DARK OPTICAL SOLITONS: PHYSICS AND APPLICATIONS

Yuri S. KIVSHAR[a], **Barry LUTHER-DAVIES**[b]

[a] *Australian Photonics Co-operative Research Centre, Optical Sciences Centre, Research School of Physical Sciences and Engineering, Australian National University, ACT 0200, Canberra, Australia*

[b] *Australian Photonics Co-operative Research Centre, Laser Physics Centre, Research School of Physical Sciences and Engineering, Australian National University, ACT 0200, Canberra, Australia*

ELSEVIER

AMSTERDAM – LAUSANNE – NEW YORK – OXFORD – SHANNON – TOKYO

ELSEVIER

Physics Reports 298 (1998) 81–197

PHYSICS REPORTS

Dark optical solitons: physics and applications

Yuri S. Kivshar[a], Barry Luther-Davies[b]

[a] *Australian Photonics Co-operative Research Centre, Optical Sciences Centre, Research School of Physical Sciences and Engineering, Australian National University, ACT 0200, Canberra, Australia*

[b] *Australian Photonics Co-operative Research Centre, Laser Physics Centre, Research School of Physical Sciences and Engineering, Australian National University, ACT 0200, Canberra, Australia*

Received April 1997; editor: A.A. Maradudin

Contents

Abstract

We present a detailed overview of the physics and applications of *optical dark solitons*: localized nonlinear waves (or 'holes') existing on a stable continuous wave (or extended finite-width) background. Together with the traditional problems involving properties of dark solitons of the defocusing cubic nonlinear Schrödinger equation, we also describe recent theoretical results on optical vortex solitons; ring dark solitons; polarization domain walls; parametric dark solitons in a dispersive $\chi^{(2)}$ medium; vector dark solitons; coupled dark–bright soliton pairs, and we discuss the

PII S0370-1573(97)00073-2

instability-induced dynamics of dark solitons in the models of generalized (i.e., non-Kerr) optical nonlinearities. Special attention is paid to the experimental demonstrations of temporal dark solitons in optical fibres and spatial dark solitons, especially dark-soliton stripes and vortex solitons, in a defocusing bulk medium.

PACS: 42.65. − k

1. Introduction

Optical solitary waves, *temporal and spatial* solitons, have been the subject of intense theoretical and experimental studies in recent years. Solitons – localized pulses in time or bounded self-guided beams in space – evolve from a nonlinear change in the refractive index of a material induced by the light intensity distribution. When the combined effects of the refractive nonlinearity and the pulse dispersion (in the case of *temporal solitons*) or beam diffraction (in the case of *spatial solitons*) exactly compensate each other, the pulse or beam propagates without change in shape and is said to be *self-trapped*. Nonlinear effects responsible for soliton formation in optical fibers are, in general, weak and Kerr-like, i.e. they induce a local index change directly proportional to the light intensity. In this case the main nonlinear equation governing the pulse evolution is the famous cubic nonlinear Schrödinger (NLS) equation for the complex amplitude envelope of the electric field which, depending on the sign of the group-velocity dispersion, has two distinct types of localized solutions, *bright or dark solitons*. These two types of waves look like *two members of a general family* of localized solutions, and this idea manifests itself in the drawing of Marc Haelterman, see Fig. 1. However, as will be seen from the results presented below, these two types of solitary waves are in fact *very different*, they have completely different nature and result from quite different physics.

In the case of temporal solitons observed in optical fibers [Hasegawa (1989); an extended overview and history can be also found in the book by Hasegawa and Kodama (1995)], the group velocity dispersion is known to vanish at a wavelength of about 1.3 μm and is *positive* at larger wavelengths and *negative* at shorter ones. As a result, since silica optical fibers have always a positive Kerr coefficient, the two different signs of group-velocity dispersion support two different types of solitons, *dark*, in the former case, and *bright*, in the latter case. A similar situation occurs for self-guided beams or spatial optical solitons [Chiao et al. (1964); see also Chiao et al. (1993)] observed in planar waveguides or in a bulk medium. Here diffraction plays a role analogous to dispersion in the temporal domain, but now the nonlinearity may be either *positive*, for the so-called self-focusing nonlinear medium, or *negative*, for self-defocusing medium. This again gives rise to two distinct types of solitons, bright and dark, respectively.

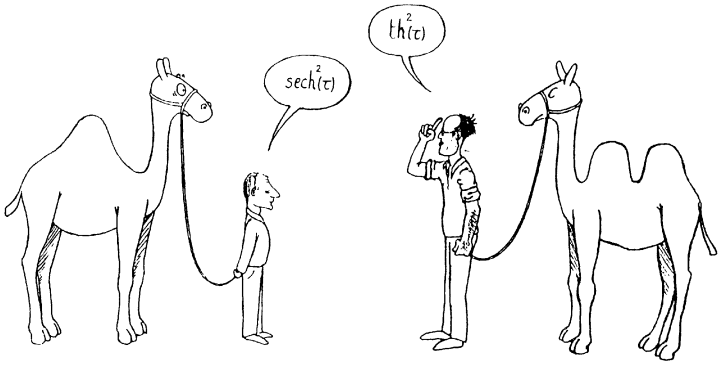

Fig. 1. Do these 'animals' belong to the same soliton family? (the drawing made by Marc Haelterman in 1989).

When the group-velocity dispersion in an optical fiber is anomalous (or, similarly, when the nonlinearity of a planar waveguide is self-focusing), a constant amplitude continuous wave is unstable due to the modulational instability [see, e.g., Hasegawa (1989)], and breaks down into a sequence of localized pulses (or beams for the spatial domain). These pulses are *bright solitons*. Propagation of bright solitons in optical fibers has been verified in a number of elegant experiments, see, e.g., the pioneering paper by Mollenauer et al. (1980), as well as more recent investigations of long-distance soliton transmission in periodically amplified fibers [e.g., Mollenauer et al. (1990)]. These results have been presented in several review papers and books [e.g., Hasegawa (1989), Agrawal (1989), Hasegawa and Kodama (1995) and Haus and Wong (1996)].

In the case of normal group-velocity dispersion in fibers (or a self-defocusing nonlineariy in waveguides), bright solitons do not exist, instead initial pulses (or spatially localized beams) undergo enhanced dispersion (or diffraction) induced broadening and chirping. In this case a constant amplitude wave is *modulationally stable* and localized pulses can appear only as "holes" on a continuous wave (cw) background, i.e., as *dark solitons*. Interest in the behaviour of such dark solitons has been motivated by several experimental observations of temporal dark solitons in optical fibers (Emplit et al., 1987; Krökel et al., 1988; Weiner et al., 1988) and spatial dark solitons in bulk media and waveguides (Andersen et al., 1990; Swartzlander et al., 1991; Allan et al., 1991; Skinner et al., 1991; Luther-Davies and Yang, 1992a,b; Duree et al., 1995; Taya et al., 1996; Z. Chen et al., 1996b). Although there has now been many successful experiments in which dark solitons have been observed in optical systems because of the relative ease of producing high intensity light beams or short (ps or fs) optical pulses, it should be remembered that the basic physics behind dark-soliton propagation on a modulationally stable background wave is quite fundamental and it applies to nonlinear problems with a different physical context. By way of illustration we note here some other experimental results including the excitation of nonpropagating π-kink surface modes in a long channel of shallow liquid driven parametrically (Denardo et al., 1990), the observation of dark-soliton standing waves in a discrete mechanical system [Denardo et al. (1992); see also the theory of this phenomenon presented by Kivshar (1993a)], the observation of high-frequency dark solitons during pulse propagation in thin magnetic films (M. Chen et al., 1993), and so on.

Optical dark solitons have been investigated in many theoretical and experimental papers and several years ago the early results in this field were summarized in two review papers (Weiner, 1992; Kivshar, 1993b). However, recent experimental achievements have increased interest in the potential applications of optical dark solitons. For example, it was demonstrated (Luther-Davies and Yang, 1992b) that various types of all-optical switches may be 'written' using structures created during propagation and interaction of dark spatial solitons. As was demonstrated earlier for bright solitons (Reynaud and Barthelemy, 1990), these induced structures can guide a weak probe beam of a different frequency or polarization thus acting as light induced structured waveguides. These kinds of devices have very interesting properties, e.g., they may conserve transverse velocity – the key characteristic used in dark spatial soliton switching – even in the presence of two-photon absorption (Yang et al., 1994); the effect which can have a dramatic destructive influence on bright spatial solitons (Silberberg, 1990a).

The purpose of this review paper is to describe, in the framework of an unified approach, the basic physics of the dark-soliton propagation using the examples taken from nonlinear waveguide optics. We present a systematic analysis of the properties of *scalar dark solitons*, in the framework of the generalized NLS equations, and *vector dark solitons* and their generalizations such as

bright–dark solitons, in the framework of coupled NLS equations. Although throughout we relate the theory to possible applications in guided wave optics, the analytical results are rather general and are applicable to other fields.

First, we discuss the physical origin and properties of dark solitons and similar localized structures in the nonlinear systems with no or small dissipation. We consider the most interesting examples, with applications in nonlinear guided wave optics, and discuss the effect of perturbations and the stability of dark solitons, and their waveguiding properties. As a generalization of the concept of dark solitons, we include a summary of results on dark solitons in quadratic or $\chi^{(2)}$ media; vector dark solitons; and dark–bright solitons; polarization domain walls; $(2+1)$-dimensional dark solitons of circular symmetry; etc. One of the important parts of our review is a summary of the experimental results demonstrating the generation and propagation of $(1+1)$- and $(2+1)$-dimensional dark solitons. We emphasize that in presenting the analytical results, we avoid the traditional restrictions associated with consideration of only the cases of integrable models (i.e., the cubic NLS equation, for scalar solitons, or the Manakov equation, for vector solitons), as has been done in many previous review papers and books on optical solitons. Instead, we concentrate on the physics of the underlying phenomena and more realistic (generally non-integrable) physical models. This involves naturally discussions of soliton stability and instability-induced evolution of dark solitons, since in nonintegrable models solitary waves can become unstable.

At the same time, we do not discuss here some phenomena which can be also related to the physics of dark solitons, such as vectorial *dark solitons of the TM type* [e.g., Y. Chen (1991a,b)], different types of *envelope shock waves* connecting background of nonequal intensities [e.g., Christodoulides (1991), Kivshar and Malomed (1993), Kivshar and Turitsyn (1993), Cai et al. (1997)], *dark surface modes* in slab waveguide structures with defocusing nonlinearity [e.g., Andersen and Skinner (1991a,b), Miranda et al. (1992) and Y. Chen and Atai (1992)], dark solitons and dark-profile modes in *discrete lattices* (Kivshar, 1993a; Kivshar et al., 1994a,c), *dark gap solitons* in the systems with periodically varying parameters such as optical waveguides with grating [e.g., Feng and Kneubühl (1993), Kivshar (1995) and Kivshar et al. (1995)]. We believe these, and some other related topics still require further analysis and deeper insight into stability as well as experimental verifications.

The structure of our review paper is as follows. In Section 2 we provide a kind of framework for the remaining chapters. First, we discuss the basic equations describing the physics of dark solitons in nonlinear optics. This includes nonlinear pulse propagation in optical fibers (temporal solitons), where weak nonlinearity can be described in the framework of the Kerr effect, and self-guided optical beams (spatial solitons) that require to introduce generalized phenomenological models of non-Kerr nonlinearities. Next, we describe the physical origin of dark solitons and discuss their difference from bright solitons by analyzing the results of modulational instability of continuous waves. As we demonstrate, this leads to a different choice of mathematical tools for analyzing these two types of solitons, and a specific role of the integrals of motion and, in the case of dark soliton, the soliton phase. To discuss solitary waves in more realistic physical models described by a perturbed cubic NLS equation (temporal solitons) or in media with non-Kerr optical response (spatial solitons), we present a summary of the results of the perturbation theory developed for dark solitons (Section 3) and also discuss the characteristic scenarios of the instability-induced dynamics dark solitons (Section 4). In particular, we analyse some effects important for optical applications,

e.g. dark-soliton jitter (Section 3.3); the effect of third-order dispersion on dark solitons (Section 3.4); and briefly discuss the role of a finite-width background in experimental observations of dark solitons (Section 3.5). In Section 5 we present several important multi-component generalizations of dark solitons for systems describing incoherent and parametric interactions between optical polarization modes or harmonics. Section 6 gives a summary of experimental results on dark solitons in optical fibers and the (1 + 1)-dimensional dark spatial solitons. Extensions of the concept of dark soliton to higher dimensions are presented in Section 7, where we discuss also the theory and experimental demonstrations of optical vortex solitons. Finally Section 8 concludes the review being served as a guide to some open, unsolved problems.

2. Dark vs. bright solitons

2.1. Optical fibers

To discuss the physics of dark solitons in optical fibers, we should start from the basic dynamical equation for the complex envelope amplitude of the electric field which can be derived taking into account the weak nonlinearity arising from the Kerr effect in a silica glass. This derivation is well-known and it is *exactly the same* as in the case of bright solitons [see, e.g., Agrawal (1989), Hasegawa (1989) and Hasegawa and Kodama (1995)]. The derivation is based on the well-known Maxwell's equations for a dielectric medium in which is assumed that the electric displacement vector $\boldsymbol{D}$ can be split up into two parts, linear and nonlinear ones. The nonlinearity arises from the Kerr effect alone, and the nonlinear part $\boldsymbol{D}_{nl}$ may be presented in the form, $\boldsymbol{D}_{nl} = n_2|\boldsymbol{E}|^2\boldsymbol{E}$, where $\boldsymbol{E}$ is the electric field, and n_2 is the Kerr coefficient.

The next important step of the derivation is the use of the fact that wave envelope function $E(z, t)$ is a slowly varying function in the propagation coordinate z and retarded time t, which can be expanded using the Fourier space variable $\Delta\omega = \omega - \omega_0$. This represents a small frequency shift of the side band from the carrier frequency ω_0, which in turn induces a small shift pf the carrier wave number, $\Delta k = k - k_0$. The expansion of the wave number $k(\omega)$ around k_0 can be therefore presented as a standard Fourier expansion,

$$k - k_0 = \left.\frac{\partial k}{\partial \omega}\right|_{\omega=\omega_0} (\omega - \omega_0) + \frac{1}{2}\left.\frac{\partial^2 k}{\partial \omega^2}\right|_{\omega=\omega_0} (\omega - \omega_0)^2 + \cdots ,$$

where the second-order derivative describes the wave dispersion. Expanding the field envelope E and taking into account simultaneously both temporal (or group-velocity) dispersion and weak Kerr nonlinearity, we arrive at the well-known *cubic* nonlinear Schrödinger (NLS) equation. In an appropriate system of normalized coordinates, this equation becomes

$$\mathrm{i}\frac{\partial u}{\partial z} - \frac{\sigma}{2}\frac{\partial^2 u}{\partial x^2} + |u|^2 u = 0 , \tag{2.1}$$

where $\sigma = \pm 1$ stands for the sign of the second-order derivative of $k(\omega)$. This sign corresponds to two distinct types of the fiber group-velocity dispersion, namely *anomalous*, when $\sigma = -1$, or *normal*, when $\sigma = +1$. The meaning of other values is the following: u is the normalized amplitude

of the electric field envelope E describing the pulse, z is the normalized distance along the fiber, and the time variable t is a retarded time measured in the reference frame moving along the fiber with the group velocity. The normalization units are well known and, as a matter of fact, they are the same as for bright solitons [see, e.g. Hasegawa (1989)],

$$z \to z/Z_0\,, \qquad x = (t - z/V_g)/t_c\,.$$

The most frequently used normalized units are

$$Z_0 = 0.322\,\frac{\pi c T^2}{\lambda_0^2 D}\,, \qquad t_c = \frac{T}{1.763}\,,$$

$$D = \frac{2\pi}{\lambda_0^2}\left\{\frac{d^2k}{d\omega^2}\right\}_{\omega=\omega_0}, \qquad V_g^{-1} = 2\left\{\frac{dk}{d\omega}\right\}_{\omega=\omega_0}.$$

Here the parameter T represents the full width at half maximum (FWHM) of the pulse intensity, and the pulse propagation is considered in the reference frame moving with the group velocity V_g.

2.2. Nonlinear waveguides

2.2.1. Why temporal and spatial solitons are different

Usually, the stationary beam propagation in planar waveguides is considered as the phenomenon similar to the pulse propagation in fibers referring to the so-called *spatio-temporal analogy* in wave propagation [Akhmanov et al. (1967); see also Svelto (1974)]. This means that the propagation coordinate z is treated as the evolution variable and the spatial beam profile along the transverse direction, for the case of waveguides, is similar to the temporal pulse profile, for the case of fibers. This analogy has been developed by many researchers, and it is based on a simple notion that both beam and pulse propagation can be described by the cubic NLS equation [see, e.g., Boardman and Xie (1993), Chiao et al. (1993)]. However, contrary to the accepted opinion, there exists a crucial difference between these two phenomena. Indeed, in the case of the nonstationary pulse propagation in fibers, the operation wavelength is usually selected near the zero of the group-velocity dispersion. This means that the absolute value of the fiber dispersion is small enough to be compensated by a weak nonlinearity such as that produced by the (very weak) Kerr effect in optical fibers which leads to a nonlinearity-induced change in the refractive index by the order of 10^{-10}. Therefore, nonlinearity in fibers is *always weak* and it is well modeled by the cubic NLS equation, which is known to be integrable by means of the inverse scattering transform [Zakharov and Shabat (1971, 1973); see also Zakharov et al. (1980)]. However, for very short (fs) pulses the cubic NLS equation should be corrected to include some additional (but still small) effects such as higher-order dispersion, induced Raman scattering, etc. (e.g., Hasegawa (1989) and Hasegawa and Kodama (1995)]. Thus, in fibers nonlinear effects are very weak and they become important on large distances (of order of hundred meters or even kilometers).

Contrary to the pulse propagation in optical fibers, the physics underlying the stationary beam propagation in planar waveguides and a bulk medium is different. In this case the nonlinear change in the refractive index should compensate for the beam spreading caused by diffraction which is not a small effect. That is why to observe spatial solitons much larger nonlinearities are usually required, and very often such nonlinearities are not of the Kerr type (e.g. they saturate at higher

intensities). This leads to the models of generalized non-linearities (see Section 2.2.3 below) with the properties of solitary waves different from those described by the integrable cubic NLS equation. For example, unlike the solitons of the integrable cubic NLS equation, solitary waves of generalized nonlinearities may be unstable, they also show some interesting properties such as fusion due to collision, etc.

Propagation distances usually involved into the phenomenon of the beam self-focusing and spatial soliton propagation are of order of millimeters or centimeters. Nevertheless, the physics of spatial solitary waves is very rich and it should be understood in the framework of nonintegrable models.

2.2.2. Basic equations

First, we consider the propagation of a monochromatic scalar electric field E in a bulk optical medium with an intensity-dependent refractive index, $n = n_0 + n_{\rm nl}(I)$, where n_0 is the linear refractive index, and $n_{\rm nl}(I)$ describes the variation in the index due to the field with the intensity $I = |E|^2$. The function $n_{\rm nl}(I)$ is assumed to be dependent only on the light intensity, and it is usually introduced phenomenologically.

Solutions of the governing Maxwell's equation can be presented in the form

$$E(\boldsymbol{R}_\perp, Z; t) = \mathscr{E}(\boldsymbol{R}_\perp, Z)\mathrm{e}^{\mathrm{i}\beta_0 Z - \mathrm{i}\omega t} + \text{c.c.}\,, \tag{2.2}$$

where c.c. denotes complex conjugate, ω is the source frequency, and $\beta_0 = k_0 n_0 = 2\pi n_0/\lambda$ is the plane-wave propagation constant for the uniform background medium, in terms of the source wavelength $\lambda = 2\pi c/\omega$, c being the free-space speed of light. Further, we assume a $(2+1)$-dimensional model, so that the Z-axis is parallel to the direction of propagation, and the X- and Y-axis are two transverse directions.

The function $\mathscr{E}(\boldsymbol{R}_\perp, Z)$ describes the wave envelope which in the absence of nonlinear and diffraction effects $\mathscr{E}$ would be a constant. If we substitute Eq. (2.2) into the two-dimensional, scalar wave equation, we obtain the generalized nonlinear parabolic equation,

$$2\mathrm{i}k_0 n_0 \frac{\partial \mathscr{E}}{\partial Z} + \left(\frac{\partial^2 \mathscr{E}}{\partial X^2} + \frac{\partial^2 \mathscr{E}}{\partial Y^2}\right) + 2n_0 k_0^2 n_{\rm nl}(I)\mathscr{E} = 0\,. \tag{2.3}$$

In dimensionless variables, Eq. (2.3) becomes the well-known generalized NLS equation, where local nonlinearity is introduced by the function $n_{\rm nl}(I)$.

For the case of the Kerr (or cubic) nonlinearity we have $n_{\rm nl}(I) = n_2 I$, n_2 being the coefficient of the Kerr effect of an optical material. Now, introducing the dimensionless variables, i.e. measuring the field amplitude in the units of $k_0\sqrt{n_0|n_2|}$ and the propagation distance in the units of $k_0 n_0$, we obtain the $(2+1)$-dimensional NLS equation in the standard form,

$$\mathrm{i}\frac{\partial u}{\partial z} + \frac{1}{2}\left(\frac{\partial^2 u}{\partial x^2} + \frac{\partial^2 u}{\partial y^2}\right) \pm |u|^2 u = 0\,, \tag{2.4}$$

where the sign ($\pm$) is defined by the type on nonlinearity, *self-defocusing* ('minus', for $n_2 < 0$) or *self-focusing* ('plus', for $n_2 > 0$).

For propagation in a slab waveguide, the field structure in one of the directions, say y, is defined by the linear guided mode of the waveguide. Then, the solution of the governing Maxwell's

equation has the structure

$$E(\boldsymbol{R}_\perp, Z; t) = \mathscr{E}(X, Z)A_n(Y)\mathrm{e}^{\mathrm{i}\beta_n^{(0)}z - \mathrm{i}\omega t} + \cdots , \tag{2.5}$$

where the function $A_n(Y)$ describes the corresponding fundamental mode of the slab waveguide. Similarly, substituting this ansatz into Maxwell's equations and averaging over Y, we come again to the renormalized equation of the form of Eq. (2.4) with the Y-derivative *omitted*, which in the dimensionless form becomes the standard cubic NLS equation

$$\mathrm{i}\frac{\partial u}{\partial z} + \frac{1}{2}\frac{\partial^2 u}{\partial x^2} \pm |u|^2 u = 0 . \tag{2.6}$$

As has been discussed above, Eq. (2.6) coincides formally with Eq. (2.1) of Section 2.1, which has been derived in the theory of pulse propagation in dispersive nonlinear optical fibers.

2.2.3. Models of optical nonlinearities

The generalized NLS Eq. (2.3) has been considered in many papers for analyzing the beam self-focusing and properties of spatial bright and dark solitons [see, e.g., Zakharov et al. (1971), Zakharov and Synakh (1975), Kaplan (1985a,b), Enns and Mulder (1989), Mulder and Enns (1989), Gatz and Herrmann (1991, 1992), Herrmann (1992), Bass et al. (1992), Snyder and Sheppard (1993), Królikowski and Luther-Davies (1992, 1993), Królikowski et al. (1993), Valley et al. (1994), Christodoulides and Carvalho (1995), Pelinovsky et al. (1996a,b), Micallef et al. (1996)]. All types of non-Kerr nonlinearities discussed in relation with the existence of solitary waves in nonlinear optics can be divided, generally speaking, into *three main classes*: (i) *competing nonlinearities*, e.g. focusing (defocusing) cubic and defocusing (focusing) quintic nonlinearity [see, e.g., Kaplan (1985a,b), Gatz and Herrmann (1991); Królikowski et al. (1993)] and also generalization to a power nonlinearity [e.g., Pelinovsky et al. (1996a) and Micallef et al. (1996)]; (ii) *saturable nonlinearities* [see, e.g., Snyder and Sheppard (1993), Królikowski and Luther-Davies (1992, 1993), Valley et al. (1994) and Christodoulides and Carvalho (1995)], and (iii) *transiting nonlinearities* [see, e.g., Kaplan (1985a,b), Enns and Mulder (1989) and Bass et al. (1992)].

Usually, the nonlinear refractive index of an optical material deviates from the linear (Kerr) dependence for larger light intensities. Nonideality of the nonlinear optical response is known for semiconductor (e.g., AlGaAs, CdS, $CdS_{1-x}Se_x$) waveguides and semiconductor-doped glasses [see, e.g., Roussignol et al. (1987), Acioli et al. (1990) and Lederer and Biehlig (1994)]. Larger deviation from the Kerr nonlinearity is observed for nonlinear polymers. For example, recently the measurements of a large nonresonant nonlinearity in single crystal PTS (p-toluene sulfonate) at 1600 nm (Lawrence et al., 1994a,b) revealed a variation of the nonlinear refractive index with the input intensity which can be modeled by *competing*, cubic-quintic nonlinearity,

$$n_{\mathrm{nl}}(I) = n_2 I + n_3 I^2 . \tag{2.7}$$

This model describes a competition between self-focusing ($n_2 > 0$), at smaller intensities, and self-defocusing ($n_3 < 0$), at larger intensities. Similar models are usually employed to describe the stabilization of wave collapse in the (2 + 1)-dimensional NLS equation [e.g., Josserand and Rica (1997) and references therein].

In a more general case, the models with competing nonlinearities can be described by power-law dependence on the beam intensity,

$$n_{\rm nl}(I) = n_p I^p + n_{2p} I^{2p}\,, \tag{2.8}$$

where p is a positive constant and usually $n_p n_{2p} < 0$.

Models with *saturable nonlinearities* are the most typical ones in nonlinear optics. For higher powers saturation of nonlinearity has been measured in many materials and consequently the maximum refractive index change has been reported [see, e.g., Coutaz and Kull (1991)]. We do not linger on the physical mechanisms behind the saturation but merely note that it exists in many nonlinear media being usually described by phenomenological models introduced more than 25 years ago [see, e.g., Gustafson et al. (1968), Reichert and Wagner (1968) and Marburger and Dawes (1968)]. The effective generalized NLS equation with saturable nonlinearity is also the basic model to describe the recently discovered (1 + 1)-dimensional photovoltaic dark solitons in photovoltaic–photorefractive materials as $LiNbO_3$ [see Valley et al. (1994)]. Unlike the phenomenological models usually used to describe saturation of nonlinearity, for the case of photovoltaic solitons this model finds its rigorous justification (Valley et al., 1994; Christodoulides and Carvalho, 1995).

There exist several models of the nonlinearity saturation. From a general point of view, the function $n_{\rm nl}(I)$ describing the nonlinearity saturation should be characterized by *three independent parameters*: the saturation intensity, $I_{\rm sat}$, the maximum change in the refractive index, n_∞, and the Kerr coefficient n_2 which appears for small I. In particular, the phenomenological model

$$n_{\rm nl}(I) = n_\infty \left\{1 - \frac{1}{(1 + I/I_{\rm sat})^p}\right\}, \tag{2.9}$$

satisfies these criteria, provided $n_2 = n_\infty p/I_{\rm sat}$. In the particular case $p = 1$, the model defined by Eq. (2.9) reduces to the well-known expression derived from the two-level model, which is used most frequently. For the case $p = 2$ the model Eq. (2.9) possesses localized solutions for bright and dark solitons in an explicit analytical form (Królikowski and Luther-Davies, 1992, 1993).

At last, *bistable solitons* introduced by Kaplan (1985a,b) usually require a special type of the intensity-dependent refractive index which changes from one type to another one, e.g., it varies from one kind of the Kerr nonlinearity, for small intensities, to another kind with different value of n_2, for larger intensities. This type of nonlinearity is known to support bistable dark solitons (Enns and Mulder, 1989; Mulder and Enns, 1989) as well. One of the simplest models of such transiting nonlinearities describes a change from one type of the Kerr dependence, to the other one, i.e.,

$$n_{\rm nl}(I) = \begin{cases} n_2^{(1)} I & I < I_{\rm cr} \\ n_2^{(2)} I & I > I_{\rm cr}\,. \end{cases} \tag{2.10}$$

A smooth transition of this kind can be modeled by the function (Enns and Mulder, 1989)

$$n_{\rm nl}(I) = n_2 I\{1 + \alpha \tanh[\gamma(I^2 - I_{\rm cr}^2)]\}\,, \tag{2.11}$$

where for $I \ll I_{\rm cr}$, $n_{\rm nl}(I) \simeq n_2^{(1)} I$, where $n_2^{(1)} = n_2[1 - \alpha \tanh^2(\gamma I_{\rm cr}^2)]$, and for $I \gg I_{\rm cr}$, $n_{\rm nl}(I) \simeq n_2^{(2)} I$, where $n_2^{(2)} = (1 + \alpha)$. Unfortunately, examples of nonlinear optical materials with such dependencies are not known yet, but the bistable solitons possess attractive properties useful for their possible futuristic applications in all-optical logic and switching devices.

2.3. When the NLS equation fails

The scalar NLS equation discussed above for both temporal and spatial wave propagation is considered to be rather universal model. It is derived from the first principles on the basis of very general assumptions about dispersive (or diffractive) and nonlinear properties of physical systems. However, the NLS model may fail in a number of cases, and therefore one should be aware of the validity limits of this simple model. Here we discuss only two main circumstances when the NLS equation fails [see also Gibbon (1990), for examples from other fields].

First of all, a standard derivation of the NLS equation is based on the so-called *multi-scale asymptotic technique*, sometimes called reductive perturbation method [e.g., Jeffrey and Kawahara (1982) and Taniuti and Nishihara (1983)]. It assumes nonresonant nonlinearities when the most important effects are described by an envelope of the field of the fundamental frequency ω propagating with the carrier wave number k. All higher-order harmonics, even being excited, are assumed to be very small and, therefore, they do not modify the field evolution on the main frequency which, in the case of the cubic nonlinearity, is described by the NLS equation. However, when some multiple frequencies are generated, they may strongly affect the wave propagation at the fundamental harmonic provided the so-called matching conditions are satisfied. For example, strong interaction between the main frequency ω and two other frequencies ω_1 and ω_2 occurs provided $\omega = \omega_1 + \omega_2$ and the phase mismatch $\Delta k = k - (k_1 + k_2)$ vanishes. This kind of three-wave mixing is possible in a medium where the lowest-order nonlinearity is quadratic. When the medium nonlinearity is cubic, the wave coupling is possible in the form of a four-wave mixing process. When any of such resonance conditions is satisfied, the envelope of the fundamental field becomes strongly coupled to a secondary field (or more than one field) and a single NLS equation becomes not valid. Coupling between the modes may also support multi-component solitary waves which might differ very much from the conventional solitons of the scalar NLS equation (see Section 5.4 below). Additionally, the intermode interaction may lead to instability of solitary waves (see, e.g., Section 5.3 below).

The second class of problems when the NLS model fails is closely related to optical spatial solitons described by non-Kerr nonlinearities. Indeed, it is well known that the NLS equation with nonlinearity stronger than cubic, e.g. a power-law focusing nonlinearity $|u|^{2q}u$, has localized solutions which blowup, so that a singularity appears in finite z. This phenomenon occurs for negative values of the system Hamiltonian under the condition $qD \geq 2$, where q is the nonlinearity power and D stands for the $(D+1)$-dimensional model [e.g., Zakharov (1972)]. Blowup (or *collapse*) in finite z means that the NLS model of this dimension fails as an envelope equation since it breaks the scales on which it was derived in the framework of the multi-scale asymptotic technique. For spatial solitons this condition means that if $D = 2$, than the cubic nonlinearity $|u|^2u$ is already sufficient to induce collapse. If $D = 1$, then one needs the quintic (or higher-order) nonlinearity to induce collapse. Blowup indicates also that the primary NLS model should be corrected, e.g. by taking into account the effects of nonparaxiality in the beam self-focusing [Feit and Fleck (1988); Fibich (1996)].

Therefore, we can conclude that the NLS equation has a multiple of uses even though its applicability must be treated with care. In nonlinear optics, it is not only generic model for describing self-guided beams or spatial solitons, in waveguides, or bulk media and pulses or temporal solitons, in optical fibers, but it allows also to describe the beam self-focusing possessing

the properties of blowup solutions. When the generalized NLS equation is valid as the main approximation, all corrections to it can be treated within the perturbation theory. However, near resonances the inclusion of higher-order corrections is very often meaningless and requires another approach [see, e.g., Oughstun and Xiao (1997), as an example of the failure of the envelope approximation for ultrashort pulses in a dispersive attenuative medium].

2.4. Modulational instability and solitons

The NLS equation has the simplest solution in the form of a continuous wave (cw) given, e.g. for the Eq. (2.6), by the expression,

$$u = u_0 e^{ikx - i\beta z}, \qquad \beta = \tfrac{1}{2}k^2 \mp u_0^2, \tag{2.12}$$

where the sign stands for the type of nonlinearity. Let us investigate the linear stability of the exact solution, Eq. (2.12), against small perturbations. To do so, we follow the standard procedure and look for solutions describing small variations around the exact solution, Eq. (2.12), in the form,

$$u = (u_0 + \xi)e^{ikx - i\beta z + i\psi}, \tag{2.13}$$

where the function ξ and derivatives of the phase ψ are assumed to be small. Substituting Eq. (2.13) into the NLS Eq. (2.6), we come to a system of two coupled linear equations for ξ and ψ. Looking for solutions to these functions in the form, $\xi, \psi \sim \exp(i\Omega z - iQx)$, we obtain the dispersion relation,

$$(\Omega - kQ)^2 = Q^2(\pm u_0^2 + \tfrac{1}{4}Q^2), \tag{2.14}$$

which shows that small excitations on the cw background, Eq. (2.12), are absolutely stable only for the case of the defocusing medium (the sign 'plus'), whereas they become unstable for the focusing nonlinearity provided $Q^2 < 4u_0^2$. In the former case, the small-amplitude waves can propagate along the background and these waves are characterized by the minimum ('sound') velocity

$$c^2 = u_0^2. \tag{2.15}$$

This property of modulational instability of the cw background is closely connected with the existence and type of solitary wave solutions of the NLS equation. Namely, spatially localized solutions with vanishing asymptotics are possible only for the case when the plane wave solution is unstable, i.e., only for the focusing nonlinearity.

Similarly, the NLS Eq. (2.1) displays the same properties of the plane wave stability and, therefore, divides localized solutions into two different classes depending on the sign parameter σ. For example, the defocusing nonlinearity, in the spatial problem, corresponds to the normal group-velocity dispersion and $\sigma = +1$, in the temporal problem.

Thus, in the case $\sigma = -1$ (anomalous dispersion) the cw solution in unstable and therefore the appropriate boundary conditions to Eq. (2.1) is $|u| \to 0$ at $x \to \pm\infty$. For these conditions Zakharov and Shabat (1971) showed that Eq. (2.1) [and, therefore, Eq. (2.6)] is exactly integrable by means of the inverse scattering transform, and it possesses localized solutions called *bright*

solitons. General solution for the bright soliton has the form,

$$u(z, x) = \frac{a e^{ivx/2 - i(v^2/4 - a^2)z}}{\cosh[a(x - vz)]}, \tag{2.16}$$

where a is the soliton amplitude and v is its velocity. At $v = 0$ this soliton has a simplified structure referred to as the fundamental bright soliton (see Fig. 2a)

$$u(z, x) = \frac{a e^{ia^2 z}}{\cosh(ax)}. \tag{2.17}$$

For $\sigma = +1$ (normal dispersion) the cw solution $|u| = u_0$ is always stable against small modulations of its shape, and, as a result, Eq. (2.1) has soliton solutions in the form of localized 'dark' pulses created on the cw background. The NLS equation with the boundary conditions $|u| \to u_0$ is also exactly integrable by the inverse scattering technique (Zakharov and Shabat, 1973) and its one-soliton solution for a single dark soliton can be written in the form,

$$u(z, x) = u_0[B \tanh \Theta + iA]\, e^{iu_0^2 z}, \tag{2.18}$$

where

$$\Theta = u_0 B(x - Au_0 z). \tag{2.19}$$

Parameters A and B are connected by a simple relation, $A^2 + B^2 = 1$, so that instead of two parameters we can use only one, introducing $A = \sin\phi$ and $B = \cos\phi$. The effective angle ϕ corresponds to the total phase shift across the dark soliton, 2ϕ. Soliton solution, Eqs. (2.18) and (2.19), has, unlike the bright soliton, Eq. (2.16), the only parameter ϕ and the function $B^2 = \cos^2\phi$ characterizes the soliton intensity at the center, i.e., the minimum soliton intensity relative to the

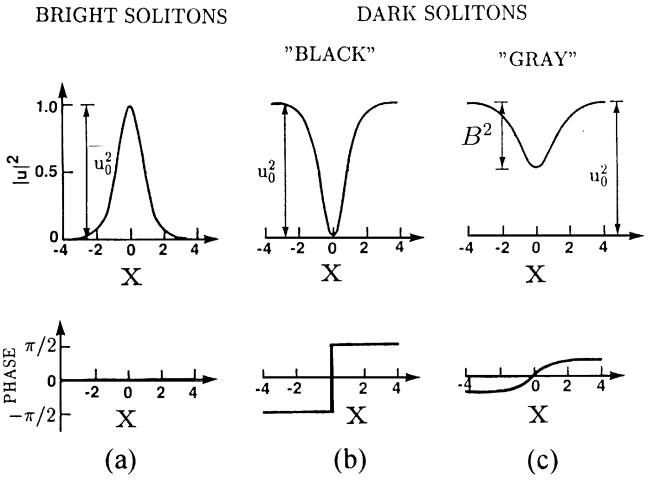

Fig. 2. Intensity and phase as functions of normalized coordinate x for bright (a), black (b) and (c) gray solitons [adapted from Tomlinson et al. (1989)].

background intensity. The soliton intensity profile $|u|^2$ has the dip-like shape (see Fig. 2b and Fig. 2c)

$$|u|^2 = u_0^2\left(1 - \frac{\cos^2\phi}{\cosh^2\Theta}\right). \tag{2.20}$$

The value $u_0 \sin\phi$ has the meaning of the soliton velocity in the x-space, i.e. the relative velocity between the dark soliton and the background.

We distinguish two limit cases of the dark soliton solution, Eq. (2.18). The so-called *fundamental dark soliton* (at $\phi = 0$)

$$u(z, x) = u_0 \tanh(u_0 x)\, e^{iu_0^2 z}, \tag{2.21}$$

is the anti-symmetric function of x with the π phase shift and zero intensity at its center (see Fig. 2b). Another limit case, when $\cos^2\phi < 1$, corresponds to the so-called *gray solitons* (see Fig. 2c) when the minimum intensity does not drop to zero [for the small-amplitude limit, see, e.g., discussions in Section 2.5.2 and also Kivshar (1993b)]. As may be seen in Fig. 2a–c, one of the major differences between bright and dark solitons is in the phase dependence: Bright solitons have a constant phase across the localized region but dark solitons have a nontrivial distribution of their phase, so that there exists a finite phase jump across the localized region. Below, we relate this difference with the different physics of these two types of solitary waves.

A dark-soliton solution of the generalized (1 + 1)-dimensional NLS equation

$$i\frac{\partial u}{\partial z} + \frac{1}{2}\frac{\partial^2 u}{\partial x^2} + g(|u|^2)u = 0, \tag{2.22}$$

propagating on a cw background with the phase velocity β/k can be always found in quadratures and presented in the following form,

$$u(z, x) = u_0[G(x) + iF(x)]\, e^{ikx - i\beta z}, \tag{2.23}$$

where the real and imaginary parts satisfy the boundary condition

$$G^2(\pm\infty) + F^2(\pm\infty) = 1,$$

u_0 being the background amplitude. This kind of solution can be presented as a (rather complicated) curve on the plane of the complex variable Λ defined by its real part, G, and imaginary part, F, i.e. $\Lambda = G + iF$, with the spatial variable x treated as an internal parameter [see Kosevich and Kovalev (1989) and Królikowski et al. (1993)]. In the particular case of the cubic NLS equation, the solution for a dark soliton is given by Eq. (2.18), so that $F = \text{const}$ and the corresponding curve on the Λ-plane is a straight line (see Fig. 3).

For some particular nonlinear functions $g(|u|^2)$, dark soliton solutions of the generalized NLS Eq. (2.22) can be found in an explicit analytical form. There exist only a few such cases: two types of dark solitary waves in the model of *cubic–quintic nonlinearity*, Eq. (2.7) [e.g., Barashenkov and Makhankov (1988), Gagnon (1989), Makhankov (1990) and Kivshar et al. (1996)], dark solitons of the so-called *threshold nonlinearity* (Snyder et al., 1993) and, at last, dark solitons in *a saturable medium* described by Eq. (2.9) at $p = 2$ (Królikowski and Luther-Davies, 1993). As has been mentioned above (see also Section 2.5.1 below), the special case of the cubic NLS Eq. (2.1) at $\sigma = +1$ or Eq. (2.6) with the sign 'minus' is exactly integrable by the inverse scattering transform

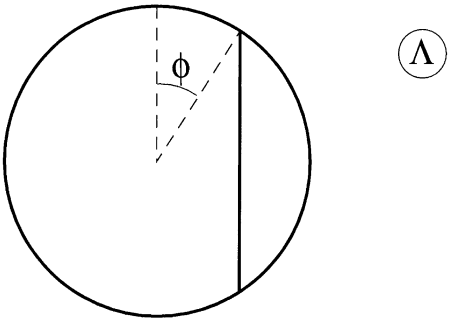

Fig. 3. Schematic presentation of a dark soliton solution of the defocusing cubic NLS equation on a complex plane Λ. Angle ϕ defines the soliton 'grayness'.

(Zakharov and Shabat, 1973; Iizuka et al., 1991) meaning that not only single dark solitons but also their superposition describing elastic collisions of N dark solitons can be formally found in an explicit analytic form [see some examples in the papers by Iizuka et al. (1991), Gagnon (1993) and Miller (1996)].

2.5. Dark solitons: mathematical tools

2.5.1. Inverse scattering transform

As is well known, the basic mathematical method to analyse any kind of wave propagation in linear media is the famous Fourier transform method. For definiteness, our discussion below assumes the case of the stationary beam propagation and spatial solitons, though it equally applies to the pulse propagation in fibers. So, making *decomposition* of the input beam $u(z = 0, x)$ into a set of linear Fourier modes, we reduce the problem of the beam propagation to a trivial oscillatory evolution of the Fourier components (or harmonics), and then construct the beam shape at any propagation distance z. In the case of a homogeneous linear medium, the only type of the Fourier modes are given by nonvanishing periodic functions, and the spectrum of the corresponding eigenvalues is continuous. However, the Fourier method is rather general and it can be also applied to analyse wave propagation in *inhomogeneous linear media*. In this case, additionally to the periodic modes with the continuous spectrum, there appear the so-called spatially localized (or guided) modes existing due to a spatial variation of the properties of the linear medium. This localized or guided modes are possible however only for special discrete eigenvalues. Therefore, a complete set of linear eigenstates which can be obtained by the Fourier method includes both discrete and continuous modes.

As is well known, the Fourier transform method cannot be used for nonlinear systems where the superposition principle does not exist. However, one may try to invent *another kind* of (nonlinear) decomposition to obtain *nonlinear modes* whose evolution will be reduced to trivial oscillations similar to that given by the Fourier transform. Such a decomposition is known to exist only for some special nonlinear equations (the so-called exactly integrable equations), and it is called *the inverse scattering transform* method. In some sense, the inverse scattering transform provides an inherent similarity between the modes of *linear inhomogeneous* systems and those of *nonlinear*

homogeneous systems where both types of localized modes, i.e., guided waves, for the former case, and solitary waves, for the latter case, correspond to a certain set of discrete eigenvalues.

The main idea of the *nonlinear decomposition* based on the inverse scattering transform is to find an appropriate *linear* eigenvalue problem which includes the input beam $u(z = 0, x)$ as an effective potential. The main property of this linear eigenvalue problem is: In spite of an explicit dependence of the potential on z, the eigenvalues are conserved quantities provided the wave field $u(z, x)$ satisfies the primary nonlinear equation. Finding the eigenvalue problem with this property, i.e., eigenvalues remain invariant when the potential evolves according to a (integrable) nonlinear evolution equation, is a common feature of the integrability technique based on the inverse scattering transform method. The property that the eigenvalues remain invariant means that if they are found (or known) for $u(z = 0, x)$, they remain the same for any z. For a given $u(z = 0, x)$, the eigenvalue problem can be solved as a scattering problem for an auxiliary eigenfunction $\Psi(x; \lambda)$, λ being a spectral problem eigenvalue. The scattering data are the amplitude $a(\lambda)$ of a transmitted wave, the amplitude $b(\lambda)$ of a reflected wave, the eigenvalues of the discrete spectrum $\{\lambda_n\}$, and the normalized coefficients b_n of the eigenfunctions of the discrete spectrum. Similar to the machinery of the standard Fourier transform method, the evolution of the scattering data $\{a(\lambda), b(\lambda), \lambda_n, b_n\}$ is trivial, and the solution of the primary nonlinear equation is then found using results of the inverse scattering method to find the function $u(z, x)$ through the z-dependent scattering data. The similar method is well-established in quantum mechanics, however here this method is used for z-dependent potential provided the conservation constrains are satisfied.

Importantly, each eigenvalue of the discrete spectrum of the scattering problem governs a localized solution, i.e., soliton, after such a reverse procedure. The soliton beam is of conserved shape due to invariance of the eigenproblem spectrum. Therefore, the stationary nature of the eigenvalues provides the important property of the stability of the soliton beams when undergoing collisions. Hence, solitons are important not only as a particular solutions of the nonlinear equation, but as an unique solution whose stability is guaranteed by the invariant property of the corresponding eigenvalue problem. Furthermore, using the scattering data one may decompose any localized input beam into a set of normal (nonlinear) modes (like linear Fourier modes) and the soliton modes are dominant nonlinear modes in such a decomposition, i.e., asymptotically a localized input beam will be transformed into a set of solitons emitting an energy excess as radiation.

As was found by Zakharov and Shabat (1971, 1973), the NLS Eq. (2.6) is exactly integrable and it may be therefore analysed by means of the inverse scattering transform method for any sign of nonlinearity (or, for temporal solitons, for any sign of the dispersion coefficient). Mathematical tools of the inverse scattering transform allow us to solve the Cauchy problem for the NLS Eq. (2.6) if the input beam profile is given. According to this method, to find which type of input beam $u(0, x)$ generates solitons and to determine soliton parameters, one has to solve the eigenvalue Zakharov–Shabat problem for the auxiliary two-component eigenfunction $(\Psi_1, \Psi_2)^T$,

$$\frac{\partial \Psi_1}{\partial x} = i\lambda \Psi_1 - iu(0, x)\Psi_2 , \qquad \frac{\partial \Psi_2}{\partial x} = -i\lambda \Psi_2 - iu^*(0, x)\Psi_2 , \tag{2.24}$$

where for the sign 'minus' in Eq. (2.6) the boundary conditions are: $u(0, x) \to u_0$, for $x \to +\infty$, and $u(0, x) \to u_0 e^{i\theta}$, for $x \to -\infty$, where the asterisk stands for complex conjugation, u_0 is the background amplitude, and θ is a constant phase.

For the NLS Eq. (2.6) with the sign 'minus', the spectral problem, Eq. (2.25), has a discrete spectrum lying in the region of real values $|\lambda| < u_0$, and the discrete spectrum is invariant in z when the coordinate evolution is included. Each real discrete eigenvalue $\lambda_n = u_0 \sin \phi_n$ corresponds to a dark soliton beam with the amplitude of the dip in the background defined by $u_0 \cos \phi_n$ that moves with the transverse 2 sin ϕ_n. Thus, the asymptotic evolution of the input localized beam is described by the eigenvalues of the discrete spectrum of the scattering problem, Eq. (2.25), so that any input beam will be transformed into a certain set of solitons for large enough propagation distances z.

From the viewpoint of experimental studies of the soliton generation by an arbitrary input beam, it is useful to know the solution of the scattering problem (and, therefore, the number and parameters of the generated solitary waves) for certain types of input beam profile. For example, let us take the shape of the input beam as the tanh-like profile, i.e.,

$$u(0, x) = u_0 \tanh(ax)\,, \tag{2.25}$$

where the ratio u_0/a is arbitrary. Then, as has been shown by Zhao and Bourkoff (1989a,b), the eigenproblem, Eq. (2.25), can be solved exactly and the eigenvalues of the discrete spectrum are defined as

$$\lambda_1 = 0\,, \quad \lambda_{2n} = -\lambda_{2n+1} = \sqrt{u_0^2 - w_n^2}\,, \quad \text{where } n = 1, 2\,, \ldots, N_0\,, \tag{2.26}$$

and positive w_n are defined as

$$w_n = u_0 \left(1 - \frac{na}{u_0}\right).$$

Maximum value N_0 is the largest integer number satisfying the condition $N_0 < u_0/a$. The first, zero eigenvalue corresponds to *a black soliton* with the zero intensity at its center, which is always created by the input beam, Eq. (2.25). The even number of the secondary eigenvalues, Eq. (2.26), correspond to N_0 symmetric *pairs of gray solitons* propagating to the left and right. Thus, the total number of dark solitons created by the input beam, Eq. (2.25), is $N = 2N_0 + 1$, and it depends on the ratio u_0/a.

The inverse scattering transform can be employed, in principle, to analyze the soliton generation in the cubic NLS equation from any type of the input profile. Several input profiles were analyzed in the literature additionally to the tanh profile, Eq. (2.25). For example, Gredeskul and Kivshar (1989b) analyzed the so-called step-like profile, $u(0, x) = u_0 e^{i\theta_1}$, for $x < 0$, and $u(0, x) = u_0 e^{i\theta_2}$, for $x > 0$, showing that it always generates a single dark soliton corresponding to the eigenvalue $\lambda_1 = -u_0 \cos[\frac{1}{2}(\theta_2 - \theta_1)]$. To generate several dark solitons by the similar modulation of the background phase, one need to use an input pulse with a several phase steps. In particular, N phase steps can generate N dark solitons in the asymptotic region provided (Kivshar and Gredeskul, 1990)

$$\Delta\tau_j > (2u_0)^{-1} |\cot(\theta_{j+1}/2) + \cot(\theta_j/2)|\,,$$

where $\Delta\tau_j$ is the distance between the $(j+1)$th and jth steps, and θ_j is the value of the jth phase jump. In particular, two steps of different signs always produce two dark solitons of opposite velocities (Gredeskul et al., 1990). Similar results can be obtained for the modulation of the background amplitude and the simple case of a boxlike input was analyzed by Zakharov and

Shabat (1973), for zero intensity in the box, and by Gredeskul and Kivshar (1989b), for a general case.

The most interesting feature of dark solitons, i.e., their thresholdless generation, was demonstrated and rigorously proven by Gredeskul and Kivshar (1989a) for the cubic NLS equation. Indeed, as is well known, generation of bright solitons requires to exceed a certain threshold defined through the input profile. Namely, bright solitons will be created by a localized input pulse provided (Kivshar, 1989) $\int_{-\infty}^{+\infty}|u(0, x)|\,\mathrm{d}x > \pi/2$. Unlike bright solitons, dark solitons can be created by an *arbitrary* initial small dip on a cw background, for example, when the input pulse has the following general form:

$$u(0, x) = u_0 e^{i\theta} + u_1(x)\,, \qquad u_1 \to 0 \quad \text{at} \quad |x| \to \infty\,. \tag{2.27}$$

As was shown by Gredeskul and Kivshar (1989a), for an arbitrary but small $u_1(x)$ (which falls off fast enough at $|x| \to \infty$), and for

$$\Delta \equiv \mathrm{Re}\left\{e^{-i\theta}\int_{-\infty}^{+\infty} u_1(x)\,\mathrm{d}x\right\} < 0\,, \tag{2.28}$$

there always exist two eigenvalues of the discrete spectrum of the spectral problem, Eq. (2.25), $\lambda_{1,2} = \pm\lambda_0 \equiv \pm u_0(1 - \frac{1}{2}\Delta^2)$, which correspond to a pair of dark solitons with equal amplitudes $u_0\Delta$ and the opposite velocities $\pm 2\lambda_0$. As a consequence of this result, *an even input pulse always produces at least a pair of dark solitons.*

2.5.2. Small-amplitude approximation

The case $B^2 = \cos^2\phi \ll 1$ in Eq. (2.18) corresponds to a shallow or small-amplitude dark soliton. This is the case when the soliton transverse velocity v is close to the limit speed c of linear waves propagating on the cw background. Importantly, in this limit we can apply a reductive perturbation technique to obtain analytical results even for the nonintegrable genreralized NLS Eq. (2.22) because in this case the dynamics of dark solitons is described by an effective Korteweg de Vries (KdV) equation [e.g., Makhankov (1990) and Kivshar (1993b)].

To discuss the dark-soliton dynamics in the small-amplitude limit, we look for solutions of the self-defocusing NLS Eq. (2.6) in the form,

$$u(z, x) = \{u_0 + a(z, x)\}\, e^{iu_0^2 z} e^{i\phi(z,x)}\,. \tag{2.29}$$

Substituting Eq. (2.29) into the NLS Eq. (2.6), we obtain two equations for the functions ϕ and a which are not defined yet. Now if one will use new variables which allow us 'to split' the propagation directions,

$$\xi = \varepsilon(x - cz)\,, \qquad \zeta = \varepsilon^3 z\,, \tag{2.30}$$

ε being an arbitrary small parameter connected with the soliton amplitude, and look for solutions in the form of the asymptotic series in ε,

$$a = \varepsilon^2 a_0 + \varepsilon^4 a_1 + \cdots, \qquad \phi = \varepsilon\phi_0 + \varepsilon^3\phi_1 + \cdots, \tag{2.31}$$

then in the lowest approximation those equations yield the simple equation for the beam phase,

$$\frac{\partial \phi_0}{\partial \xi} = -\frac{c a_0}{u_0}\,. \tag{2.32}$$

and the KdV equation for the beam amplitude,

$$2c\frac{\partial a_0}{\partial \zeta} + 6u_0 a_0 \frac{\partial a_0}{\partial \xi} - \frac{1}{4}\frac{\partial^3 a_0}{\partial \xi^3} = 0\,. \tag{2.33}$$

Eq. (2.33) has a sech^2-type solution describing a soliton, so that the dark soliton in this small-amplitude limit can be obtained as an asymptotic expansion, Eqs. (2.29) and (2.30), calculated with the help of the KdV soliton solution [e.g., Kivshar (1993b)].

For the NLS Eq. (2.6) the established link between the small-amplitude dark solitons and solitons of the KdV Eq. (2.33) is not a remarkable fact because both these models are exactly integrable, and we can obtain, in principle, analytical results for them separately with the same completeness. However, the most important result is that such a property is also valid for the generalized NLS Eq. (2.22). For example, for the generalized NLS equation we can derive [e.g., Kivshar et al. (1993)] the following KdV equation:

$$2c\frac{\partial a_0}{\partial \zeta} - 2u_0[3g'(u_0^2) + u_0^2 g''(u_0^2)]a_0\frac{\partial a_0}{\partial \xi} - \frac{1}{4}\frac{\partial^3 a_0}{\partial \xi^3} = 0\,, \tag{2.34}$$

where

$$c^2 = u_0^2 g'(u_0^2)$$

is the limit speed of linear waves in the NLS model of generalized nonlinearity. Additionally, the approach based on the small-amplitude approximation of dark solitons is very useful to analyse the influence of different perturbations on the dark-soliton dynamics using the known analytical results for the KdV solitons [see, e.g., Kivshar and Afanasjev (1991a) and Kivshar (1993b)]. This approach was also extended to the case of the anomalous dispersion in the perturbed NLS equation (Frantzeskakis, 1996).

2.6. Integrals of motion

A difference between bright and dark solitons can be also seen in the definition of the integrals of motion of the NLS model for vanishing (bright) and non-vanishing (dark) boundary conditions. Being mostly interested in the case of spatial solitons, we consider the cubic NLS equation in the form of Eq. (2.6) with the self-defocusing (negative) nonlinearity.

Eq. (2.6) can be treated as the Euler equation which follows from the Lagrangian with the density,

$$\mathscr{L} = \frac{\mathrm{i}}{2}\left(u^*\frac{\partial u}{\partial z} - \frac{\partial u^*}{\partial z}u\right) - \frac{1}{2}\left|\frac{\partial u}{\partial x}\right|^2 - \frac{1}{2}|u|^4\,, \tag{2.35}$$

corresponding to the system Hamiltonian,

$$H_{\rm tot} = \frac{1}{2}\int_{-\infty}^{+\infty}\left\{\left|\frac{\partial u}{\partial x}\right|^2 + |u|^4\right\} {\rm d}x\,. \tag{2.36}$$

Because the cubic NLS Eq. (2.6) is exactly integrable, it possesses *an infinite number* of integrals of motion. However, our primary interest is in the nonintegrable generalized NLS models, so that we are interested only in the fundamental invariants which exist also in a general case and have a clear physical meaning. Because the system described by the NLS equation is conservative, the total energy defined by Eq. (2.36) is conserved. Additionally, we consider also the field momentum,

$$M_{\rm tot} = \frac{\rm i}{2}\int_{-\infty}^{+\infty}\left(u\frac{\partial u^*}{\partial x} - u^*\frac{\partial u}{\partial x}\right){\rm d}x\,, \tag{2.37}$$

and the power,

$$P_{\rm tot} = \int_{-\infty}^{+\infty}|u|^2\,{\rm d}x\,. \tag{2.38}$$

Invariants, Eqs. (2.36), (2.37) and (2.38), can be formally introduced for any types of the boundary conditions to Eq. (2.6). However, it is easy to see that in the case of nonzero boundary conditions, the values defined by Eqs. (2.36), (2.37) and (2.38) are *divergent*. Indeed, let us calculate these values for the exact cw solution, Eq. (2.12), and obtain,

$$P_{\rm cw} = u_0^2 L\,, \qquad M_{\rm cw} = k u_0^2 L = kP\,, \qquad H_{\rm cw} = \frac{P^2}{2L} + \frac{M^2}{2P}\,, \tag{2.39}$$

where L defines a spatial extension of the cw beam. It is clear that these values are not finite provided $L \to \infty$. Obviously, the similar problem appears if we use the invariants, Eqs. (2.36), (2.37) and (2.38), for the case of dark soliton which corresponds to the same nonvanishing boundary conditions. However, for a dark soliton itself it is possible to introduce finite (or renormalized) expressions for these invariants.

We consider the most general form of a dark soliton propagating on the cw background wave, Eq. (2.12). The solution of Eq. (2.6) describing a dark soliton with the velocity v moving on a running background with the propagation constant β can be written in the following form

$$u(x,z) = u_0\{B\tanh[u_0 B(x - vz)] + {\rm i}A\}\,{\rm e}^{{\rm i}kx - {\rm i}\beta z + {\rm i}\theta_0}\,, \tag{2.40}$$

where, as above, the parameter $\beta = \frac{1}{2}k^2 + u_0^2$ characterizes the dispersion relation for the background wave, $\theta(0)$ is a constant phase, and the soliton and background parameters, A, B, and v are connected by the relations,

$$u_0 A = v - k\,, \qquad A^2 + B^2 = 1\,. \tag{2.41}$$

In such a form, the dark soliton solution, Eq. (2.40), is characterized by three independent parameters, two of them, u_0 and k, describe the amplitude and wave number of the cw background, while only one, e.g., A, characterizes the dark soliton itself. The asymptotics of the solution, Eq. (2.40), coincide with those of the cw solution, Eq. (2.12). However, the presence of a dark soliton on the background manifests itself in different phases at $x \to \pm\infty$, i.e., the plane wave

soliton is shifted in phase, and the total phase shift across the dark soliton is

$$\Delta\theta = 2\left[\tan^{-1}\left(\frac{A}{B}\right) - \frac{\pi}{2}\right] = -2\tan^{-1}\left(\frac{B}{A}\right). \tag{2.42}$$

Let us define the renormalized integrals of motion which characterize the dark soliton itself. It is clear that the integrals of motion, Eqs. (2.36), (2.37) and (2.38), describe a complex object 'background + dark soliton', and we should modify the integrals to remove the corresponding contributions of the cw background. After such a *renormalization procedure* the integrals of motion calculated for the solution, Eq. (2.40), become finite. We will present this renormalization for the simpler case $k = 0$, i.e. when the cw background is at rest.

It is clear that the power, Eq. (2.38), should be renormalized calculating a difference between the total power, Eq. (2.38), and the corresponding value, Eq. (2.39), contributed from the background

$$P_{\mathrm{r}} = \int_{-\infty}^{\infty} \mathrm{d}x\,(u_0^2 - |u|^2)\,. \tag{2.43}$$

Calculating P_r for the solution, Eq. (2.40), we find $P_r = 2u_0B$. This value is often called *complimentary power* of a dark soliton.

The similar procedure can be used to renormalize the system Hamiltonian,

$$H_r = \frac{1}{2}\int_{-\infty}^{\infty} \mathrm{d}x\left\{\left|\frac{\partial u}{\partial x}\right|^2 + (|u|^2 - u_0^2)^2\right\}, \tag{2.44}$$

and for the dark soliton solution, Eq. (2.40), it takes the form

$$H_r = \tfrac{4}{3}(c^2 - v^2)^{3/2}\,. \tag{2.45}$$

Renormalization of the field momentum is a bit tricky. From the integral of motion, Eq. (2.37), we should take away a contribution of the background which this time is given by *the phase difference* produced by the presence of the dark soliton, Eq. (2.42). Because the momentum of the cw background has the form $M = ku_0^2L$ [see Eq. (2.39)], this phase difference gives a nonzero contribution even at $k = 0$. Indeed, this contribution is calculated as $u_0^2\int k(x)\,\mathrm{d}x = u_0^2\Delta\theta$, where $k(x)$ describes a local change of the background wavenumber. As a result, the renormalized momentum of a dark soliton is defined as

$$M_{\mathrm{r}} = \frac{\mathrm{i}}{2}\int_{-\infty}^{\infty} \mathrm{d}x\left(u\frac{\partial u^*}{\partial x} - u^*\frac{\partial u}{\partial x}\right) - u_0^2\Delta\theta\,, \tag{2.46}$$

where $\Delta\theta$ is given by Eq. (2.42). Substituting the solution, Eq. (2.40), at $k = 0$ into Eq. (2.46), we find

$$M_{\mathrm{r}} = -2v\sqrt{c^2 - v^2} + 2c^2\tan^{-1}\left(\frac{\sqrt{c^2 - v^2}}{v}\right), \tag{2.47}$$

where c^2 is defined in Eq. (2.15).

Differentiating the formulas, Eqs. (2.47) and (2.45), over the soliton velocity v, we recover the simple relation

$$\frac{\partial H_{\mathrm{r}}}{\partial M_{\mathrm{r}}} = v\,, \tag{2.48}$$

which indicates that the renormalized integrals of motion satisfy the standard expression of classical mechanics so that a dark soliton, similar to a bright soliton, can be regarded as an effective particle.

For the case of the generalized NLS Eq. (2.22), we can also introduce the renormalized invariants which are free of any divergence and characterize the dark soliton itself. In a similar way, we define the complementary power P_{r},

$$P_{\mathrm{r}} = \int_{-\infty}^{+\infty} (u_0^2 - |u|^2)\,\mathrm{d}x \tag{2.49}$$

the renormalized field momentum,

$$M_{\mathrm{r}} = \frac{\mathrm{i}}{2}\int_{-\infty}^{+\infty}\left(u\frac{\partial u^*}{\partial x} - u^*\frac{\partial u}{\partial x}\right)\left(1 - \frac{u_0^2}{|u|^2}\right)\mathrm{d}x\,, \tag{2.50}$$

and the renormalized Hamiltonian,

$$H_{\mathrm{r}} = \int_{-\infty}^{+\infty}\left\{\frac{1}{2}\left|\frac{\partial u}{\partial x}\right|^2 + \int_{u_0^2}^{|u|^2}[g(u_0^2) - g(I)]\,\mathrm{d}I\right\}\mathrm{d}x\,. \tag{2.51}$$

All these values remain finite for any type of the nonlinear function $g(I)$ in the generalized NLS Eq. (2.22).

2.7. Physical interpretation of dark solitons

As has been mentioned above, the Fourier transform method is a useful tool for linear systems where it employs the familiar superposition principle. This method can be also applied to analyse linear wave propagation in *inhomogeneous media* when, additionally to the periodic modes with the continuous spectrum, there appear spatially localized (or guided) modes existing due to spatial variations of the properties of the linear medium. This localized or guided modes are possible however only for special discrete eigenvalues. Therefore, a complete set of *linear eigenstates* which can be obtained by the Fourier method includes both *discrete* and *continuous* modes.

For nonlinear systems the Fourier method cannot be used and the superposition principle is not valid. However, as was discussed in Section 2.5.1, the inverse scattering transform for a certain class of nonlinear equations provides a qualitative similarity between the modes of *linear inhomogeneous* systems and those of *nonlinear homogeneous systems* in the sense that both types of localized modes, i.e. guided waves, for the former case, and solitary waves, for the latter case, correspond to a certain set of discrete eigenvalues.

We may wonder if this kind of similarity can be formulated in a direct way, when a nonlinear equation does not allow the application of the inverse scattering transform. As was advanced by Snyder and coauthors (Snyder et al., 1993, 1995), such a similarity does exist for a rather wide class

of stationary (and, sometimes, periodic) solutions of the Maxwell's equations and it provides a complete analogy between guided waves as modal solutions of the waveguide optics, from one side, and solitary waves of generalized nonlinearities, from the other side.

To demonstrate this property, we follow the papers by Snyder et al. (1991, 1993, 1995) and consider the stationary (1 + 1)-dimensional evolution of the TE field $E(x, z) = \mathscr{E}(x)\mathrm{e}^{-\mathrm{i}\beta z}$ in a homogeneous medium with the intensity-dependent refractive index n. Then, the envelope function $\mathscr{E}(x)$ is a solution of the scalar wave equation,

$$\left\{\frac{\mathrm{d}^2}{\mathrm{d}x^2} + k_0^2 n^2(|\mathscr{E}|^2) - \beta^2\right\}\mathscr{E}(x) = 0\,, \tag{2.52}$$

which is more general than the generalized NLS Eq. (2.22) derived from Eq. (2.52) in the paraxial approximation.

Now, as was pointed out by Snyder et al. (1991), a spatially localized solitary wave solution $\mathscr{E}(x)$ of Eq. (2.52) can be treated as a guided mode of the effective linear waveguide that it induces. Indeed, let us define the *linear* waveguide using the so-called self-consistency relation (Snyder et al., 1991, 1993)

$$n_{\mathrm{lin}}^2(x) \equiv n^2(|\mathscr{E}(x)|^2)\,, \tag{2.53}$$

provided the solution $\mathscr{E}(x)$ of the nonlinear Eq. (2.52) is known. Then, it immediately follows that $\mathscr{E}(x)$ is also a solution of the *linear* eigenvalue problem, Eq. (2.52), with the spatial-dependent refractive index defined by Eq. (2.53). This simple notion allows to borrow from the literature on linear optical waveguides [e.g., Snyder and Love (1973)] to find analytical solutions and the nonlinear media corresponding to them. For example, a slab waveguide is found to correspond to the so-called threshold nonlinearity [e.g., Snyder et al. (1991)]. Additionally, the interpretation of solitary waves as modes of the induced waveguides provides a simple physics which, for example, can explain why some kind of solitary waves are possible (Snyder et al., 1995).

As an example, we consider a linear waveguide with a refractive index profile of the form

$$n_{\mathrm{lin}}^2(x) = n_\infty^2 + (n_0^2 - n_\infty^2)\,\mathrm{sech}^2(x/a)\,, \tag{2.54}$$

where a is the characteristic profile half-width. All modes of this waveguide can be expressed with the help of Legendre functions [e.g., Snyder and Love (1973)]. In particular, the fundamental bound mode is given by the familiar expressions

$$\mathscr{E}(x) = \mathscr{E}_0\,\mathrm{sech}^s(x/a)\,, \tag{2.55}$$

with the propagation constant $\beta^2 = (k_0 n_\infty)^2 + (s/a)^2$. Self-consistency condition, Eq. (2.53), allows to conclude that the mode, Eq. (2.54), corresponds to a bright soliton of the Kerr medium provided $s = 1$ at a fixed value of the waveguide parameter,

$$V^2 \equiv (k_0 a)^2(n_0^2 - n_\infty^2) = 2\,.$$

Thus, a bright solitary wave can be treated as the bound mode of the linear waveguide it induces. As for dark solitons, it is clear from their unbounded fields that, if a dark soliton is a mode of its induced linear waveguide, than it must be a radiation mode, that is, a mode of the continuous spectrum. Dark solitary waves constructed from modes of linear waves were discussed by

Snyder et al. (1993), who provided a simple physical picture of dark solitons through reflectionless plane-wave scattering from a linear dielectric waveguide.

For the sech-type waveguide, Eq. (2.54), the fields of radiation modes consist of an incident plane wave and its reflections, except for integer values of the parameter s introduced as $V^2 = s(s+1)$, where V is the waveguide parameter defined above. For these particular values of s, *there is no reflection wave*. For example, for $s = 1$ and the waveguide parameter $V = \sqrt{2}$, the radiation reflectionless mode of the sech-type waveguide, Eq. (2.54), has the form of a dark soliton of the cubic (or Kerr) medium,

$$\mathscr{E}(x) = \mathscr{E}_0 \frac{e^{iqx}}{(1 - iQ)} [\tanh(x/a) - iQ] , \tag{2.56}$$

where $Q = aq$, and q is a real continuous variable ($0 < q < k_0 n_\infty$) related to the direction of the incident plane wave, and it also defines the propagation constant, $\beta^2 = (k_0 n_\infty)^2 - q^2$. Thus, the elementary physics of reflectionless plane-wave scattering from a linear waveguide allows a deeper insight into the theory of dark solitons.

3. Perturbation theory and applications

3.1. Equations for soliton parameters

3.1.1. Direct method

Renormalized integrals of motion for dark solitons allows us to apply a straightforward technique for describing the soliton perturbation-induced dynamics. The approach based on the invariants is the simplest one, and it can be regarded as a direct method whereas more involved technique is based on the inverse scattering transform [e.g., Kivshar and Malomed (1989)].

First, we consider the case of *a constant background* when a perturbation does not change the parameters of the cw solution. We consider the perturbed NLS equation,

$$i\frac{\partial u}{\partial z} + \frac{1}{2}\frac{\partial^2 u}{\partial x^2} - |u|^2 u = \varepsilon P(u) , \tag{3.1}$$

where the term $\varepsilon P(u)$ in the right-hand side stands for a small perturbation. Because the perturbation is assumed do not change the cw background, it should vanish as $|x| \to \infty$. To find the equation for the evolution of the soliton parameters, first we introduce the new function $v(x, z)$ to make the renormalization procedure more straightforward,

$$u(x, z) = u_0 v(x, z)\, e^{-iu_0^2 z} , \tag{3.2}$$

and obtain the equation for v,

$$i\frac{\partial v}{\partial \zeta} + \frac{1}{2}\frac{\partial^2 v}{\partial \xi^2} + (1 - |v|^2)v = \varepsilon \tilde{P}(v) , \tag{3.3}$$

where $\varepsilon\tilde{P}(v)$ is a renormalized perturbation $\varepsilon P(u)$. Considering only the case of a nonpropagating background wave, we may now analyze how the parameters of the dark soliton solution be

changed due to the perturbation from the right-hand side of Eq. (3.3). At $\varepsilon = 0$, the dark soliton can be written in the form,

$$v(\zeta, \xi) = \cos\phi \tan\Theta + \mathrm{i}\sin\phi\,, \qquad \Theta = \eta(\xi - \Omega\zeta)\,, \tag{3.4}$$

where $\zeta = u_0^2 z$, $\xi = u_0 x$, $\eta = \cos\phi$, and $\Omega = \sin\phi$. This solution is characterized by the soliton phase angle ϕ ($|\phi| < \pi/2$) which describes the 'darkness' of the soliton through the simple relation

$$|u|^2 = 1 - \frac{\cos^2\phi}{\cosh^2\Theta}\,. \tag{3.5}$$

To treat analytically the influence of a small perturbation $\varepsilon\tilde{P}(v)$ on the parameters of the dark soliton, Eq. (3.4), we use the so-called *adiabatic approximation* of the perturbation theory for solitons [see, e.g., Kivshar and Malomed (1989)]. According to this approach, the parameters of the dark soliton, Eq. (3.4), are considered as slowly varying in z but with the functional shape which remains unchanged, i.e., it is assumed to be described by Eq. (3.4), where we should modify Z as the following:

$$\Theta = \cos\phi(\zeta)\left[\xi - \int \mathrm{d}\zeta' \sin\phi(\zeta')\right]. \tag{3.6}$$

To derive the equation for the perturbation-induced evolution of the soliton phase $\phi(\zeta)$, we start from the renormalized Hamiltonian of the unperturbed system,

$$H_\mathrm{r} = \frac{1}{2}\int_{-\infty}^{\infty} \mathrm{d}\xi \left\{ \left|\frac{\partial v}{\partial \xi}\right|^2 + (|v|^2 - 1)^2 \right\},$$

which for the soliton solution, Eq. (3.4), takes the value $H_\mathrm{r} = \frac{4}{3}\cos^3\phi$ [cf. Eq. (2.45)]. Calculating the derivative of H_r over ζ and using Eq. (3.3), we find the result (Kivshar and Yang, 1994a)

$$\frac{\mathrm{d}\phi}{\mathrm{d}\zeta} = \frac{\varepsilon}{8\cos^2\phi\sin\phi}\, Re\left\{ \int_{-\infty}^{+\infty} \mathrm{d}\xi\, \tilde{P}(v)\frac{\partial v^*}{\partial \zeta} \right\}, \tag{3.7}$$

where the functions in the right-hand side of Eq. (3.7) should be also calculated in the adiabatic approximation using the solution given by Eq. (3.4). The similar equation can be obtained by the equivalent approach based on the Lagrangian technique, as was shown by Kivshar and Królikowski (1995a).

If the perturbation $\varepsilon\tilde{P}(v)$ in Eq. (3.7) does not vanish at $|x| \to \infty$, *it will certainly affect the background wave*. This is the standard case of dissipative perturbations which produce a slow decay of the background amplitude (Kivshar and Yang, 1994a; Yang et al., 1994). Taking the limit $|x| \to \infty$ and interesting in the evolution of the nonpropagating background $u_\mathrm{b}(z)$ (i.e., that which does not depend on x), we obtain the equation for the background amplitude u_b

$$\mathrm{i}\frac{\mathrm{d}u_\mathrm{b}}{\mathrm{d}z} - |u_\mathrm{b}|^2 u_\mathrm{b} = \varepsilon P(u_\mathrm{b})\,. \tag{3.8}$$

Eq. (3.8) allows to find the law describing the background evolution in the presence of perturbations. Generally, a solution of Eq. (3.8), $u_\mathrm{b}(z)$, may be presented in the form, $u_\mathrm{b}(z) = u_0(z)\exp[\mathrm{i}\theta(z)]$, where the function $u_0(z)$ and $\theta(z)$ characterize the change of the background amplitude and phase,

respectively. To describe now the evolution of a dark soliton on this varying background we should *remove* the background by the transformation [cf. Eq. (3.2)]

$$u(z, x) = u_0(z)\, e^{i\theta(z)} v(x, z)\,, \tag{3.9}$$

and to find an effective nonlinear equation for the function $v(x, z)$. In many cases (e.g., see below) such an equation can be transformed into a perturbed NLS Eq. (3.3) after a change of the variables, so that this will alow to apply immediately the result given by Eq. (3.7).

3.1.2. Method based on the inverse scattering technique

To derive the adiabatic equation for the soliton parameters, we can employ the perturbation theory based on the inverse scattering transform, similar to that developed for bright solitary waves and also for some other nonlinear models [e.g., Kivshar and Malomed (1989)]. The first effort to derive the adiabatic equations for the parameters of a dark soliton by means of the inverse scattering transform was attempted by Konotop and Vekslerchik (1994). However, these authors based their theory of the assumption that the phase of a dark soliton is fixed by the boundary condition and it does not change. This assumption led to an artificial singularity and required to introduce one more parameter for describing the soliton evolution. As is clear from the results presented above (see also Section 4.1), the local phase of the soliton is not a conserved quantity and, therefore, the assumption made by Konotop and Vekslerchik (1994) is, generally speaking, wrong. That is why the equations derived by those authors have narrow applicability limits and can be used for very special classes of perturbations only.

A correct approach should take into account the evolution of the background which supports a dark soliton, similar to the invariant-based method discussed above. Here we give a sketch of another way to derive the equations for the soliton parameters.

We consider the perturbed NLS equation in the following form:

$$i\frac{\partial u}{\partial z} + \frac{1}{2}\frac{\partial^2 u}{\partial x^2} + (u_0^2 - |u|^2)u = \varepsilon P(u)\,, \tag{3.10}$$

where we keep explicitly the background intensity u_0^2 because, in general, it may vary under the action of perturbations. We assume the validity of the adiabatic approximation when the structure of the dark soliton solution remains unchanged but its parameters become dependent on the evolution variable z. This means that the main relation between the soliton parameters, $\lambda_n^2 + w_n^2 = u_0^2$, still remains valid for z, even when the background varies. Differentiating this relation, we come to the equation

$$\frac{d\lambda_n}{dt} = -\frac{w_n}{\lambda_n}\frac{dw_n}{dt} + \frac{u_0}{\lambda_n}\frac{du_0}{dt}\,, \tag{3.11}$$

which defines the evolution of the soliton velocity. However, this equation should be completed by two others. First, the evolution of the spectral parameter can be determined by the technique of the inverse scattering similar to that developed by Konotop and Vekslerchik (1994),

$$\frac{dw_n}{dt} = \frac{i\varepsilon}{2a'(\lambda_n)b_n}\int_{-\infty}^{+\infty}\{P(u)\Psi_2^2(x, \lambda; z) - P^*(u)\Psi_1^2(x, \lambda; z)\}\, dx\,, \tag{3.12}$$

where $\Psi_{1,2}(x, \lambda; z)$ are the so-called Jost functions introduced in Section 2.5.1. As for the background, its evolution cannot be self-consistently determined by the soliton parameters and, to derive the corresponding equations, we should analyze the perturbed NLS equation in the asymptotic limit $|x| \to \infty$. Taking this limit in the NLS Eq. (3.10), we obtain two equations for the background intensity u_0 and phase θ,

$$\frac{\mathrm{d}u_0}{\mathrm{d}z} = R_1 \sin\theta + R_2 \cos\theta\,, \tag{3.13}$$

$$\frac{\mathrm{d}\theta}{\mathrm{d}z} = \frac{1}{u_0}(R_1 \cos\theta - R_2 \sin\theta)\,, \tag{3.14}$$

where $R_1 \equiv \mathrm{Re}\{\varepsilon P(u_0 \mathrm{e}^{\mathrm{i}\theta})\}$ and $R_2 \equiv \mathrm{In}\{\varepsilon P(u_0 \mathrm{e}^{\mathrm{i}\theta})\}$. Eqs. (3.13) and (3.14) are equivalent to Eq. (3.8) obtained in Section 3.1.1 and, together with Eqs. (3.11) and (3.12) present a full system of equations for the background and soliton parameters.

A development of a complete perturbation theory for dark solitons based on the inverse scattering transform, which will take into account not only the evolution of the soliton parameters but also radiation generated under the action of an external perturbation [see discussions of the importance of radiative effects in Burtsev and Camassa (1997)] still remains an open problem.

3.2. Physical applications

In this section we apply the adiabatic equations derived above to analyze several particular cases which correspond to physically important perturbations. From these examples it follows how to take properly into account the effect of the varying background on the dynamics of dark solitons.

3.2.1. Effect of gain and loss

As is well-known, in the problem of the propagation of spatial solitons nonlinearity is usually associated with two-photon absorption which, in fact, appears as a by-product of enhanced nonlinearity [see, e.g., Silberberg (1990a) and references therein]. In the presence of either two-photon absorption (TPA) or nonlinear gain, the stationary self-localized states of a light wave are no longer possible but in the case of a combined effect, when two-photon absorption is compensated by a gain, the stationary solution in the form of a fundamental dark soliton can exist. To describe the effect of TPA on dark solitons, we consider the NLS equation modified as follows [see, e.g., Silberberg (1990a) and Yang et al. (1994)],

$$\mathrm{i}\frac{\partial u}{\partial z} + \frac{1}{2}\frac{\partial^2 u}{\partial x^2} - |u|^2 u = -\mathrm{i}K|u|^2 u\,, \tag{3.15}$$

where K is the normalized TPA coefficient defined as $K = \beta/2k_0 n_2$, where k_0 is the free-space wave vector, β and n_2 are the intensity-dependent absorption and refractive index coefficients, respectively.

As is well known, in the absence of TPA (i.e., at $K = 0$), Eq. (3.15) describes the case of a defocusing Kerr nonlinearity and the background wave $u = u_0 \exp(-\mathrm{i}u_0^2 z)$ is modulationally stable. Nonlinear absorption, even small, leads to an attenuation of the cw background so that its

amplitude and phase become slowly dependent on $Ku_0^2(0)z$ according to

$$u_0(z) = \frac{u_0(0)}{\sqrt{1 + 2Ku_0^2(0)z}}, \tag{3.16}$$

$$\theta(z) = \int_0^z u_0^2(z')\,\mathrm{d}z' = \frac{1}{2K}\ln[1 + 2Ku_0^2(0)z]\,. \tag{3.17}$$

To separate the evolution of the background and dark soliton, we apply the following transformation:

$$u(z, x) = u_0(z)\,\mathrm{e}^{\mathrm{i}\theta(z)}v(z, x)\,, \tag{3.18}$$

where $u_0(z)$ and $\theta(z)$ change according to Eqs. (3.16) and (3.17). Then, the function v satisfies the equation

$$\mathrm{i}\frac{\partial v}{\partial \zeta} + \frac{1}{2}\frac{\partial^2 v}{\partial \xi^2} - (|v|^2 - 1)v = -\mathrm{i}K(|v|^2 - 1)v\,, \tag{3.19}$$

where ζ and ξ are new coordinates which are connected with z and x by the following differential relations, $\mathrm{d}\zeta = u_0^2(z)\,\mathrm{d}z$ and $\mathrm{d}\xi = u_0(z)\,\mathrm{d}x$. After such a transformation, the resulting equation has *a vanishing perturbation* and it can be treated by the perturbation theory for solitons. The equation for the soliton phase angle ϕ in the primary variables takes the form

$$\frac{\mathrm{d}\phi}{\mathrm{d}z} = \frac{1}{3}Ku_0^2(z)\sin(2\phi)\,, \tag{3.20}$$

where the background amplitude $u_0(z)$ evolves according to Eq. (3.16). Eq. (3.20) may be easily integrated to give the result

$$\phi(z) = \tan^{-1}\{\tan\phi(0)[1 + 2Ku_0^2(0)z]^{1/3}\}\,. \tag{3.21}$$

One of the main characteristics of the dark-soliton switching devices is the so-called soliton steering angle (Luther-Davies and Yang, 1992b). It is easy to see that the total shift of the dark soliton along the x-axis is given by the relation $\int^z \mathrm{d}z'\,u_0(z')\sin\phi(z')$, so that the steering angle X may be defined through the local transverse velocity,

$$W(z) = \tan\chi = u_0(z)\sin\phi(z)\,. \tag{3.22}$$

The important conclusion based on Eq. (3.22) is the following: When the dark soliton propagates in the presence of TPA on a decaying background $u_0(z)$, the function $\sin\phi(z)$ grows slowly keeping, at least for small $\phi(0)$, the product of Eq. (3.22) almost constant (Yang et al., 1994). This simply means that the steering angles for switching devices based on dark soliton propagation are almost preserved in a Kerr nonlinear medium in the presence of TPA. From the physical point of view, this important property simply follows from the nature of nonlinear absorption: the background intensity decays faster than the central minimum in the soliton forcing the soliton.

Fig. 4a shows the evolution of the background $u_0(z)$, the soliton phase angle $\sin\phi(z)$, and the transverse soliton velocity $W(z) = u_0(z)\sin\phi(z)$. The analytical results (solid curves) based on Eqs. (3.16) and (3.21) are in perfect agreement with the results of the numerical simulations (opened diamond marks) and, as may be seen, the steering angle is almost preserved provided $\phi(0)$ is small.

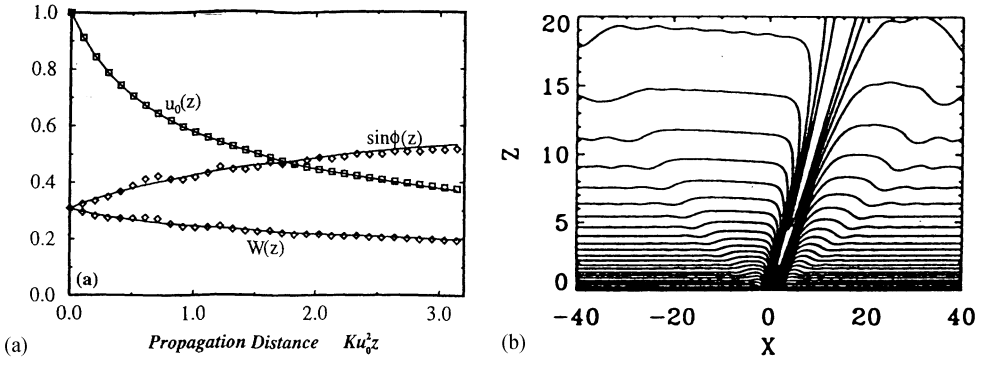

Fig. 4. (a) Evolution of the background amplitude, $u_0(z)$, the function sin $\phi(z)$, and the transverse velocity of the dark soliton, $W(z)$ in a Kerr medium with TPA at $K = 0.05$. The solid curves are from Eqs. (3.20) and (3.21), the diamond marks are obtained from a numerical simulation of Eq. (3.15) for $\phi(0) = 0.1\pi$. (b) Contour plots corresponding to the evolution presented in (a) (Kivshar and Yang, 1994a).

Small deviations of the numerical data from the adiabatic relationship are caused by transition radiation which slightly changes the intensity of the background (see Fig. 4b).

It is important to compare the result of Eq. (3.22) with the corresponding result of linear absorption described by the contribution $\varepsilon P(u) = -\mathrm{i}\gamma u$ on the right-hand side of Eq. (3.15) instead of the term $-\mathrm{i}K|u|^2u$. As follows from the corresponding perturbed NLS equation, in this case the background wave decays exponentially

$$u_0(z) = u_0(0)\,\mathrm{e}^{-\gamma z}\,, \qquad \theta(z) = \int_0^z u_0^2(z')\,\mathrm{d}z' = \frac{u_0^2(0)}{2\gamma}\,(1 - \mathrm{e}^{-2\gamma z})\,. \tag{3.23}$$

As in the case of the TPA-induced dynamics, first of all we remove the background evolution by the transformation, Eq. (3.18), where this time the functions $u_0(z)$ and $\theta(z)$ are defined by Eq. (3.23). The important result of such a transformation is that the effective Eq. (3.19) for the function $v(\zeta, \xi)$ is the NLS equation *without* any perturbation. This immediately implies that the transformation, Eq. (3.18), does allow to exclude the effect of the linear absorption considering the pulse evolution in the new reference frame, so that the soliton phase angle does not change, $\mathrm{d}\phi/\mathrm{d}z = 0$. The similar conclusion follows from the analysis presented by Lisak et al. (1991); see also Giannini and Joseph (1990), who however used a different method which does not allow a generalization to the case of nonlinear loss.

3.2.2. Stabilization of dark solitons

Linear or/and nonlinear absorption affects the background but it can be compensated by a gain. In the presence of both linear gain and TPA, the background can be stabilized but the dark soliton is still unstable (Kivshar and Yang, 1994a). This result of the perturbation theory is in agreement with the existence of the exact solution of the complex Ginzburg–Landau equation which is known to be unstable (Sakaguchi, 1991; Y. Chen, 1992b). However, as was recently pointed out by Ikeda et al. (1995) [see also Ikeda et al. (1997)], a dark soliton can be stabilized by *a nonlinear gain.*

Indeed, as we demonstrated above, the effect of a linear gain is trivial, so that it does not allow to compensate for TPA. If, however, we assume the gain to be strong enough to include some higher-order terms, i.e.,

$$\varepsilon P(u) = \delta u + \gamma_1 |u|^2 u + \gamma_2 |u|^4 u \,,$$

the effective equation for the dark-soliton angle becomes (Ikeda et al., 1995, 1997)

$$\frac{\mathrm{d}\phi}{\mathrm{d}z} = \left\{ \frac{\gamma_1}{3} u_0^2(z) - \frac{2\gamma_2}{15} u_0^4(z) \left[2\cos^2 \phi - 5 \right] \right\} \sin(2\phi) \,, \tag{3.24}$$

where $u_0^2(z)$ satisfies the equation for the background field,

$$\frac{\mathrm{d}u_0}{\mathrm{d}z} = -(\delta u_0 + \gamma_1 u_0^2 + \gamma_2 u_0^4)\, u_0 \,,$$

which shows that u_0 is stably stationary at $u_0 = 1$ provided $\delta + \gamma_1 + \gamma_2 = 0$ and $\gamma_1 + 2\gamma_2 > 0$. This condition can be made consistent with the stability of the dark soliton defined by Eq. (3.24), allowing to control dark solitons by varying nonlinear gain (Ikeda et al., 1995, 1997). This result was verified by Ikeda et al. (1995, 1997) by means of direct numerical simulations of the perturbed NLS equation.

Maruta and Kodama (1995) suggested a completely different idea of the dark-soliton stabilization by means of a synchronized phase modulation. In their approach, the effective perturbation of the NLS equation appears in the form $\varepsilon P(u) = \mu \cos(\omega x) u$, where μ is the phase-modulation coefficient, and ω is the modulation frequency synchronized with the initial pulse separation of a sequence of dark solitons. As was shown by Maruta and Kodama (1995), this perturbation leads to a nontrivial variation of the soliton phase which can display a stable dynamics near the fixed point $\phi = 0$ (corresponding to a black soliton with the zero minimum amplitude at its center) due to the effect of phase-locking between the soliton and periodically varying perturbation.

An interesting method to compensate for the amplitude variation of a dark soliton in a lossy medium was suggested by Kim et al. (1996). They demonstrated that dark solitons are stabilized when phase-sensitive amplification and spectral filtering are used together. Indeed, in a periodically amplified system, the spectral filtering are used together. Indeed, in a periodically amplified system, the spectral filtering was shown to inhibit the sideband instabilities typical for both cw waves and solitons, including dark solitons as earlier demonstrated by Allen et al. (1994, 1995). From the other side, a phase-sensitive amplification inhibits to the destabilization of the constant-intensity background wave caused by the filtering (Kim et al., 1996).

3.2.3. Raman self-frequency shift

Perturbation theory for dark solitons can be also effectively applied for analyzing the dark solitons in optical fibers. One of the important perturbations acting on dark solitons in fibers appears when the pulse duration in fibers reaches the subpicosecond regime. Then, it becomes necessary to include higher-order dispersion effects that are presented by higher-order derivatives in the effective NLS equation for the wave envelope. Stimulated Raman scattering (SRS) is known to be one of the dominant effects for very short optical pulses. For bright solitons this effect causes the so-called self-frequency shift [Mitschke and Mollenauer (1986), Gordon (1986), see also

Hasegawa and Kodama (1995)], whereas for dark solitons, a self-frequency shift at the initial stage of the pulse evolution (Weiner et al., 1989) leads finally to a decay of dark solitons (Kivshar, 1990a,b; Kivshar and Afanasjev, 1991b; Uzunov and Gerdjikov, 1993; Kivshar and Yang, 1994a).

From the physical point of view, SRS originates from the noninstantaneous, delayed response of the fiber nonlinearity. This effect may be described in the time domain by a response function that has a form of a decaying sinusoidal oscillations (Stolen et al., 1989). The Raman contribution to the nonlinear refractive index may be taken into account in a rather general form,

$$n_2|u|^2 \to n_2\left[(1-\alpha)|u|^2 + \alpha\int_{-\infty}^{t} \mathrm{d}t'\,|u(t')|^2 f(t-t')\right], \tag{3.25}$$

where α is the fraction of the total (low frequency) nonlinearity with a delayed response, and $f(t)$ is the Raman response function [see, e.g., Stolen et al. (1989)]. The Raman response function of fused silica is extremely short, so that Eq. (3.25) may be considered in local approximation expanding the function $|u(t-s)|^2$ in the integrand of Eq. (3.25) (here $s = t - t'$) in the Taylor series around t to obtain a local perturbation to the NLS equation,

$$\varepsilon P(u) = \varepsilon u\frac{\partial}{\partial t}(|u|^2)\,, \tag{3.26}$$

ε being proportional to the Raman gain parameter α. In such a form, the effect of SRS may be analysed as a perturbation to the standard NLS dynamics and for dark solitons it was investigated numerically (Weiner et al., 1989; Kivshar and Afanasjev, 1991b; Zhao and Bourkoff, 1992) and analytically (Kivshar, 1990a; Kivshar and Afanasjev, 1991b). As a matter of fact, the general formula describing the dark-soliton propagation in the presence of SRS was obtained by Uzunov and Gerdjikov (1993), whereas its small-amplitude limit was derived even earlier by Kivshar (1990a) within the asymptotic approach based on the perturbed Korteveg–de Vries equation. In general, the effect is described by the perturbed NLS equation

$$\frac{\partial u}{\partial z} - \frac{1}{2}\frac{\partial^2 u}{\partial t^2} + |u|^2 u = -\tilde{\varepsilon}u\int_{-\infty}^{t} |u(t')|^2 G(t-t')\,\mathrm{d}t'\,. \tag{3.27}$$

To write Eq. (3.27), we assume that the first term of the expansion

$$u(t)\int \mathrm{d}s\, f(s)|u(t-s)|^2 \to |u|^2 u\int_{-\infty}^{+\infty} f(s)\,\mathrm{d}s - u\frac{\partial}{\partial t}(|u|^2)\int_{-\infty}^{+\infty} sf(s)\,\mathrm{d}s\,, \tag{3.28}$$

is already included into the main Kerr-type nonlinearity $|u|^2u$ so that the "renormalized" response function $G(s)$ has the property $\int_{-\infty}^{+\infty} G(s)\,\mathrm{d}s = 0$. If the parameter $\tilde{\varepsilon}\max(G)$ is small, we may treat the right-hand side of Eq. (3.27) as a perturbation. Applying the perturbation theory to the dark soliton, Eq. (3.4)) [with the change $z \to -z$ because of the difference in the signs for Eqs. (2.25) and (3.27)], and changing the order of integration, one may come to the following equation for the soliton phase angle:

$$\frac{\mathrm{d}\phi}{\mathrm{d}z} = \tilde{\varepsilon}u_0\cos\phi\int_{-\infty}^{+\infty} \mathrm{d}s\; G\left(\frac{s}{u_0\cos\phi}\right)F(s)\,, \tag{3.29}$$

where

$$F(s) = \frac{2[s(3 - \tanh^2 s) - 3 \tanh s]}{\sinh^2 s \tanh^2 s}. \tag{3.30}$$

As follows from Eq. (3.30), the local approximation may be used only in the case when the Raman response function is short in comparison with the soliton width $(u_0 \cos \phi)^{-1}$. In this case we may simply expand the function $F(s)$ into the Fourier series as $F(s) \simeq F(0) + sF'(0)$ and obtain the resulting equation in the form of a perturbed NLS equation as an expansion in the inverse width of the soliton $(u_0 \cos \phi)$, this value is assumed to be small in comparison with the inverse characteristic decay T of the response function. The result is (Uzunov and Gerdjikov, 1993; Kivshar and Yang, 1994a)

$$\frac{d\phi}{dz} = \frac{4}{15} \varepsilon u_0^3 \cos^3 \phi , \tag{3.31}$$

where

$$\varepsilon \equiv \tilde{\varepsilon} \int_{-\infty}^{+\infty} yG(y)\, dy . \tag{3.32}$$

The small-amplitude limit of the result, Eq. (3.32), was obtained earlier by Kivshar (1990a) with the help of the KdV soliton approximation.

Fig. 5 shows the evolution of a dark soliton with an initial negative (a) or positive (b) velocity in the presence of the SRS contribution at $\varepsilon = 0.1$. Comparison of the numerical simulation results with Eq. (3.31) is presented in Fig. 5c as the soliton phase angle given by the function $\sin \phi$ vs the propagation distance at two different initial values, $\phi(0) = -0.2\pi$ and $\phi(0) = +0.2\pi$. As may be seen from those figures, Eq. (3.31) describes rather well the soliton dynamics which, as a matter of

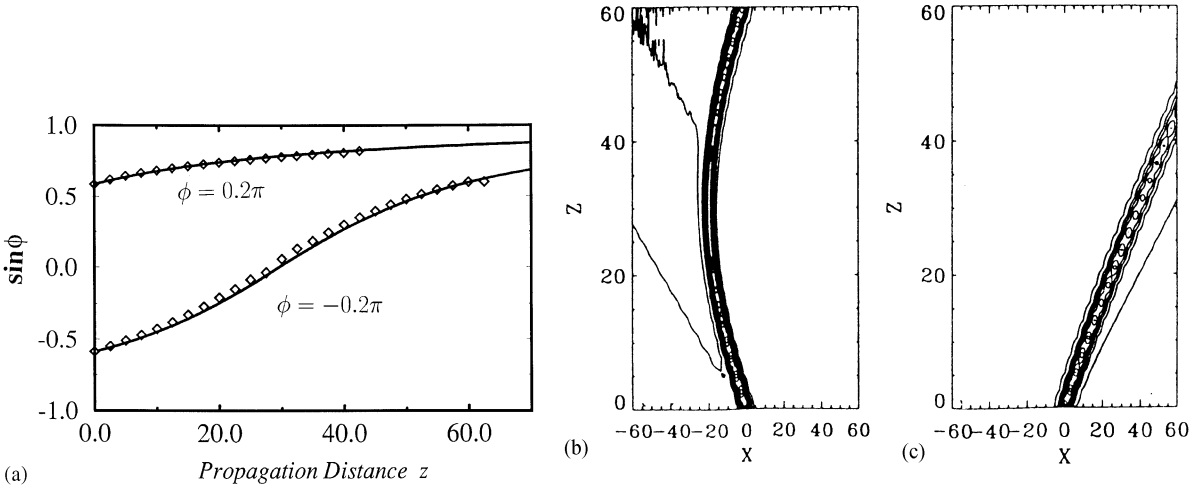

Fig. 5. (a) Change of the phase angle of a dark soliton under the action of the Raman self-scattering effect for $\varepsilon = 0.1$, $\phi = -0.2\pi$ and $\phi = 0.2\pi$. (b), (c) Contour plots for the same initial data, $\phi = -0.2\pi$ and $\phi = 0.2\pi$, respectively (Kivshar and Yang, 1994a).

fact, corresponds to transformation of a dark soliton with arbitrary parameters into a small-amplitude soliton due to the continuous SRS-induced frequency and position shift.

3.3. Dark-soliton jitter

For long-distance propagation of temporal bright solitons, losses should be compensated for by a periodic amplification. As was firstly predicted by Gordon and Haus (1986), an undesirable effect of periodic amplification will cause, through amplified spontaneous emission, a random frequency shift of the solitons that in turn results in a temporal jitter at the output of the fiber links. The jitter parameters observed experimentally (Mollenauer et al., 1990) showed excellent agreement with the model of Gordon and Haus (1986).

For bright solitons, the main result of the Gordon–Haus effect can be demonstrated in a few lines. We start from the NLS Eq. (2.1) with $\sigma = -1$ and present its bright soliton solution in the form [cf. Eq. (2.16)]

$$u_s(t, z) = \frac{a}{\cosh \xi} \exp(i\Omega t - iqz), \tag{3.33}$$

where $\xi = a(t - \Omega z)$ and $q = (\Omega^2 - a^2)/2$. As can be seen from Eq. (3.33), the bright soliton has two independent parameters, the soliton amplitude a and frequency shift Ω which are defined, in particular, by two invariants, the power P_{tot} and momentum M_{tot},

$$P_{tot} = \int_{-\infty}^{+\infty} |u|^2 \, dt, \qquad M_{tot} = \frac{i}{2} \int_{-\infty}^{+\infty} \left(u^* \frac{\partial u}{\partial t} - u \frac{\partial u^*}{\partial t} \right),$$

which for the soliton solution, Eq. (3.33), take the values $P_s = 2a$ and $P_s = -2a\Omega$.

Following the main ideology of Gordon and Haus (1986), we consider now the effect of adding small perturbation δu to the soliton field u_s. Such a nonsolitonic field produces a change in the soliton parameter, radiation corrections being of the second order in δu. The frequency fluctuations $\delta\Omega$ can be then found from the energy and momentum conservation (Gordon and Haus, 1986). Let us now consider that the nonsolitonic correction is a noise arising from a broadband amplifier. If the amplifier bandwidth is greater than the spectral width of the solitons, then we may consider that its effective noise contribution is white. To describe such a noise, we take the addendum δu as a stochastic complex filed with the statistical properties $\langle \delta u(t) \rangle = \langle \delta u^*(t) \rangle = 0$ and the only nonzero pair correlator, $\langle \delta u(t) \delta u^*(t') \rangle = D\delta(t - t')$. Parameter D is the mean value of the random fluctuations, and it is proportional to the mean number of photons per mode at the amplifier output (Gordon and Haus, 1986). Averaging directly the calculated value $\delta\Omega$ with the help of this correlator, we find that

$$\langle \delta\Omega^2 \rangle = \frac{D}{2a^2} \int_{-\infty}^{+\infty} \left| i \frac{\partial u}{\partial t} + \Omega u \right|^2 dt. \tag{3.34}$$

Calculating the right-hand side of Eq. (3.34) for the soliton solution, we recover the famous result of Gordon and Haus (1986),

$$\langle \delta\Omega^2 \rangle = \tfrac{1}{3} Da. \tag{3.35}$$

We now consider the case of dark solitons that occur in the normal fiber dispersion regime described by Eq. (2.1) at $\sigma = +1$. We follow the original paper by Kivshar et al. (1994a). To simplify the problem, we first apply the transformation $u = u_0 v(t, z) \exp(\mathrm{i}u_0^2 z)$, so that the function $v(t, z)$ satisfies the NLS equation of the form

$$\mathrm{i}\frac{\partial v}{\partial z} - \frac{1}{2}\frac{\partial^2 v}{\partial t^2} + u_0^2(|v|^2 - 1)v = 0\,, \tag{3.36}$$

which has a dark soliton solution of the form of Eq. (2.18).

To calculate the jitter, we use two invariants, the renormalized Hamiltonian H_r and renormalized momentum M_r defined is Section 2.6. Calculating the values of M_r and H_r for the soliton solution, one can find the results $M_r = 2\sin\phi\cos\phi$ and $H_r = \frac{4}{3}u_0\cos^3\phi$. As above, we consider the effect of adding a small perturbation δv to the soliton field v_s, which for the primary field u means the selection of the fluctuations in the form: $u = u_0(v_s + \delta v)\exp(\mathrm{i}u_0^2 z)$. The frequency fluctuations $\delta\Omega$, where $\Omega = u_0\sin\phi$, depend on the fluctuations of the background amplitude δu_0 and of the internal phase angle $\delta\phi$. From the conservation identities resulting from the Hamiltonian and the renormalized momentum, one can be find that $\delta\Omega = \alpha(\phi)\delta H_r + \beta(\phi)\delta M_r$, i.e.,

$$\delta\Omega = 2\,\mathrm{Im}\left\{\int_{-\infty}^{+\infty}\delta v\left[\alpha(\phi)\frac{\partial v^*}{\partial z} - \beta(\phi)\frac{\partial v^*}{\partial t}\right]\mathrm{d}t\right\}, \tag{3.37}$$

where

$$\alpha(\phi) = -\frac{3\sin\phi}{4\cos^3\phi}\,, \quad \beta(\phi) = \frac{u_0(3\sin^2\phi + \cos^2\phi)}{4\cos^3\phi}\,.$$

Applying the same reasoning as in the case of the bright soliton, we obtain the following result (Kivshar et al., 1994a)

$$\langle\delta\Omega^2\rangle = \frac{2D}{u_0^2}\int_{-\infty}^{+\infty}\left|\alpha(\phi)\frac{\partial v}{\partial z} - \beta(\phi)\frac{\partial v}{\partial t}\right|^2\mathrm{d}t\,, \tag{3.38}$$

where, as above, we have assumed that the field δv is a stochastic complex noise with the only nonzero correlator

$$\langle\delta v(t)\delta v^*(t')\rangle = \frac{D}{u_0^2}\,\delta(t - t')\,. \tag{3.39}$$

Substituting the exact soliton solution into Eq. (3.38), we finally obtain the result

$$\langle\delta\Omega^2\rangle = \frac{8D}{3u_0^2}\cos^3\phi[\alpha(\phi)\Omega - \beta(\phi)]^2 = \frac{D}{6}\cos\phi\,. \tag{3.40}$$

Validity of this result was discussed by Kivshar et al. (1994a).

To make a comparison between the cases of bright and dark solitons, we must consider a black soliton of the same amplitude as the bright one. We then set $u_0 = a = 1$ and $\phi = 0$. For this choice of parameters Eqs. (3.35) and (3.40) may be now compared to yield the simple relation

$$\langle\delta\Omega^2\rangle_{\mathrm{dark}} = \tfrac{1}{2}\langle\delta\Omega^2\rangle_{\mathrm{bright}}\,.$$

Let us now consider the consequences of this result for soliton-based transmission systems. We assume a fiber link of length L equipped with N amplifiers. Because the noise of amplified spontaneous emission, each amplifier induces a random frequency shift $\delta\Omega$ that slightly modifies the velocity of the solitons that propagate over the length $z_L = L/N$ of the fiber sections. The frequency parameter Ω represents, in soliton units, the inverse group velocity of the soliton. It is possible to show (Gordon and Haus, 1986) that the distribution of the times of arrival of the solitons at the output of the link has a variance jitter given by $\langle \delta t^2 \rangle = L^3 \langle \delta\Omega^2 \rangle / 3z_L$. Introducing the temporal jitter of the transmission as being the standard deviation of this distribution, $\langle \delta t^2 \rangle^{1/2}$, we obtain the following relation:

$$\langle \delta t^2 \rangle_{\text{dark}}^{1/2} = \frac{1}{\sqrt{2}} \langle \delta t^2 \rangle_{\text{bright}}^{1/2} . \tag{3.41}$$

This result shows that the temporal jitter of the fundamental dark solitons is $\sqrt{2}$ lower than that obtained with bright solitons. This result is in perfect agreement with the conclusions of the numerical investigation reported earlier by Hamaide et al. (1991).

The calculations presented above have been recently extended by Panoiu et al. (1995) to include the SRS effect on the jitter of dark solitons. The SRS effect was taken into account as a local perturbation, Eq. (3.26), to the NLS equation. It was shown that the simultaneous action of random fluctuations and SRS effect can, in some cases, compensate each other leading to the lowering jitter. This is, in particular, the case of the background fluctuations when there exists a distance where the dark-soliton jitter completely vanishes (Panoiu et al., 1995).

3.4. Effect of third-order dispersion

Experimental demonstration of long-distance transmission and data coding with the help of dark solitons [see Section 6.1 below and also Nakazawa and Suzuki (1995a,b)] has led to renewed efforts to explore this type of soliton for optical communications. In order to reduce the operating power, the transmission wavelength should be selected closer to the zero of the group-velocity dispersion where, however, the soliton propagation is influenced by the third-order dispersion. The effect of the third-order dispersion on bright solitons is now well understood (Wai et al., 1986, 1990; Menyuk and Wai, 1992). Under the action of the third-order dispersion, a bright soliton develops a nonvanishing asymptotics in the form of a tail (Menyuk and Wai, 1992). Wai et al. (1990) showed that the tail amplitude A is exponentially small in the third-order dispersion coefficient β, $A \sim \exp(-1/\beta)$, and can be calculated using asymptotic analysis 'beyond all orders'. As was pointed out, this result is consistent with Menyuk's robustness hypothesis (Menyuk, 1993), according to which autonomous, homogeneous, Hamiltonian deformations of integrable equations lead to solitary waves that radiate beyond all orders if they radiate at all.

The effect of third-order dispersion on dark solitons was investigated first in the framework on the small-amplitude approximation (Kivshar, 1991a,b; Kivshar and Afanasjev, 1991a) and reviewed by Kivshar (1993b) [see also the recent paper by Frantzeskakis (1996), where the more general case was analyzed). It was shown that, in the framework of the small-amplitude approximation when an effective KdV equation is valid, the third-order dispersion does not affect strongly the existence and properties of gray solitons. However, Kivshar and Afanasjev (1991a) found an

interesting feature of dark solitons near the zero point of the group velocity dispersion. Namely, dark solitons exist as 'humps' (instead of 'dips') on the background of the amplitude u_0 in the region, $1 < \delta < 4$, where $\delta \equiv \alpha^{3/2}/\beta u_0$, α and β are dispersion coefficients defined below. Such *antidark solitons* match exactly the conventional dark solitons at the critical points, where they are described by one of two modified versions of the KdV equation (Grimshaw et al., 1997). Since, the dark and antidark solitons can exist in the same region of the soliton parameters, Afanasjev and Kivshar (1991a) suggested that a head-on collision between them can occur. This head-on collision was investigated analytically by Huang and Velarde (1996) who applied an asymptotic expansion technique to show that the soliton can preserve their identities only to the second order. Huang and Velarde (1996) calculated also the phase shift of the solitons after the collision.

Effect of the third-order dispersion on dark solitons of large or moderate amplitude was analyzed by Afanasjev et al. (1996) [see also Karpman (1993)] who also carried out numerical simulations to confirm the phenomenon of the dark-soliton resonance decay predicted by the theory. In this section, discussing the effect of the third-order dispersion on dark solitons, we follow the work by Afanasjev et al. (1996).

As is well known [e.g., Hasegawa (1989)] the pulse propagation in optical fibers near the zero of the group-velocity dispersion is described by the perturbed NLS equation which we write here in the form,

$$\mathrm{i}\frac{\partial u}{\partial z} - \alpha\frac{\partial^2 u}{\partial t^2} + 2|u|^2 u = \mathrm{i}\beta\frac{\partial^3 u}{\partial t^3}\,, \tag{3.42}$$

where α and β are the corresponding dispersion coefficients. When $\beta \neq 0$, the information about the existence of localized solutions can be obtained by analyzing the asymptotics. We take $u = (u_0 + \xi)\exp(2\mathrm{i}u_0^2 z)$ and linearize Eq. (3.42) for small ξ. Then, for a stationary wave moving with the velocity v, we seek a solution in the form $v \sim (\xi_\mathrm{r} + \mathrm{i}\xi_\mathrm{i})\exp(\mathrm{i}k\zeta)$, where $\zeta = t - vz$, and obtain the equation for $\kappa \equiv k^2(v)$,

$$(v - \beta\kappa)^2 = \alpha(\alpha\kappa + 4u_0^2)\,. \tag{3.43}$$

Quadratic Eq. (3.43) has two roots. Following Afanasjev et al. (1996), we consider $v^2 < c^2$, where $|c| = 2\sqrt{\alpha}u_0$ is the effective speed of sound. Then, one root, say κ_-, is always negative, and it corresponds to exponentially decaying soliton tails. However, for any $\beta \neq 0$ Eq. (3.43) has an additional, positive root, say κ_+, which describes a nonvanishing oscillating tail of the dark soliton.

Existence of nonvanishing tails can be usefully viewed as a resonant generation of linear waves, which takes place provided the speed of the solitary wave v coincides with the phase velocity V_ph of the linear waves. Indeed, the condition $V_\mathrm{ph} = v$ leads immediately to Eq. (3.43). From the physical point of view, this result implies that the solitary wave acts as a source generating trailing oscillations which with the leading front propagating with the wave group velocity V_g. This process is demonstrated in Fig. 6a and Fig. 6b for the case of a black soliton and $\beta = 0.18$. At the initial stage of the soliton evolution some transition radiation is excited. This radiation propagates to the left, moving with the sound speed c, and quickly separates from the dark soliton, as is seen in Fig. 6a. The radiation creates an additional, small-amplitude dark soliton (see Fig. 6b) which is, according to Kivshar and Afanasjev (1991a), is stable in the presence of the third-order dispersion.

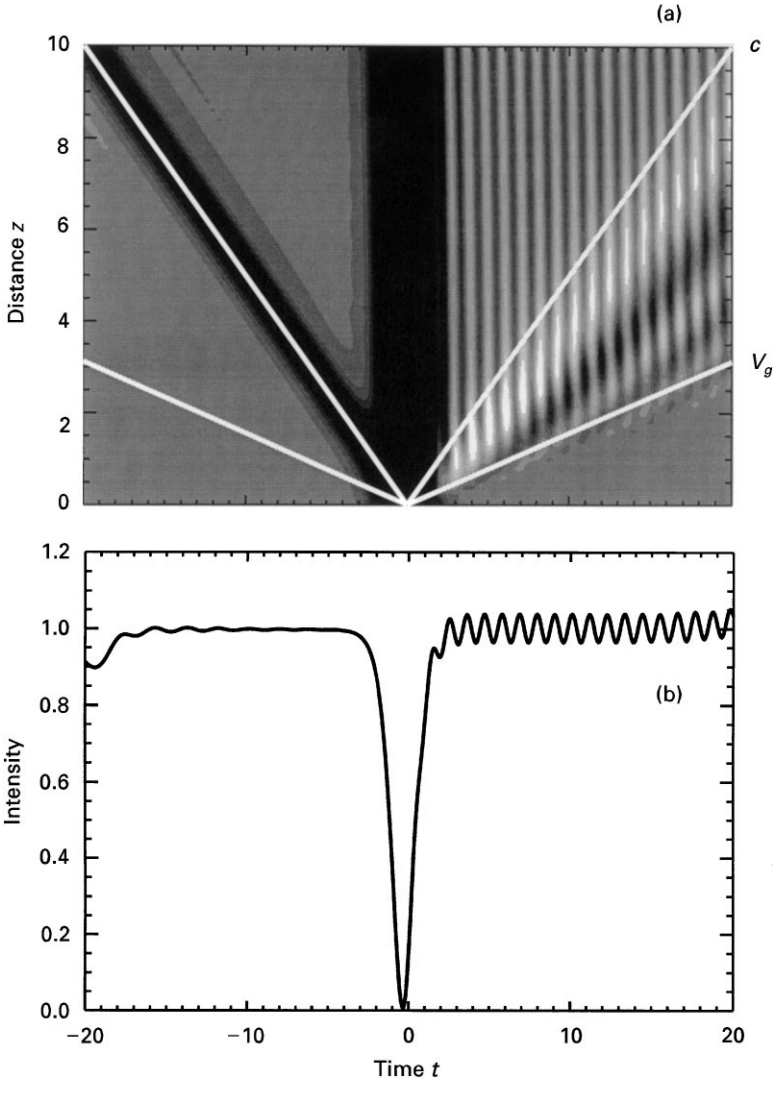

Fig. 6. Formation of a nonvanishing oscillating tail for a black soliton at $\beta = 0.18$. (a) Grey-scale plot, in which the white lines show the propagation with the sound velocity c. (b) Intensity profile at $z = 10$ (Kivshar and Afanasjev, 1996).

An oscillating tail is formed from the right of the soliton, and its front propagates with the group velocity V_g which is different from the velocity of the dark soliton v and sound velocity c. As a result of the generation of a continuously growing tail, the soliton amplitude decreases and its velocity increases, i.e., the soliton decays. Fig. 7 shows subsequently the evolution of the field intensity at the soliton center, $I_{\min} = u_0^2 v^2/c^2$, vs. propagation distance z, which varies from zero to approximately 0.8. Similar dynamics was also reported for initially grey solitons of moderate amplitudes (Afanasjev et al., 1996).

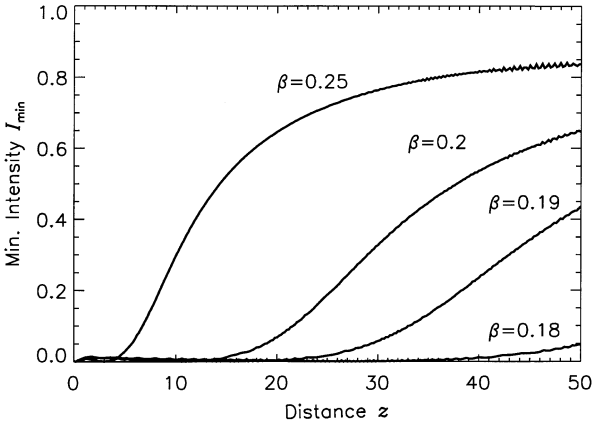

Fig. 7. Long-term adiabatic decay of a black soliton in the presence of the third-order dispersion. Shown is the evolution of the minimum soliton intensity $I_{\min}(z)$ at different values of β (Kivshar and Afanasjev, 1996).

Calculation of the oscillation amplitude is a delicate task which requires all orders of the asymptotic expansion (Wai et al., 1990; Kivshar and Malomed, 1991). However, a qualitatively correct result can be obtained considering the linear equation for the soliton perturbations $\xi = u - u_s$. As was shown by Karpman (1993) and Afanasjev et al. (1996), the corresponding solution can be found in a cumbersome form, but its general structure is given by the expression:

$$\xi = A\theta(\zeta)\theta(-\zeta + V_g z)\sin(\sqrt{\kappa_+}\zeta + \phi),$$

where $\theta(x) = 1$ for $x > 0$ and $\theta(x) = 0$ for $x < 0$, and $\zeta = t - vz$. The dependence of the tail amplitude A on β and v, can be presented as the following (Afanasjev et al., 1996)

$$A \sim CB(\kappa_+)\mathrm{csch}\left(\frac{\pi\sqrt{\alpha}}{u_0\cos\theta}\sqrt{\kappa_+}\right), \tag{3.44}$$

where C is a constant and B is an algebraic function of κ_+, a positive root of Eq. (3.43). Using the first-order expansion for small β, $k = \sqrt{\kappa_+} \approx \alpha/\beta$, one can easily show that the tail amplitude depends on β exponentially, i.e. in the similar fashion as for bright solitons (Wai et al., 1986, 1990). However, the special feature of dark solitons is the algebraic factor $\sqrt{1 - v^2/c^2}$ in the exponent which demonstrates that the radiation amplitude becomes exponentially small for any fixed β but in the limit $v^2 \to c^2$. This explains the validity of the small-amplitude approximation used earlier by Kivshar and Afanasjev (1991a). Indeed, as the amplitude of the dark soliton decreases, for a fixed value of β the amplitude of the oscillating tail decays exponentially fast. This means that the oscillation amplitude becomes beyond all orders of the asymptotic expansion in the soliton amplitude, and in this limit the soliton radiation and decay are negligible.

3.5. Background of finite extent

In experiments reporting dark solitons, localized beams (or pulses) have been created on a background beam (or pulse) of a finite extend (Emplit et al., 1987; Krökel et al., 1988;

Weiner et al., 1988; Swartzlander et al., 1991; Allan et al., 1991; Luther-Davies and Yang, 1992a,b). Therefore, the interpretation of the experimental results as the observation of dark-soliton propagation could be questionable because the background, being only in several times longer than the dark beams or pulses observed, spreads significantly due to dispersion, in the temporal case, or diffraction, in the spatial case.

However, Tomlinson et al. (1989) demonstrated, by means of direct numerical simulations, that optical dark solitons superimposed upon backgrounds only 10 times wider than the soliton width can exhibit stable soliton-like propagation for relatively short distances. During the propagation, the background spreads, reduces its intensity, and develops a frequency chrip (in the temporal case) but, nevertheless, dark pulses created on such a finite-width background adiabatically maintain their soliton characteristics. As has been pointed out by Gredeskul et al. (1990), for the finite-width background the corresponding eigenvalue problem of the associated IST (see Section 2.5.1 above) has no eigenvalues of the discrete spectrum and the dark pulses created on a vanishing background correspond instead to the so-called *quasi-stationary states* of the eigenvalue problem, Eq. (2.24). This simply means that the dark beams created on a finite-width background never become proper solitons, and they should disappear as soon as the propagation distances increase.

However, these results are correct from the mathematical point of view but they do not give a clear physical explanation to the following fact: *Why dark pulses, even being not proper solitons, do not change significant when the background itself spreads, reduces its intensity, and develops a frequency chirp?*. The answer to this question follows from the analysis done by Kivshar and Yang (1994b) which we briefly discuss below.

It is known that for vanishing boundary conditions the NLS equation describes the spreading pulses (or beams) which undergo enhanced broadening and chirping. Let us take such a quasi-linear background in a rather general form,

$$u(x, z) = u_0(x, z)\, \mathrm{e}^{\mathrm{i}\theta(x,z)}\,, \tag{3.45}$$

where we just introduce the background amplitude, $u_0(x, z)$, and phase, $\theta(x, z)$. We consider now the evolution of a dark pulse *superimposed* upon such a spreading background, looking for a solution of the NLS equation in the form,

$$u(x, z) = u_0(x, z)\, \mathrm{e}^{\mathrm{i}\theta(x,z)} v(x, z)\,, \tag{3.46}$$

where $v(x, z)$ falls off fast as x increases. Substituting Eq. (3.46) into the NLS equation and assuming that the function $u_0(x, z)\exp[\mathrm{i}\theta(x, z)]$ is a solution of the NLS equation, we obtain the following equation for the function $v(x, z)$,

$$\mathrm{i}\frac{\partial v}{\partial z} + \frac{1}{2}\frac{\partial^2 v}{\partial x^2} - u_0^2(|v|^2 - 1)v = -2\frac{\partial}{\partial x}\left[\ln(u_0 \mathrm{e}^{\mathrm{i}\theta})\right]\frac{\partial v}{\partial x}\,, \tag{3.47}$$

where $u_0 \equiv u_0(x, z)$ is the background amplitude introduced above. Introducing slow variables ζ and ξ according to the relations, $\mathrm{d}\zeta \approx u_0^2(x, z)\,\mathrm{d}z$, $\mathrm{d}\xi \approx u_0(x, z)\,\mathrm{d}x$, and taking the pulse $v(\zeta, \xi)$ as a dark soliton, Eq. (3.4), the pulse evolution due to such a perturbation can be effectively analysed

with the help of Eq. (3.7), giving the evolution equation for the soliton phase angle,

$$\frac{\mathrm{d}\phi}{\mathrm{d}\zeta} = \frac{1}{2}\cos^2\phi \int_{-\infty}^{+\infty} \frac{\mathrm{d}\Theta}{\cosh^2\Theta}\left(\frac{1}{u_0}\frac{\partial u_0}{\partial\Theta}\right), \tag{3.48}$$

where $u_0 = u_0(Z, \zeta)$ is considered in the reference frame moving with the soliton [see Eq. (3.6)].

Eq. (3.48) is valid for an arbitrary background, and it clearly shows that the evolution of a dark soliton *does not depend on the background phase*, so that the enhanced frequency chirp developed by the background does not affect the dark pulse and it maintains adiabatically its properties. Additionally, as follows from Eq. (3.48), the change of the soliton angle depends not on the extension and intensity of the background but rather on its *local slope*.

In particular, these results indicate that properly selecting the input background shape we may keep the steering angle of the dark soliton, $W = u_0 \sin\phi$ almost unchanged because the effect of the background decay can be completely compensated by the internal dynamics of the dark soliton. This effect was indeed demonstrated numerically (Kivshar and Yang, 1994b) comparing the soliton evolution for the constant and varying backgrounds.

4. Instability-induced soliton dynamics

4.1. Stability of dark solitons

Optical dark solitons are of both fundamental and technological importance if they are stable under propagation. For temporal solitons in optical fibers, nonlinear effects are weak and the model based on the cubic NLS equation is valid is most of the cases. Therefore, being described by the integrable or nearly integrable models, solitons are always stable, or their dynamics can be affected by (generally small) external perturbations which can be treated in the framework of perturbation theory. For spatial solitons in waveguides or bulk media, higher powers are usually required, so that real optical materials demonstrate essentially non-Kerr change of the nonlinear refractive index with the increase of the light intensity. Generally speaking, the nonlinear refractive index always deviates from Kerr for larger input powers, e.g., it saturates. Therefore, models with a more general intensity-dependent refractive index are employed to analyze spatial dark solitons and, as we discuss here, dark solitary waves in such non-Kerr materials can become unstable.

Stability of *bright solitons* of the generalized NLS Eq. (4.2) has been extensively investigated for many years, and the criterion for the soliton stability has been derived by different methods (see, e.g., Vakhitov and Kolokolov (1973), Weinstein (1985), Kuznetsov et al. (1986), Kusmartsev (1989) and Mitchell and Snyder (1993)]. Stability of bright solitons in the generalized NLS equation of any dimension is given by the simple criterion (Vakhitov and Kolokolov, 1973)

$$\frac{\mathrm{d}P}{\mathrm{d}\beta} = \frac{\mathrm{d}}{\mathrm{d}\beta}\left(\int_V |E(\boldsymbol{r}, z)|^2\,\mathrm{d}\boldsymbol{r}\right) > 0\,,$$

where P is the total soliton power and β is the soliton propagation constant. Stability of self-guided in nonlinear waveguide structures can be also given in some cases by the same criterion (e.g., Jones

and Moloney (1986) and Mitchell and Snyder (1993)] but, generally, it is more complicated and depends on a particular structure and the type of nonlinearity.

Different scenarios of the instability-induced dynamics of bright solitons have been found and analyzed both analytically and numerically [see, for a review, e.g., Kuznetsov et al. (1986)]. Recently, Pelinovsky et al. (1996a) developed an asymptotic analytical approach to describe the dynamics of unstable solitons (e.g. diffraction-induced decay, collapse, or switching to a novel stable state). All these results allow to say, as we believe, that the picture of the instabilities of bright solitons is complete.

In contrast to bright solitons, the stability criterion for dark solitons of the generalized NLS equation has not been understood until recently and, even more, this issue created a lot of misunderstanding in the past. In particular, we notice some efforts to employ, by analogy with bright solitons, the soliton complementary power [see, e.g., Enns and Mulder (1989)] and to use this value for analyzing the soliton bistability (Mulder and Enns, 1989; Bass et al., 1992), a statement that a black dark soliton (a dark soliton with zero intensity at its center) is always stable (Mitchell and Snyder, 1993), etc. However, as was already noticed by Królikowski et al. (1993), the complimentary power does not define stability of dark solitons.

From a historical point of view, the first efforts to analyze the stability of dark solitons were stimulated by numerical simulations done by Barashenkov and Kholmurodov (1986) who observed instability of the so-called 'bubbles', localized waves of rarefaction of the Bose gas condensate. These nontopological solitary waves belong, in the $(1 + 1)$-dimensional case, to the family of dark solitons of the NLS equation with the cubic–quintic nonlinearity, Eq. (2.7), and they survive in higher dimensions [see, e.g., Barashenkov and Makhankov (1988)]. Although quiescent bubbles were found to be always unstable regardless of dimension [Barashenkov et al. (1989), see also a proof given by De Bouard (1995)], in numerical simulations it was revealed that the moving bubbles can be stabilized at nonzero velocities (Barashenkov and Kholmurodov, 1986). Later Bogdan et al. (1989) [see also Barashenkov and Panova (1993)] explained this phenomenon through the multivalued dependence of the bubble energy vs. the renormalized bubble momentum.

However, it was believed for a long time that kink-type dark solitons (e.g., black solitons) are always stable [see, e.g., Mitchell and Snyder (1993)]. Instability of black solitons was observed for the first time by Kivshar and Królikowski (1995b) in numerical simulations of the NLS equation with the saturable nonlinearity, Eq. (2.9), at $p = 2$. These authors used the variational principle to link the instability to the existence of multivalued solution in terms of the system invariants, and also derived the instability threshold condition by using the asymptotic expansions.

Even it was known for some time that the stability criterion for dark solitons should be defined through the renormalized soliton momentum,

$$\frac{\mathrm{d}M_{\mathrm{r}}}{\mathrm{d}v} = \frac{\mathrm{d}}{\mathrm{d}v}\left\{\frac{\mathrm{i}}{2}\int_{-\infty}^{+\infty}\left(u\frac{\partial u^*}{\partial x} - u^*\frac{\partial u}{\partial x}\right)\left(1 - \frac{u_0^2}{|u|^2}\right)\mathrm{d}x\right\} > 0\,,$$

and this was shown to be consistent with the results of numerical simulations (Barashenkov and Kholmurodov, 1986; Barashenkov et al., 1989; Kivshar and Afanasjev, 1996) and the variational principle for bubble-type (Bogdan et al., 1989) and kink-type (Kivshar and Królikowski, 1995b) dark solitons, the rigorous proof of this stability criterion was presented only recently by Barashenkov (1996), with the help of the Lyapunov function, and Pelinovsky et al. (1996b), with the help of

the asymptotic expansions near the instability threshold. The first approach does not allow to describe the instability itself but it is more general, whereas the second method is valid in the vicinity of the instability threshold being however sufficient to determine the instability domain.

We would like to note that the stability of dark solitons can be also formulated by using another definition of the renormalized momentum M_r, e.g., that introduced for any dimension by Jones and Roberts (1982),

$$\boldsymbol{M}_r = \frac{i}{2}\int_V [(u-1)\nabla u^* - (u^*-1)\nabla u]\,d\boldsymbol{r}\,.$$

This invariant was used by Kuznetsov and Rasmussen (1995) to analyze the transverse instability of a dark-soliton stripe and vortex line in a cubic NLS equation.

In this chapter we follow the approach based on the asymptotic multiscale analysis developed by Pelinovsky et al., 1996b) which allows to describe both *linear* and *nonlinear* regimes of the instability-induced dynamics of dark solitons. We also describe the results of a detailed numerical simulations of different scenarios of the evolution of unstable dark solitons.

4.2. Asymptotic approach

4.2.1. Stationary solutions

We consider the generalized NLS Eq. (2.22) and look for stationary solution on a cw background in the form

$$u(x,z) = \psi(x,z)\,e^{ig(q)z}\,, \tag{4.1}$$

where $q = u_0^2$ is the background intensity and the function ψ satisfies the conditions $\psi(x,z) \to q$ for $x \to \pm\infty$. Substituting Eq. (4.1) into Eq. (2.22), we obtain the equation

$$i\frac{\partial\psi}{\partial z} + \frac{1}{2}\frac{\partial^2\psi}{\partial x^2} + [g(|\psi|^2) - g(q)]\psi = 0\,. \tag{4.2}$$

Now, dark soliton ψ_s is defined as a localized travelling-wave solution of Eq. (4.2),

$$\psi_s(\xi) = \Phi(\xi)\,e^{i\theta(\xi)}\,, \tag{4.3}$$

where $\xi = x - vz$ and two *real* functions, $\Phi \equiv \Phi(\xi; v, q)$ and $\theta \equiv \theta(\xi; v, q)$, depend on two parameters, the soliton velocity v and the intensity q of the cw background. These functions satisfy the following ordinary differential equations,

$$\frac{d\theta}{d\xi} = v\left(1 - \frac{q}{\Phi^2}\right), \tag{4.4}$$

$$\frac{1}{2}\frac{d^2\Phi}{d\xi^2} + \frac{v^2}{2}\left(\Phi - \frac{q^2}{\Phi^3}\right) + [g(\Phi^2) - g(q)]\Phi = 0\,. \tag{4.5}$$

Eqs. (4.3), (4.4) and (4.5) describe a dark soliton defined by two parameters, the soliton velocity v and the background intensity q. For the soliton solution of the form of Eq. (4.3) we can define the renormalized invariants, the renormalized or complementary power, Eq. (2.49), renormalized

momentum, Eq. (2.50), and renormalized Hamiltonian, Eq. (2.51). Defined for the soliton solution, Eq. (4.3) with the index 's', these invariants take the form

$$P_s(v, q) = \frac{1}{2}\int_{-\infty}^{+\infty} (\Phi^2 - q)\, d\xi\,, \tag{4.6}$$

$$M_s(v, q) = -v\int_{-\infty}^{+\infty} \frac{(\Phi^2 - q)^2}{\Phi^2}\, d\xi\,, \tag{4.7}$$

$$H_s(v, q) = \int_{-\infty}^{+\infty} \left\{ \frac{1}{2}\left(\frac{d\Phi}{d\xi}\right)^2 + \frac{v^2}{2}\frac{(\Phi^2 - q)^2}{\Phi^2} + \int_q^{\Phi^2} [g(q) - g(I)]\, dI \right\} d\xi\,. \tag{4.8}$$

Besides, we can find the analytical expression for the total phase shift S_s of the background wave across the dark soliton,

$$S_s(v, q) = v\int_{-\infty}^{+\infty} \left(1 - \frac{q}{\Phi^2}\right) d\xi\,. \tag{4.9}$$

4.2.2. Equation for soliton velocity

As has been shown by Pelinovsky et al. (1996b), the analysis of stability of dark soliton solutions, Eqs. (4.3), (4.4) and (4.5) can be carried out in the framework of the perturbation theory if a change of the soliton parameters is slow in time. Soliton instability is weak near the instability threshold when the velocity v of the unstable dark soliton is close to a critical value v_c defined by the instability threshold equation $\partial M_s/\partial v|_{v=v_c} = 0$. Moreover, we suppose that the amplitude of instability-induced perturbations remains small for an extended time interval and the localized wave is close to a dark soliton ψ_s with slowly (adiabatically) varying parameters. Therefore, we can introduce a small parameter ε which characterizes a small perturbation of the unstable dark soliton, and look for solutions ψ to Eq. (4.2) in the form of the following asymptotic (multi-scale) expansion,

$$\psi = \{\psi_s(\xi; v, q) + \varepsilon\psi_1(\xi; v, q; X, T) + \varepsilon^2\psi_2(\xi; v, q; X, T) + O(\varepsilon^3)\}\, e^{iR(X,T)}\,,$$

where

$$\xi = x - \frac{1}{\varepsilon}X_s(T)\,, \quad X_s(T) = \int_0^T v(T')\, dT'\,, \quad X = \varepsilon x\,, \quad T = \varepsilon z\,,$$

and $\varepsilon \ll 1$. Here the functions $v(T)$ and $R(x, T)$ describe the slowly varying soliton velocity and local phase, respectively, X and T stand for 'slow' variables, and $X_s(T)$ is the coordinate of the soliton center (minimum amplitude) with respect to the X-axis.

Generally speaking, solutions to the linear inhomogeneous equations for $\psi_1, \ldots$ may diverge exponentially along the inner interval as $\xi \to \infty$. Such divergences usually break down the asymptotic expansion procedure. However, in the vicinity of the instability threshold, where $\partial M_s/\partial v \sim O(\varepsilon)$, the first-order correction ψ_1 can be expressed in an implicit form (Pelinovsky et al., 1996b) and then a bounded solution of the second-order perturbation correction ψ_2 has to be found. In this way, the function ψ_2 does not display exponentially diverging terms if the velocity of

the perturbed dark soliton satisfies a certain differential equation, *solvability condition* [see Eq. (4.10) below].

Using the method of matched asymptotics, Pelinovsky et al. (1996b) have shown that near the instability threshold the evolution of the soliton velocity v as derived from the conservation of momentum, is described by the following equation:

$$\frac{\mathrm{d}}{\mathrm{d}T}\left[\frac{1}{\varepsilon}M_{\mathrm{s}}(v,q)+\mu_{\mathrm{s}}(v,q)\frac{\mathrm{d}v}{\mathrm{d}T}\right]=K_{\mathrm{s}}(v,q)\left(\frac{\mathrm{d}v}{\mathrm{d}T}\right)^2, \tag{4.10}$$

where M_{s} is the soliton renormalized momentum, Eq. (4.7), and the coefficients are defined as

$$\mu_{\mathrm{s}}(v,q)=\frac{2c}{q}\left(\frac{\partial P_{\mathrm{s}}}{\partial v}\right)^2+\frac{q}{2c}\left(\frac{\partial S_{\mathrm{s}}}{\partial v}\right)^2, \tag{4.11}$$

and

$$K_{\mathrm{s}}(v,q)=\frac{1}{(c^2-v^2)}\left[\frac{2cv}{q}\left(\frac{\partial P_{\mathrm{s}}}{\partial v}\right)^2+2c\frac{\partial P_{\mathrm{s}}}{\partial v}\frac{\partial S_{\mathrm{s}}}{\partial v}+\frac{vq}{2c}\left(\frac{\partial S_{\mathrm{s}}}{\partial v}\right)^2\right], \tag{4.12}$$

where P_{s} and S_{s} are defined by Eqs. (4.6) and (4.9), respectively, and c is the limiting velocity of linear waves, $c^2=qg'(q)$.

Similar calculations based on the conservation of the energy (Hamiltonian) show that the first-order variations of the renormalized momentum δM and energy δH of a perturbed dark soliton are related by the equation (see Section 2.6),

$$v\delta M+\delta H=0\,. \tag{4.13}$$

However, neither momentum nor energy of the perturbed dark soliton is conserving and this reveals *essentially dissipative character* of the instability-induced dynamics of unstable dark solitons. Such a dissipative dynamics of the dark soliton instability is explained by generation of the radiation fields propagating away from the perturbed dark soliton to the right and to the left. The profile of the radiation fields can be obtained in the following explicit form (Pelinovsky et al., 1996b),

$$U^{\pm}=\zeta_{\pm}(v,q)\frac{\mathrm{d}v}{\mathrm{d}T}\quad\text{at}\quad X=X_{\mathrm{s}}(T)\,, \tag{4.14}$$

where

$$\zeta_{\pm}(v,q)=-\frac{1}{c(c\mp v)}\left(c\frac{\partial P_{\mathrm{s}}}{\partial v}\pm\frac{q}{2}\frac{\partial S_{\mathrm{s}}}{\partial v}\right). \tag{4.15}$$

Asymptotic Eq. (4.10) cannot be generally integrated. Nevertheless, it describes a rather simple dynamics of the dark soliton instability and related evolution of the radiation fields of Eq. (4.14). The specific features of this dynamics are analysed below for three particular cases. Here we describe more general features of the instability-induced dark-soliton dynamics.

First, we consider a linear approximation of the asymptotic Eq. (4.10) substituting $v=v_0+v_1\mathrm{e}^{\lambda T}$, where v_0 is the (initial) velocity of the unperturbed dark soliton and v_1 is its small deviation caused by an initial) perturbation. Neglecting nonlinear terms in Eq. (4.10) we find the

instability growth rate λ,

$$\lambda = -\frac{1}{\varepsilon\mu_s(v_0, q)}\left(\frac{\partial M_s}{\partial v}\right)_{v=v_0}. \tag{4.16}$$

The result of Eq. (4.16) gives the criterion of the dark soliton instability, and it proves that dark solitons become unstable provided $\partial M_s/\partial v|_{v=v_0} < 0$ [we notice that the coefficient $\mu_s(v_0, q)$ is always positive, see the definition in Eq. (4.11)]. Therefore, the bifurcation analysis implies that *all dark solitons with negative slope of the renormalized momentum $M_s(v)$ are unstable*.

Next, we analyse the general conditions when the instability of dark solitons can occur. Let us first consider the small-amplitude limit, when $|v| \to c$. In this limit dark solitons can be described by an effective KdV equation (see Section 2.5.2), and the derivative $(\partial M_s/\partial v)$ can be found explicitly (Pelinovsky et al., 1996b), and it is *always positive*. Therefore, small-amplitude dark solitons of the generalized NLS equation are *always stable* and the instability can occur only for dark solitons of larger amplitude (or smaller velocity v).

However, in the limit of small velocities, $v \to 0$, the slope $\partial M_s/\partial v$ *can become negative* provided

$$\left(\frac{\partial S_s}{\partial v}\right)\bigg|_{v=0} < \frac{2}{q}P_s\bigg|_{v=0} < 0\,.$$

For many models, the total phase shift S_s is given by a monotonic function rising from the value $-\pi$, at $v \to 0$ ('black' soliton) to zero, at $v \to c$ (small-amplitude or 'grey' solitons), see Fig. 8a and Fig. 8b. For example, this situation is typical for the Kerr and power-law nonlinearity, $g(I) \sim I^p$, as well as for the generalized Kerr model with the nonlinearity $g(I) = I + \beta I^2$. For these models the slope $\partial S_s/\partial v$ is always positive and instabilities of dark solitons cannot occur. However, for some more complicated but still physically important models the instability of dark solitons does take place and the general form of the renormalized momentum for such cases is shown in Fig. 8a and Fig. 8b. We discuss these instabilities below.

Nonlinear dynamics of an unstable dark soliton and radiation fields emitted have been analyzed by Pelinovsky et al. (1996b). In a region of small velocities near the critical value v_c, one can apply a small-amplitude (but still nonlinear) approximation substituting $v = v_0 + \varepsilon V(T)$, in order to simplify Eq. (4.10) and reduce it to the form,

$$\mu_s(v_0, q)\frac{dV}{dT} + \frac{1}{\varepsilon}\left(\frac{\partial M_s}{\partial v}\right)_{v=v_0} V + \frac{1}{2}\left(\frac{\partial^2 M_s}{\partial v^2}\right)_{v=v_0} V^2 = 0\,. \tag{4.17}$$

This equation resembles the motion equation of an effective particle of mass μ_s and velocity V under the action of a nonlinear dissipative force. Type of the instability scenario depends essentially on a sign of the initial perturbation and the particular form of the dependence $M_s(v)$. In a general case, dark solitons of larger intensity and smaller velocity are unstable in the linear approximation while small-amplitude solitons with the velocities close to the limit velocity c are stable. Therefore, for this type of the functions $M_s(v)$ the derivative $(\partial^2 M_s/\partial v^2)|_{v=v_0}$ in Eq. (4.17) is positive and any perturbation with $V(0) > 0$ leads to a bounded scenario of the dark soliton instability. This process corresponds to a transformation of an unstable dark soliton into a stable soliton of larger velocity and smaller amplitude, described by a simple solution of Eq. (4.17)

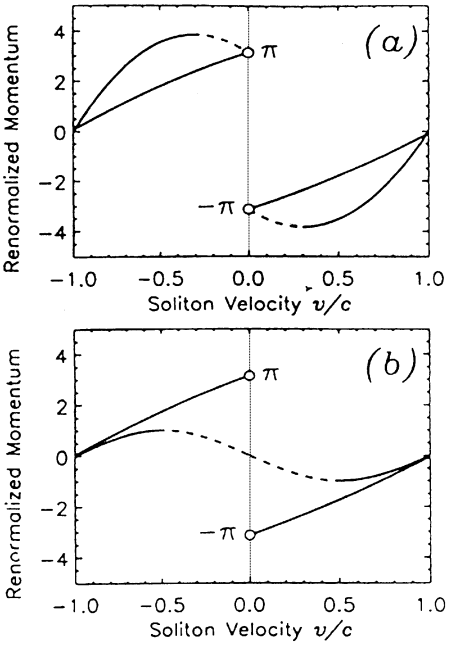

Fig. 8. Schematic presentation of the renormalized momentum $M_s(v)$ of the dark soliton for two distinct cases: (a) the minimum intensity vanishes when $v \to 0$, and (b) the minimum intensity remains finite for $v \to 0$. In both the cases the negative slope indicates unstable dark solitons (Pelinovsky et al., 1996b).

(see Pelinovsky et al., 1996b),

$$V = \frac{V_0 V_f}{(V_f - V_0)\, e^{-\lambda T} + V_0}, \tag{4.18}$$

where λ is defined by Eq. (4.16) ($\lambda > 0$), V_0 is the initial velocity of the unstable dark soliton, and V_f is the final velocity of stable solitons defined as

$$V_f = -\frac{2}{\varepsilon}\left(\frac{\partial M_s}{\partial v}\right)\Big|_{v=v_0}\left\{\left(\frac{\partial^2 M_s}{\partial v^2}\right)\Big|_{v=v_0}\right\}^{-1}. \tag{4.19}$$

This result is valid only if the renormalized momentum of the perturbed dark soliton is a conserved quantity during the soliton transformation. However, this quantity does not conserve beyond the quadratic approximation and the change ΔM between the value of the renormalized momentum M_f for the final stable dark soliton and that for the initial unstable soliton, M_0, can be calculated directly from Eq. (4.10) as follows,

$$\Delta M = \varepsilon \int_{-\infty}^{+\infty} K_s(v, q)\left(\frac{dv}{dT}\right)^2 dT = \frac{\varepsilon^3 \lambda (\Delta V)^2}{6} K_s(v_0, q), \tag{4.20}$$

where the coefficient K_s is defined above in Eq. (4.12). We note that this coefficient can have, in general, *an arbitrary sign* and, therefore, transitions from unstable to stable dark solitons can lead

to either increasing or decreasing of the value of the soliton renormalized momentum. As a matter of fact, the type of the momentum change is determined by a balance between the radiation field U^+ propagating to the same direction as the perturbed dark soliton and the field U^- propagating to the opposite direction. These radiation fields can be also calculated analytically with the help of Eq. (4.14),

$$U^{\pm} = \frac{\lambda \Delta V}{4}\,\zeta_{\pm}(v_0, q)\,\mathrm{sech}^2\left[\frac{\lambda}{2(c \mp v_0)}\,(X \mp cT)\right], \tag{4.21}$$

which coincide, with an accuracy of the amplitude factor, with the sech^2-type profile of the stationary dark soliton solutions to the generalized NLS equation in the small-amplitude approximation (see Section 2.5.2). Evolution of the radiation field given by Eq. (4.21) obeys asymptotically the KdV equations with $\alpha > 0$. It is well-known that the sech^2-type initial condition in the KdV equation leads to a generation of solitons only if the wave amplitude is negative. In the opposite case, i.e., when the input amplitude of the localized pulse is positive, the initial profile, Eq. (4.21), transforms into linear dispersive waves. A simple analysis indicates (Pelinovsky et al., 1996b), that in the limit $v_0 \to 0$ the coefficient ζ_+ is *positive* while the coefficient ζ_- is *negative*. Moreover, it is possible to show that the sign of the coefficient ζ_- remains unchanged throughout the instability region so that the counter-propagating radiation field, described by the function U^-, should always generate a stable (shallow) dark soliton as a result of the transformation of the primary unstable dark soliton. On the other hand, the radiation field, described by the function U^+, decays into dispersive waves if $\zeta_+(v_0, q) > 0$ or it can also produce an additional (stable) dark soliton provided $\zeta_+(v_0, q) < 0$.

4.3. Examples of non-Kerr dark solitons

4.3.1. Competing nonlinearities

In the case of competing nonlinearities, e.g. focusing plus defocusing, the dark solitons of Eq. (4.2) display features different from those for dark solitons of the cubic NLS equation. Due to self-focusing at smaller intensities, the minimum amplitude of a dark soliton may not reach zero even at $v = 0$, provided the parameter of the cubic nonlinearity is large enough. As a result, the total phase shift $S_s(v)$ and, therefore, the renormalized momentum $M_s(v)$ tend to zero in both the limits, $v \to 0$ and $v \to c$. This leads to the appearance of a negative slope of $M_s(v)$ for small v and, correspondingly, to instability of dark solitons, see Fig. 8b. This phenomenon is observed for the generalized NLS Eq. (4.2) with competing power-law nonlinearity, Eq. (2.8), which we write here in the dimensionless form,

$$g(I) = \tfrac{1}{2}(\alpha I^p - \beta I^{2p})\,, \tag{4.22}$$

where α and β are both positive. The first term describes the self-focusing effect for smaller intensities, and therefore it may prevent the existence of black solitons with zero minimum intensity. For $p = 1$ the generalized NLS Eq. (4.2) with Eq. (4.22) corresponds to the focusing cubic and defocusing quintic nonlinearity which describes a deviation from the Kerr medium of an optical material (see also Introduction). Remarkably, the model, Eq. (4.2), with competing nonlinearity, Eq. (4.22), at $p = 1$ possesses an explicit analytical solution for dark soliton [probably first found by Barashenkov and Makhankov (1988)]. Therefore, although the general analysis of the

competing nonlinearities is qualitatively valid for any value of p, below we restrict ourselves by the case $p = 1$ when the results can be obtained analytically.

Exact solution for a dark soliton of the cubic-quintic nonlinearity can be found in the form

$$\Phi^2(\xi) = 1 - \frac{2k^2}{a + b\cosh(2k\xi)}, \tag{4.23}$$

$$a = (\tfrac{4}{3}\beta - 1), \quad b = \sqrt{a^2 - \tfrac{4}{3}\beta k^2}, \tag{4.24}$$

where, for simplicity, we take $q = 1$ and $\alpha = 2$. Soliton amplitude k is related to the soliton velocity v as $k^2 + v^2 = \beta - 1$.

First, the condition $k^2 > 0$ yields $|v| < c(\beta) = \sqrt{\beta} - 1$. This shows that the dark soliton, Eqs. (4.23) and (4.24), exists only for $\beta > 1$ (see Fig. 9a). Then, we use the instability criterion defined above and evaluate the slope of the function $M_s(v)$, the dark soliton becomes unstable for $\partial M_s(v)/\partial v < 0$. We check that the negative slope of $M_s(v)$ appears only for $1 < \beta < 1.5$ where the dark soliton at $v = 0$ has a nonzero amplitude at the minimum, $\Phi^2(0) = (3 - 2\beta)/\beta$. The function $M_s(v)$ for the particular case $\beta = 1.2$ is shown in Fig. 9b. The instability region is shown in Fig. 9a.

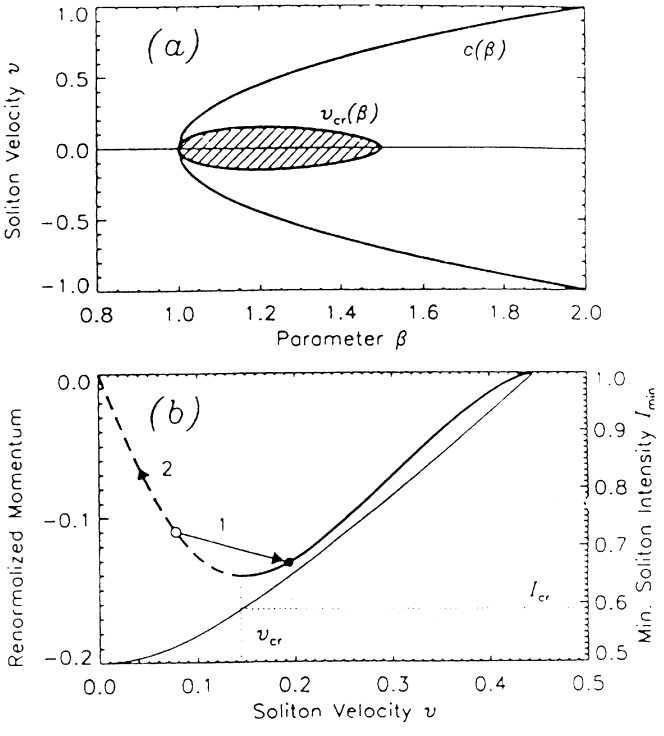

Fig. 9. (a) Regions of existence, $|v| < c(\beta)$, and instability, $|v| < v_{cr}(\beta)$, of the dark soliton Eqs. (4.23) and (4.24). (b) Renormalized momentum $M_s(v)$ for the dark soliton, Eqs. (4.23) and (4.24), at $\beta = 1.2$. Thick dashed and solid branches correspond to unstable ($v < v_{cr}$) and stable ($v > v_{cr}$) dark solitons, respectively. Thin solid curve depicts the change of the minimum soliton intensity I_{min}. Arrows 1 and 2 correspond to the evolution of the unstable soliton presented in Figs. 10 and 11, respectively (Pelinovsky et al., 1996b).

To study the evolution of unstable dark solitons, Pelinovsky et al. (1996b) performed numerical simulations. The dark soliton, Eqs. (4.23) and (4.24), was perturbed

$$\psi_{\mathrm{pert}}(\xi) = \{\Phi(\xi) + \varepsilon[1 - \Phi^2(\xi)]\}\, \mathrm{e}^{\mathrm{i}\theta(\xi)},$$

which does not change the soliton phase. Initial velocity v_0 of the unstable soliton was chosen in the unstable region, while ε was taken both positive and negative in the interval $0.0001 < |\varepsilon| < 0.02$. The numerical simulations revealed two completely different scenarios of the dynamics of the unstable dark solitons depending on the sign of ε. Some of these features, including the splitting of an unstable dark soliton, were reported earlier by Barashenkov and Kholmurodov (1986).

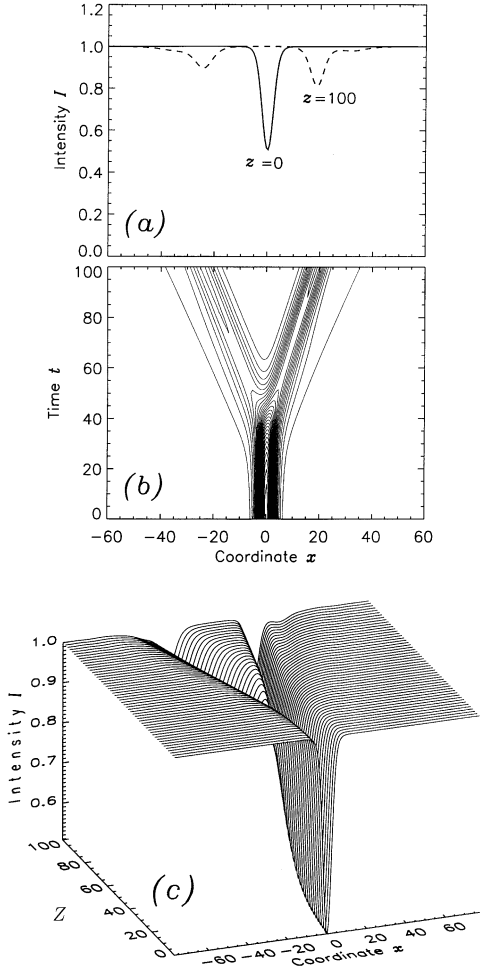

Fig. 10. Splitting of an unstable dark soliton, Eqs. (4.23) and (4.24), for $\beta = 1.2$, $v_0 = 0.02$, and $\varepsilon = +0.005$. (a) Intensity profiles at $z = 0$ (solid curve) and $z = 100$ (dashed curve), and the corresponding (b) contour plot and (c) propagation dynamics (Pelinovsky et al., 1996b).

The first scenario is observed for $\varepsilon > 0$, when initially the soliton amplitude is slightly decreased. Effectively, this corresponds to a 'push' of the unstable soliton toward the stable branch of $M_s(v)$ in Fig. 9b (curve 1) existing for larger values of v. Example of such simulations for the case $v_0 = 0.04$ is shown in Fig. 10a–c where the soliton splitting is observed.

The second scenario of the soliton instability takes place for $\varepsilon < 0$. In this case, the unstable dark soliton is 'pushed' deeper into the instability region (see curve 2 in Fig. 9b). The corresponding simulations for the case $v_0 = 0.04$ are presented in Fig. 11a–c where we observe the formation of two kinks propagating in the opposite directions. This scenario of the soliton instability can be called '*collapse of dark solitons*'.

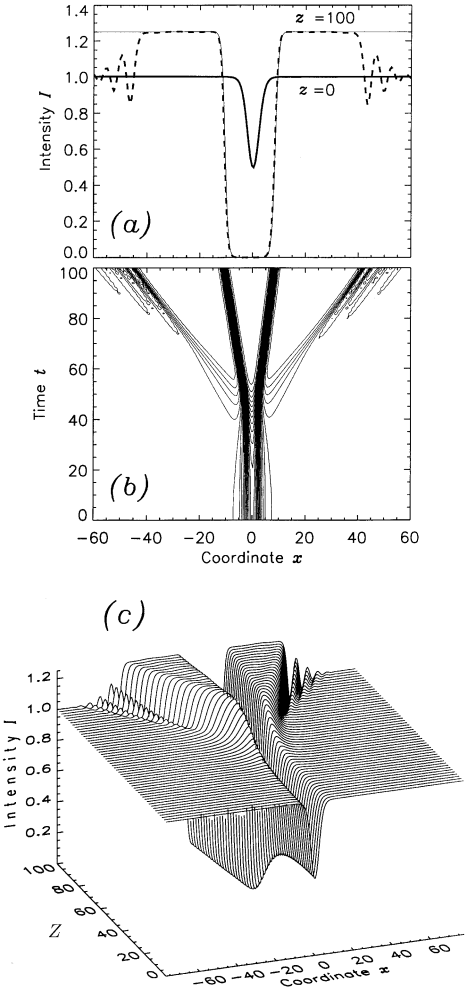

Fig. 11. 'Collapse' of the unstable dark soliton, Eqs. (4.23) and (4.24), into two kinks for $\beta = 1.2$, $v_0 = 0.02$, and $\varepsilon = -0.005$. (a) Intensity profiles at $z = 0$ (solid curve) and $z = 100$ (dashed curve), and the corresponding (b) contour plot and (c) propagation dynamics. Thin solid curve in (a) presents, for a comparison, the exact kink solution, Eq. (4.25) (Pelinovsky et al., 1996b).

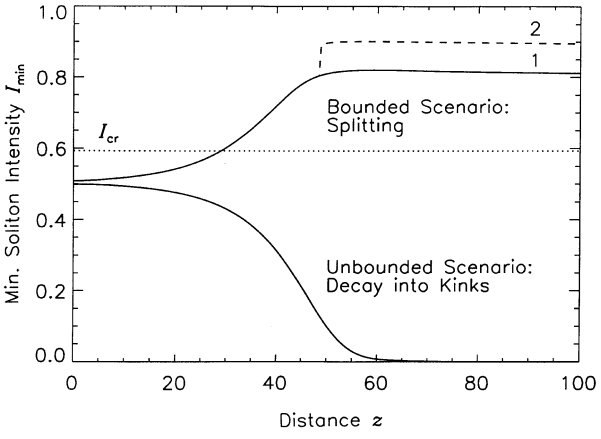

Fig. 12. Change of the minimum soliton intensity $I_{\min}$ for two scenarios of the soliton instability presented in Figs. 10 and 11: splitting (upper solid, 1, and dashed, 2, curves), and decay into kinks (collapse) (lower solid curve). The dotted line displays the critical intensity $I_{\rm cr}$, which corresponds to the instability threshold $v = v_{\rm cr}$ and it is defined in Fig. 9b (Pelinovsky et al., 1996b).

Thus, the dark solitons evolve asymmetrically in dependence of the type of the initial perturbation. Fig. 12 shows the change of the minimum soliton intensity for both the scenarios. In the first case ($\varepsilon > 0$), the initial exponential growth of the perturbation amplitude (thick solid curve) saturates at approximately $z = 55$, and the unstable dark soliton splits into two stable solitons of smaller amplitudes (see curves 1 and 2 in Fig. 12) which move after the splitting into the opposite directions as shown in Fig. 10b and Fig. 10c. When the initial soliton velocity is selected far from the threshold value $v_{\rm c}$, more than two secondary solitons are generated. In the other case ($\varepsilon < 0$), the exponential growth of the initial perturbation allows the minimum intensity to reach zero (see Fig. 12, thin solid line). Then, the region of zero intensity starts to spread out while the background intensity increases outside the localized wave (see Fig. 11b). Finally, this process results in formation and steady-state propagation of two kink structures. These kinks are described by the exact solutions to the generalized NLS Eqs. (4.2) and (4.22) at $p = 1$,

$$\psi_k(\xi, z) = \frac{\sqrt{q_{\rm c}}}{\sqrt{1 + {\rm e}^{\pm \Delta \xi}}}\, {\rm e}^{{\rm i}\omega_{\rm c} z}\,, \tag{4.25}$$

where $q_{\rm c} = 3\alpha/4\beta$, $\omega_{\rm c} = 2\beta q_{\rm c}^2$, and $\Delta^2 = 3\alpha^2/4\beta$. The kink of Eq. (4.25) connects two stable background waves, the cw background of a selected intensity $q_{\rm c}$ with the zero-intensity background.

4.3.2. Saturable nonlinearity

In this section we consider the generalized NLS model, Eq. (4.2), with the saturable nonlinearity, Eq. (2.9), which we write in the following dimensionless form:

$$g(I) = \frac{1}{2}\left[\frac{1}{(1 + aI)^p} - 1\right], \tag{4.26}$$

where the parameter a has the meaning of a ratio of the maximum intensity I_{max} to the saturation intensity, I_{sat}, i.e., $a = I_{max}/I_{sat}$, and the parameter p is the saturation index. This type of nonlinearity in the generalized NLS Eq. (4.2) is used to analyze the effect of saturation of the nonlinear refractive index at larger intensities (see also Introduction). In the case $p = 1$ the nonlinearity, Eq. (4.26), appears also in the theory of photovoltaic bright and dark solitons (Valley et al., 1994; Christodoulides and Carvalho, 1995). On the other hand, the model, Eqs. (4.2) and (4.26), at $p = 2$ is known to exhibit explicit soliton solutions in the form of bright and dark solitons (Królikowski and Luther-Davies, 1992, 1993). With the help of these exact solutions, it has been recently revealed that dark solitons supported by the saturable nonlinearity have a total phase shift larger than the limit value π realized at the black soliton at $v = 0$ (Królikowski et al., 1993). These solitons are clearly observed in numerical simulations to be stable in some region of the parameter region. Later the instability of dark solitons has been pointed out exactly for the same model (Kivshar and Królikowski, 1995b). Here, we present the results for the case $p = 2$ which displays essentially the same dynamics of the dark soliton instabilities as the model, Eqs. (4.2) and (4.26), for other values of p.

Fig. 13a presents the regions of existence, $v < c(a)$, and instability, $v < v_{cr}(a)$, of the dark solitons in the model defined by Eqs. (4.2) and (4.26) at $p = 2$ and $q = 1$. The dashed line in Fig. 13a depicts

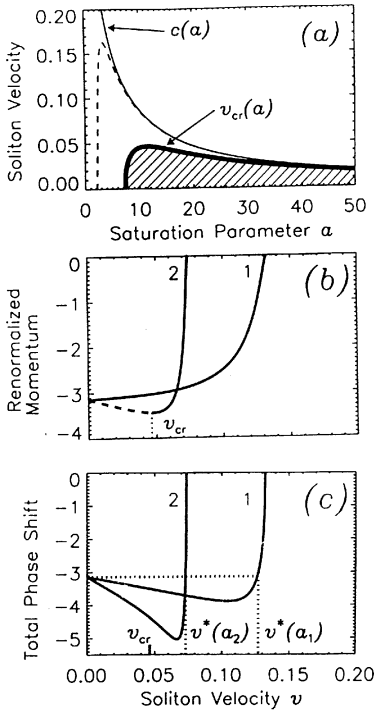

Fig. 13. (a) Regions of existence, $v < c(a)$, and stability, $v < v_{cr}(a)$, of dark solitons in the saturable model, Eqs. (3.42) and (4.26) at $p = 2$. Dashed curve shows the region where a dark soliton has a total phase shift larger than π. Renormalized momentum $M_s(v)$ (b) and the total phase shift $S_s(v)$ (c) calculated for dark solitons at two values of the saturation parameter a: $a = 6$ (curves 1) and $a = 12$ (curves 2). Critical velocity v_{cr} corresponds to the instability threshold (Pelinovsky et al., 1996b).

the region of the parameter plane where the dark solitons have the total phase shift larger than π [see also discussions in Królikowski et al. (1993)]. the typical dependencies of the renormalized momentum $M_s(v)$ and the total phase shift $S_s(v)$ are shown for $a = 6$ and $a = 12$ in Fig. 13b and Fig. 13c, respectively. It is clearly seen that the appearance of a large phase shift of the large-amplitude dark solitons serves as a pilot of their instability. However, among the dark solitons with the phase shift larger than π there exist both stable solitons, realized for smaller amplitudes and larger velocities, and unstable solitons, realized for larger amplitudes and smaller velocities (see Fig. 13a).

Next, the development of the dark soliton instability in the saturable model described by Eqs. (4.2) and (4.26) at $p = 2$ is presented in Fig. 14a–c. If follows that the instability-induced soliton dynamics in this model displays features which are different from those for the case of competing nonlinearities. Indeed, being perturbed by a small perturbation, the unstable black soliton transforms symmetrically into a stable grey soliton which corresponds to a positive slope of the function $M_s(v)$ as shown in Fig. 14a. Despite the change of the soliton velocity is small for the nonlinearity (4.26) at $p = 2$ the change of the minimum soliton intensity (see Fig. 14b) and the soliton position (see Fig. 14c) clearly indicate an initial, exponential growth of the perturbations at

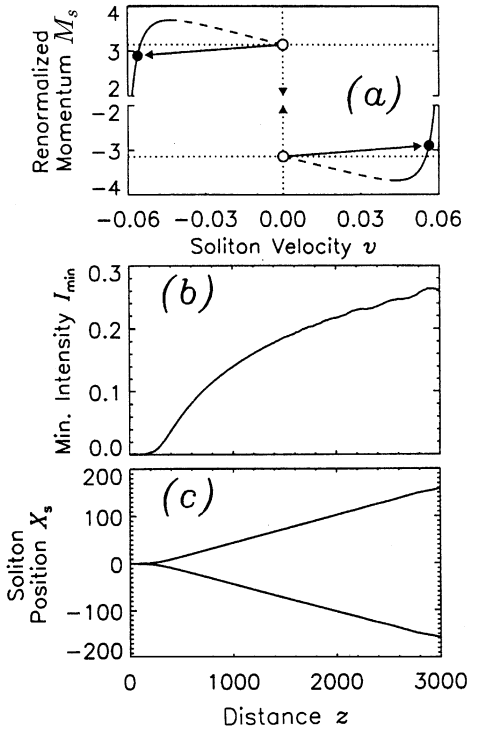

Fig. 14. Dynamics of an unstable black soliton in the model, Eqs. (3.42) and (4.26) at $p = 2$ and $a = 12$. Shown are: (a) renormalized momentum $M_s(v)$ and transitions corresponding to a transformation of an unstable 'black' soliton into a stable 'grey' soliton depending on a sign of the initial perturbation, (b) change of the minimum soliton intensity I_{min}, (c) change of the soliton position (Pelinovsky et al., 1996b).

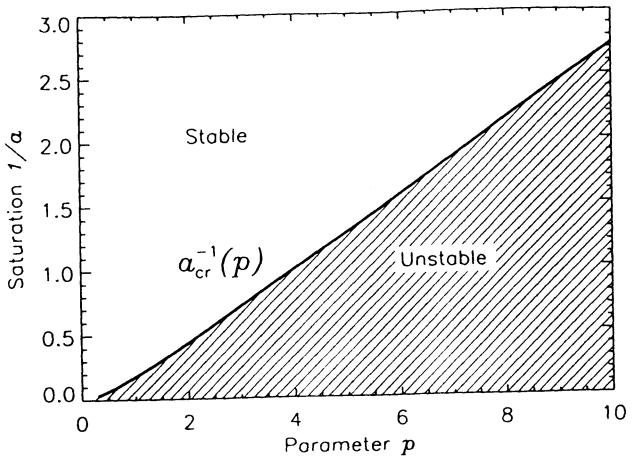

Fig. 15. Stability threshold curve for dark solitons of the generalized model of saturable medium, Eq. (4.26), as the dependence of the critical saturation intensity a_{cr}^{-1} vs. the parameter p (Kivshar and Afanasjev, 1996).

the unstable black soliton and, then, their saturation at the level which corresponds to a stable grey soliton. The development of the instability of a grey soliton occurs basically in the same manner. The novel feature is asymmetric transitions to the right and to the left (see Pelinovsky et al., 1996b).

The similar instability exists for any p in the model described by Eqs. (4.2) and (2.9). Fig. 15 presents the threshold of the instability of a black soliton for the model, Eqs. (4.2) and (4.26), as a function of the saturation parameter p (Kivshar and Afanasjev, 1996).

4.3.3. Transiting nonlinearity

In this section we consider one more example of the model of optical solitons described by the generalized NLS Eq. (4.2). This is the case of bistable solitary waves introduced, for the first time, for bright solitons by Kaplan (1985a,b). In the case of dark solitons, bistability can appear when the branch of unstable solitons is found for intermediate values of the soliton velocity allowing transitions between two (or more) types of solitons belonging to stable branches. For the first time, the bistability of dark solitons was discussed by Enns and Mulder (1989), Mulder and Enns (1989) and Bass et al. (1992), who however used the complementary power P_s for discussing the bistability regimes. As has been clarified above, the complementary power can possess both positive and negative slopes, but it does not characterize the soliton stability and therefore bistable regimes should be analyzed in the framework of the renormalized soliton momentum [see Pelinovsky et al. (1996b)].

The typical nonlinearity displaying soliton bistability was suggested by Enns and Mulder (1989) and it is a kind of defocusing *transiting nonlinearity*,

$$g(I) = -I\{1 + \alpha \tanh[\gamma(I^2 - I_0^2)]\}\,, \tag{4.27}$$

which describes a smooth transition from one linear dependence for small intensities, $I \ll I_0$, when $g(I) = [\alpha \tanh(\gamma I_0^2) - 1]I$, to the other linear dependence for large intensities, $I \gg I_0$, when

$g(I) \sim -(1+\alpha)I$. Parameters α, I_0 in Eq. (4.27) characterize the amplitude and threshold intensity of the nonlinearity transition, while $\gamma^{-1/2}$ determines the characteristic width of the transition region.

The renormalized soliton momentum $M_s(v)$ for dark solitons of the model, Eq. (4.2), with the transiting nonlinearity, Eq. (4.27), at $\alpha = 0.5$, $\gamma = 10$, and varying I_0, is shown in Fig. 16a. There exists a rather narrow region of the soliton velocities where the momentum $M_s(v)$ has a negative slope indicating a possibility of bistable dark solitons.

Fig. 16b presents an enlarged part of one of the dependencies $M_s(v)$ of Fig. 16a which displays stable (solid) and unstable (dashed) branches. The instability region, $v_{cr}^{(1)} < v < v_{cr}^{(2)}$, where, at $I_0 = 0.6$, $v_{cr}^{(1)} \approx 0.955$ and $v_{cr}^{(2)} \approx 1.014$, is rather narrow, and it is defined by the criterion $\partial M_s(v)/\partial v < 0$. The characteristic feature of the transiting nonlinearity is the stability of black solitons, which belong to one of the stable branches. Thus, in this case the unstable branch corresponds to *grey solitons*.

Numerical simulations of the instability-induced dynamics of dark solitons in the model, Eqs. (4.2) and (4.27), have been performed for a dark soliton with the initial velocity $v_0 = 0.96$ (see Pelinovsky et al., 1996b). The dynamics displays indeed two types of the transitions (switching) of a dark soliton from the unstable to one of the stable (1 or 2) branches of the stationary solutions. The first type of the soliton switching describes a transition to a stable dark soliton with larger value of the minimum intensity and larger velocity, as shown by the curves 1 in Fig. 17a–c.

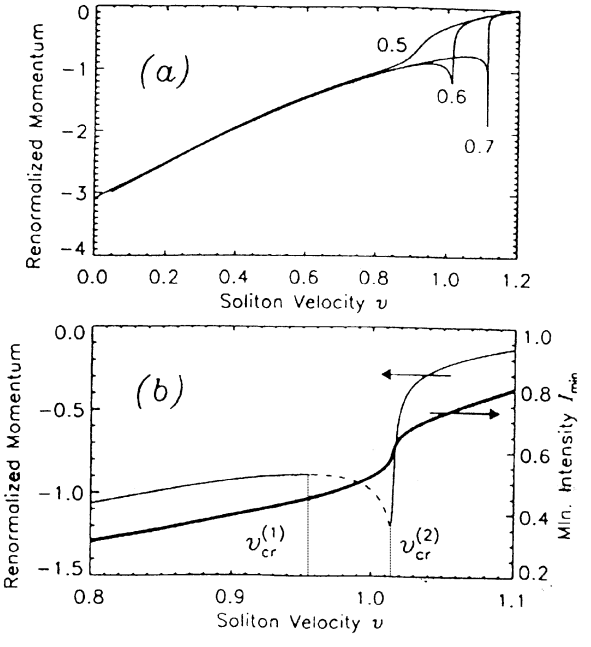

Fig. 16. (a) Renormalized momentum $M_s(v)$ for dark solitons supported by the transiting nonlinearity, Eq. (4.27) for $\alpha = 0.5$, $\gamma = 10$ and different values of the parameter I_0: 0.5, 0.6, and 0.7, shown next to the curves. (b) Stable (thin solid) and unstable (dashed) branches of the soliton renormalized momentum $M_s(v)$ for the case $\alpha = 0.5$, $\gamma = 10$, and $I_0 = 0.6$. The thick solid curve displays a change of the minimum soliton intensity I_{min} vs. soliton velocity v (Pelinovsky et al., 1996b).

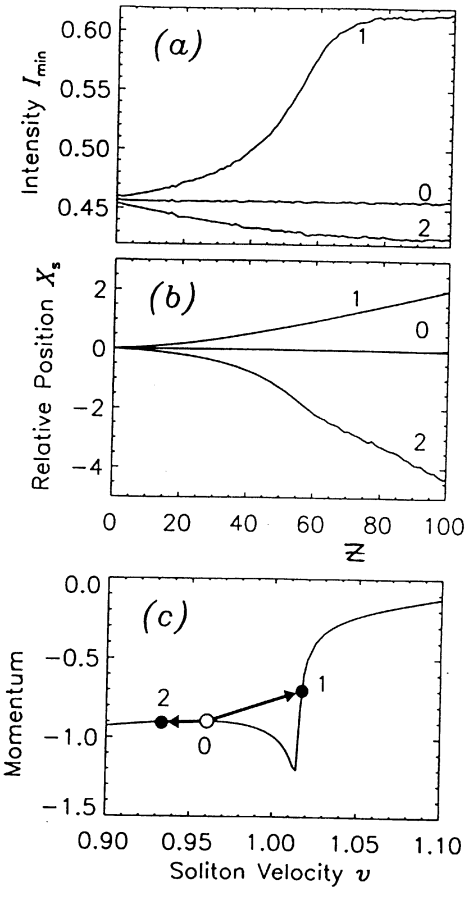

Fig. 17. Dynamics of the unstable dark soliton in the model, Eq. (3.42), with the transiting nonlinearity, Eq. (4.27), for $\alpha = 0.5$, $\gamma = 10$, and $I_0 = 0.6$. Soliton initial velocity $v_0 = 0.96$. Shown are (a) evolution of the minimum soliton intensity $I_{\min}$, and (b) change of the relative position of a soliton on a moving background, for both the unperturbed soliton (curves 0) and two types of the bounded scenario for the evolution of a perturbed dark soliton (curves 1 and 2). Transitions from the unstable branch to the stable branches (1 or 2) are shown in (c) by arrows on the plot of the renormalized momentum (Pelinovsky et al., 1996b).

The second type describes a transition to another stable dark soliton, with smaller value of the minimum intensity $I_{\min}$ and smaller velocity v, as shown by the curves 2 in Fig. 17a–c. In the latter case, the transition is observed with negligible radiation and, therefore, at almost unchanged value of the soliton renormalized momentum.

5. Multi-component dark solitons

5.1. Mode interaction: general overview

Solitary waves discussed above are described by one-component scalar fields. This is the simplest case of *single-frequency* pulses in optical fibers or *scalar* TE electric field in optical waveguides

under the condition of *nonresonant* optical nonlinearities. If either or both of these conditions is not satisfied, the scalar generalized NLS equation is not valid (see, e.g., Section 2.3) and the field of the main frequency (or main polarization) becomes coupled to other components. This is the case of the so-called multi-mode wave propagation which usually leads to *multi-component solitary waves*.

For the pulse propagation in a nonlinear optical fiber, such a situation appears in multi-mode fibers due to coupling between the modes through nonlinearities and nonuniformities of the optical material, and the pulse propagation is then described by a system of coupled NLS equations [see, e.g., Crosignani and DiPorto (1981, 1982)]. The same physics is behind the birefringency effect which leads to a coupling between two polarizations (Menyuk, 1989). Different in physics, the interaction between pulses or beams of two different frequencies lead to the similar system of coupled NLS equations, provided the four-wave mixing is neglected (see, e.g., Ryskin (1994), and references therein).

Nonlinear interaction between two polarizations arising from the tensor nature of the nonlinear $\chi^{(3)}$ susceptibility was first discussed by Maker et al. (1964) who showed that the nonlinear polarization in an isotropic medium may be written in the form

$$P_{\mathrm{NL}} = \chi^{(3)}[A(\omega)\boldsymbol{E}(\boldsymbol{E}\cdot\boldsymbol{E}^{*}) + B(\omega)\boldsymbol{E}^{*}(\boldsymbol{E}\cdot\boldsymbol{E})]\,.$$

The effect of this vectorial interaction between perpendicular polarizations on modulational instability and solitary waves was first considered in the pioneering paper by Berkhoer and Zakharov (1970).

Generally speaking, there exist *five* principally different cases of the coupling between two modes in a Kerr medium and corresponding vectorial solitary waves (for simplicity, we assume the case of the temporal solitons and focusing nonlinearity):

- Bright solitons, each in the mode with the anomalous dispersion (*vector bright solitons*) [e.g., Berkhoer and Zakharov (1970), Manakov (1974), Tratnik and Sipe (1988), Christodoulides and Joseph (1988) and Menyuk (1989)];
- Bright soliton in the mode with the anomalous dispersion coupled to a dark soliton in the mode with normal dispersion (*normal dark–bright pair*) [e.g., Afanasjev et al. (1989a,b), Wang and Yang (1990), Hong et al. (1991), Kivshar (1992) and Buryak et al. (1996a)];
- Bright soliton in the mode with normal dispersion exists due to mutual coupling to a dark soliton in the mode with anomalous dispersion (the so-called *inverted dark–bright pair*) [e.g., Trillo et al. (1988) and Afanasjev et al. (1989a)];
- Two dark solitons, each in the mode with the normal dispersion (*vector dark solitons*) [e.g., Kivshar and Turitsyn (1993), Haelterman and Sheppard (1994d,e), Radhakrishnan and Lakshmanan (1995) and Sheppard and Kivshar (1997)];
- Bright pulse supported by a dark soliton, both modes are with the normal dispersion (*soliton-induced waveguides*, in the linear limit, or *dark–bright pair*, in a nonlinear regime) [e.g., Christodoulides (1988) and Sheppard and Kivshar (1997)].

All these cases are described by two NLS equations, coupled due to crossphase modulation. These coupled equations become *asymmetric* for the interaction between envelope of different carrier frequencies or some additional coupling terms, e.g. due to *four-wave mixing* effect, may appear.

There is a little known about vectorial dark solitons and dark–bright in non-Kerr materials and in the systems described by the equations different from the coupled NLS equations. We would like

to mention dark-soliton pairs in a nonlinear coupler (Ankiewicz et al., 1994), which are probably all unstable, families of unstable multimode dark–bright solitons predicted for a photorefractive medium with a refractive index change of opposite sign for different polarization (Królikowski et al., 1996), and incoherently coupled dark–bright solitons pairs in a biased photorefractive medium (Christodoulides et al., 1996). Stability of this kind of vectorial solitons is one of the most important issues and, after very recent advances in the stability of multi-parameter solitary waves (Buryak et al., 1996b) we can expect some progress in the near future.

There exists a variety of different problems involving multi-component wave interaction and, as a matter of fact, a systematic approach to multi-component dark solitons as solitons of nonlinear equations describing such interaction is absent. That is why, in this section we discuss only a few the most characteristic examples of solitary waves existing on a nonvanishing background (e.g., dark–bright soliton pairs, polarization domain walls, and dark solitons in $\chi^{(2)}$ materials) just to show how the concept of dark soliton can be generalized to include more than one field. However, we notice that there exist more open questions than solved problems in the theory of multi-component dark solitons.

5.2. Dark–bright solitons

5.2.1. Model and exact solutions

We consider the interaction between either (i) two waves of different frequencies ω_1 and ω_2, or (ii) two waves of the same frequency ω but belonging to two different polarizations. Then, for the slowly varying wave envelopes u_1 and u_2, the most important nonresonant interaction between the waves is due to the cross-phase modulation effect, and the problem can be described by the system of two coupled NLS equations

$$\mathrm{i}\left(\frac{\partial u_1}{\partial \zeta} + \delta \frac{\partial u_1}{\partial \xi}\right) + \gamma_1 \frac{\partial^2 u_1}{\partial \xi^2} + g_1(|u_1|^2 + \sigma|u_2|^2)u_1 = 0\,, \tag{5.1}$$

$$\mathrm{i}\left(\frac{\partial u_2}{\partial \zeta} - \delta \frac{\partial u_2}{\partial \xi}\right) + \gamma_2 \frac{\partial^2 u_2}{\partial \xi^2} + g_2(|u_2|^2 + \sigma|u_1|^2)u_2 = 0\,. \tag{5.2}$$

In nonlinear optics, Eqs. (5.1) and (5.2) appear in two different physical situations. In the first, or *spatial* case, these equations describe interaction between two continuous waves of distinct frequencies ω_1 and ω_2 with ξ standing for the transverse coordinate, and $\gamma_j = 1/2k(\omega_j)$ take into account the mode diffraction. In the second, or *temporal* case, ξ stands for time, $\delta = \frac{1}{2}(\delta_1 - \delta_2)$, where $\delta_j = \mathrm{d}k(\omega_j)/\mathrm{d}\omega_j$ are the modal group velocities, and $\gamma_j = -\frac{1}{2}\mathrm{d}^2k(\omega_j)/\mathrm{d}\omega_j^2$ describe the modal dispersions (see Sections 2.1 and 2.2.2).

We are interested below in stationary solutions of Eqs. (5.1) and (5.2), when the (small) group-velocity mismatch is compensated due to the nonlinearity-induced shift of the carrier frequency, so that we apply the transformation,

$$u_1 = W\frac{\sqrt{|\gamma_2|}}{\sqrt{g_2|\gamma_1|}}\,\mathrm{e}^{\mathrm{i}k_1\xi - \mathrm{i}\omega_1\zeta}\,, \qquad u_2 = \frac{U}{g_1}\,\mathrm{e}^{\mathrm{i}k_2\xi - \mathrm{i}\omega_2\zeta}\,,$$

where $\omega_j = \pm \delta k_j + \gamma_j k_j^2$ ($j = 1, 2$) are the nonlinearity-induced shifts of the wave frequency, and $k_j = \pm \delta/2\gamma_j$. Then, the dimensionless envelopes W and U satisfy the following system of coupled NLS equations:

$$\mathrm{i}\frac{\partial W}{\partial t} + s\frac{\partial^2 W}{\partial x^2} + (\eta|W|^2 + \sigma|U|^2)W = 0\,, \tag{5.3}$$

$$\mathrm{i}\rho\frac{\partial U}{\partial t} + r\frac{\partial^2 U}{\partial x^2} + \left(\frac{|U|^2}{\eta} + \sigma|W|^2\right)U = 0\,, \tag{5.4}$$

where $t = \zeta$, $x = \xi/\sqrt{|\gamma_1|}$, $\rho = |\gamma_1|/|\gamma_2|$, and $\eta = g_1/\rho g_2$. The sign functions $r \equiv \mathrm{sgn}(\gamma_1) = \pm 1$ and $s \equiv \mathrm{sgn}(\gamma_2) = \pm 1$ describe the type of the group-velocity dispersion, negative or positive. This is the most general system describing two incoherently coupled nonlinear modes in a Kerr medium.

The parameters η and ρ produce an effective asymmetry between the modes for the case of the interaction between waves of the different frequencies, e.g., $\eta = (\omega_1/\omega_2)^2$ and $\rho = (\omega_1/\omega_2)^3$. The coefficient σ in Eqs. (5.3) and (5.4) is the parameter of the cross-phase modulation which can be defined in terms of parameters of the corresponding physical problems [see, e.g., Agrawal (1989), and Menyuk (1989)], and usually $0 < \sigma \leq 2$. For example, in fiber optics the system of Eqs. (5.3) and (5.4) describes interaction between either two waves of the same carrier frequency but belonging to different polarizations, or two waves of the same polarization but different frequencies. For two waves of different frequencies ω_1 and ω_2, one usually has ($\eta = \omega_1^2/\omega_2^2$) $\sigma = 2$, whereas for two waves of different polarizations in a birefringent optical medium, ($\eta = 1$) $\sigma = \frac{2}{3}$ (Menyuk, 1989).

As has been mentioned in Section 5.1, Eqs. (5.3) and (5.4) allow the existence of five different types of localized solutions for solitary waves. In this section we are interested in finding coupled soliton states, *dark–bright vector solitons*, which combine dark (in the W-component) and bright (in the U-component) solitary waves, so that we look for stationary solutions of the system of Eqs. (5.3) and (5.4) in the form,

$$W(\zeta, \tau) = w(x, t)\,\mathrm{e}^{\mathrm{i}\eta t}\,, \quad U(\zeta, \tau) = u(x, t)\,\mathrm{e}^{\mathrm{i}\frac{\beta}{\rho}t}\,\mathrm{e}^{\mathrm{i}\theta}\,, \tag{5.5}$$

where $x = \zeta - v\tau$, $t = \tau$, $\theta = r\rho(\frac{V}{2}x + \frac{v^2}{4}t)$, $w = w_r + \mathrm{i}w_i$ and u are complex and real functions, respectively. The following boundary conditions are posed: $|w(x)|^2 \to 1$ and $u(x) \to 0$ as $x \to \pm\infty$. Substitution of Eq. (5.5) into Eqs. (5.3) and (5.4) yields the system of equations,

$$\begin{aligned}
&\mathrm{i}\frac{\partial w}{\partial t} - \mathrm{i}v\frac{\partial w}{\partial x} - \frac{\partial^2 w}{\partial x^2} + [\eta(|w|^2 - 1) + \sigma|u|^2]w = 0\,,\\
&\mathrm{i}\rho\frac{\partial u}{\partial t} - r\frac{\partial^2 u}{\partial x^2} - \beta u + \left(\frac{|u|^2}{\eta} + \sigma|w|^2\right)u = 0\,,
\end{aligned} \tag{5.6}$$

which defines a family of *stationary two-parameter solitons*, $w = w_0(x) = w_{0\mathrm{r}}(x) + \mathrm{i}w_{0\mathrm{i}}(x)$ and $u = u_0(x)$, provided that the t-derivatives are omitted. These localized solutions are defined by two independent parameters, the propagation constant β and soliton velocity v.

Because Eq. (5.6) are not integrable, most localized solutions can be found only numerically. However, there exists a special sub-class of analytical solutions of Eq. (5.6) describing a

one-parameter family of dark–bright solitons,

$$w_0(x) = \cos\varphi \tanh(\gamma x) + \mathrm{i}\sin\varphi\,, \quad u_0(x) = a\,\mathrm{sech}(\gamma x)\,, \tag{5.7}$$

where $\gamma^2 = \eta(1-\sigma^2)/(2+2\eta\sigma) - v^2/4$, $a^2 = 2\gamma^2(\eta+\sigma)/(1-\sigma^2)$, $\tan\varphi = -v/(2\gamma)$, and $\beta = \gamma^2 + \sigma$. These analytical solutions exist only for $\sigma^2 < 1$ (and at $r = +1$) and they can be characterized by one continuous parameter (e.g., the soliton velocity V) generalizing the zero-parameter family of solitons found earlier by Afanasjev et al. (1989a,b). However, the exact solutions give only a *subset* of a more general family of vector solitons of Eq. (5.6). Each of these *stationary* solutions generates the corresponding *nonstationary* solitons through the standard Galilean transformation.

5.2.2. Soliton-induced waveguides

To explain the existence and some of the features of the bright–dark localized solutions of the model described by Eqs. (5.3) and (5.4) we study bifurcations from the one-component solutions. This analysis also allows to introduce an important physical concept of the soliton-induced waveguides and light guiding.

First, we consider the solution of Eqs. (5.3) and (5.4) as a one-component dark soliton and add small perturbations writting, $U = \mathrm{O}(\varepsilon)$, and $W = W_s(x,t) + \mathrm{O}(\varepsilon^2)$, where W_s is the one-component dark soliton ($s = -1$),

$$W_s(x,t) = \mathrm{e}^{\mathrm{i}\eta t}\tanh(x\sqrt{\eta/2})\,, \tag{5.8}$$

with the background amplitude $W_0 = 1$. It is easy to verify from Eqs. (5.3) and (5.4) that the term $\mathrm{O}(\varepsilon)$ in the expansion for W is zero. Substituting this expansion into Eqs. (5.3) and (5.4), we obtain, to the leading order, two decoupled equations, of which the equation for U is

$$\mathrm{i}\rho\frac{\partial U}{\partial t} + r\frac{\partial^2 U}{\partial x^2} + \sigma|W_s|^2 U = 0\,. \tag{5.9}$$

Stationary solutions of Eq. (5.9) can be presented in the form

$$U(x,t) = \mathrm{e}^{\mathrm{i}(\Lambda/\rho)t} f(X)\,; \quad X = x\sqrt{\eta/2}\,, \tag{5.10}$$

where the function $f(X)$ is a solution of the following eigenvalue problem

$$r\frac{\mathrm{d}^2 f}{\mathrm{d}X^2} - \frac{2\sigma}{\eta\cosh^2 X} f = \frac{2}{\eta}(\Lambda - \sigma) f\,, \tag{5.11}$$

with Λ to be determined.

The eigenvalue problem, Eq. (5.11), is well known in many branches of physics. In particular, in optical waveguide theory it is the model equation of the sech^2-profile graded index planar waveguide (Snyder and Love, 1973). For $r = -1$ the eigenvalue problem of Eq. (5.11) has solutions $f(X)$ that decay as $X \to \pm\infty$ only if $\Lambda < \sigma$ (the so-called *guide or bound modes*). The number of such bound modes depends on the parameter σ/η. In particular, for $\sigma/\eta = 2$ we have two localized solutions [see, e.g., Snyder and Love (1973)]. The lowest-order (symmetric) solution $U_1 = \mathrm{sech}^{\nu} X$ exists for $\nu = 1.56$ and it appears at the critical value $\Lambda = \Lambda_1 = 0.78$. This corresponds to a bifurcation of the vector soliton (W, U) in which a symmetric function U branches from

the one-component dark soliton W_s, and it describes a linearized limit of the coupled dark and bright solitons.

In contrast, for $r = +1$ there exist no localized eigenfunctions of the problem described by Eq. (5.11) which in this case describes the so-called 'anti-waveguide'. This means that, if coupled bright and dark solitons are possible, they should correspond to a nonzero threshold energy and they have no linear limit described by an effective linear guided mode.

The phenomenon described above is usually referred to as *soliton-induced waveguiding* of a weak probe beam, $U \ll |W_s|$, and it was widely discussed in the literature. Probably for the first time, the use of an effective waveguide created by the refractive index change due to an intense electromagnetic beam was discussed by Askar'yan (1962) who analyzed the effect of the beam gradient on electrons and atoms and suggested it for directing electrons and plasma transport. In application to the light guiding by solitary beams, there exist many papers discussing basically the same idea for both spatial and temporal solitons [see, e.g., Manassah (1991)]. The use of dark solitons as induced waveguides was suggested and verified experimentally by Luther-Davies and Yang (1992a,b).

For temporal solitons in fibers, the phenomenon of the soliton-induced waveguide can be used for compression of bright pulses by dark solitons. This effect was suggested by Jin et al. (1993) who however did not mention the physical origin of this effect due to waveguiding properties of dark solitons. Jin et al. (1993) demonstrated numerically that bright pulses can be compressed in the region of normal dispersion (which is inaccessible in the soliton compression scheme) by coupling it to a dark soliton of a finite width background. The best compression ratio of this scheme was reported to be 3.3 (Jin et al., 1993). The effect of pulse walk-off on the compression of bright pulses by dark solitons was discussed by Cao and Zhang (1996) who demonstrated that the walk-off is crucial leading to asymmetric pulses, much lower compression ratios and longer compression lengths. They also pointed out that asynchronous coupling of the bright pulse with a dark soliton can improve the compression scheme.

When the amplitude of the probe beam U grows, it cannot be described any longer by the effective linear Eq. (5.11) and therefore the full system of two incoherently coupled NLS equations should be considered. In the framework of this model, the case of the soliton-induced waveguide at $r = -1$ corresponds to the linear limit of the dark-bright solitary wave. General solutions of this kind have been not investigated yet in details, including the stability analysis similar to the case of the opposite dispersions discussed in Section 5.3. However, it was recently found that the integrable case of the Manakov equations ($\sigma = \rho = \eta = 1$) for defocusing nonlinearity allows a detailed analysis (Radhakrishnan and Lakshmanan, 1995; Sheppard and Kivshar, 1997) and the existence of N-soliton solutions describing interaction of dark–bright vector solitons (Sheppard and Kivshar, 1997). How the main features of these solitary waves survive in a more general nonintegrable model has not been understood yet, and this issue requires the further analysis.

5.3. Modes with opposite dispersions

For the case of opposite dispersions, i.e, at $r = +1$, the dark soliton behaves like an anti-waveguide and therefore it cannot guide a small-amplitude probe beam. The important question then is to find if the soliton guiding will become possible in a nonlinear regime, which is described by the coupled NLS equations, with the dark–bright vector solitary waves. Also, stability of these solitary waves seems to be the important issue to be analyzed.

To find localized solutions of the model of Eq. (5.6) describing the coupled bright and dark solitons in the case of opposite dispersions, Buryak et al. (1996a) used a numerical scheme based on a relaxation technique to solve three coupled ordinary differential equations of the second order. As a result, they found that in a physically important domain of the system parameters η and σ, i.e. $\eta \sim 1$ and $0 < \sigma \leq 2$, they system of Eq. (5.6) possesses a two-parameter family of stationary solutions with the asymptotics $|w(x)|^2 \to 1$ and $u(x) \to 0$ at $x \to \pm\infty$. Such solitons exist in a certain region, $\beta > \beta_{cr} = \sigma$ and $|v| < v_{max}(\beta)$ [see Buryak et al. (1996a)]. The exact solutions given by Eq. (5.7) correspond to a parabolic curve in this plane. This dark–bright solitons was characterized by Buryak et al. (1996a) by two integral quantities, *the power of the bright soliton* in the u-component,

$$P_u(\beta; v) = \int_{-\infty}^{+\infty} |u|^2 \, dx \,, \tag{5.12}$$

and *the renormalized momentum of the dark soliton* in the w-component which is defined as follows:

$$M_w(v; \beta) = \frac{i}{2} \int_{-\infty}^{+\infty} \left\{ w^* \frac{\partial w}{\partial x} - w \frac{\partial w^*}{\partial x} \right\} \left\{ 1 - \frac{1}{|w|^2} \right\} dx \,. \tag{5.13}$$

Note that the power P_u is an integral of motion of the system, Eq. (5.6), whereas the second conserved quantity is the total momentum $M_{tot} = M_u + M_w$, where

$$M_w(v; \beta) = \frac{i}{2} \rho \int_{-\infty}^{+\infty} \left\{ u^* \frac{\partial u}{\partial x} - u \frac{\partial u^*}{\partial x} \right\} dx \,. \tag{5.14}$$

Typical examples of dark–bright solitons and the change of the functions $P_u(\beta)$ at $v = 0$ and $M_w(v)$ at $\beta = 1.5$ are displayed in Fig. 18a and Fig. 18b, respectively. An important conclusion following from these plots is that, for almost all values of β and v within the region of the soliton existence soliton bistability is observed. The lowest order (i.e., one-soliton) solutions belong to two main branches which differ by the value of the phase jump across the dark-component (see inserts in Fig. 18b). In particular, for $v = 0$ one of the branches corresponds to a dark soliton with the (maximum) phase jump equal exactly to π (point and insert E in Fig. 18b) whereas the other one, to a dark soliton with *no phase jump* (point D). For any nonzero velocity v, the solitons of the lower branch also possess a phase jump (see the change of the soliton profiles in Fig. 18b, when going along the sequence D → F → H). As the velocity v increases, the difference between the phase jumps of the solitons of the two types becomes smaller and exactly at $|v| = v_{max}(\beta)$ the two branches merge (point H in Fig. 18b). The *critical* point H, where the derivative $\partial M_w/\partial v$ tends to infinity, separates the solutions into two distinct families. As β approaches its minimum value, $\beta_{cr} = \sigma$, the soliton amplitudes decrease (see the insert C in Fig. 18a), and we can apply the small-amplitude approximation suggested by Kivshar (1991b). For example, for $\sigma^2 < 1$ we obtain the asymptotic dependence

$$P_u(\beta; v) \approx \frac{4\eta(2\eta - v^2)\sqrt{\beta - \sigma}}{[2\eta(1 - \sigma^2) - v^2]} \,,$$

shown in Fig. 18a for the case $v = 0$ as a dashed curve.

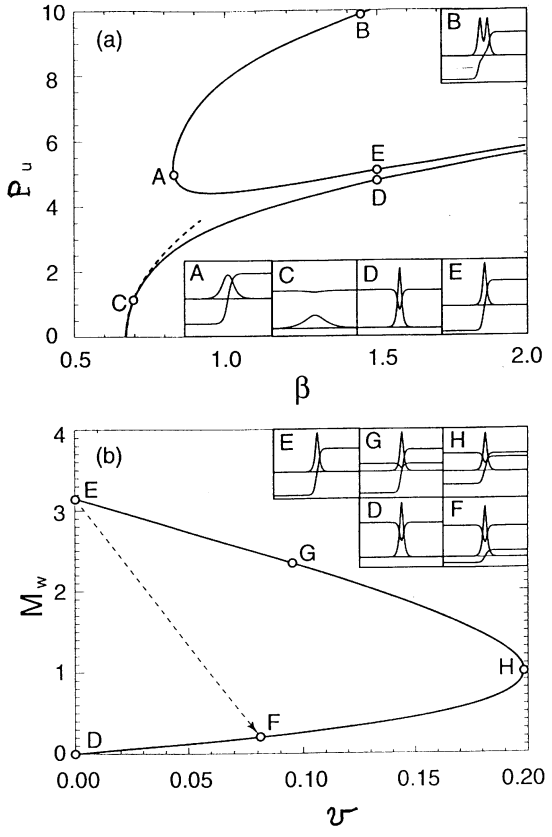

Fig. 18. (a) Characteristic dependence of the energy Q_u, Eq. (5.12), vs. β for $V = 0$, $\sigma = \frac{2}{3}$, and $\eta = 1$. Upper branch describes a transition from one-hump (e.g., points E and A) to two-hump (e.g., point B) solitons. Dashed curve is the analytical result (Kivshar, 1992). (b) Characteristic dependence of the renormalized momentum M_w, Eq. (5.13), vs. V ($V > 0$) for $\beta = 1.5$. Inserts show the profiles of the bright component (vanishing at $x \to \pm\infty$) and dark component, both real (antisymmetric) and imaginary (symmetric) parts (Buryak et al., 1996a,b).

The general stability criterion for dark–bright solitons in the model, Eq. (5.6), has to be obtained analytically by Buryak et al. (1996a,b) using the multi-scale asymptotic method proposed earlier (Pelinovsky et al., 1995). This criterion, as has been revealed recently, is a particular case of the general criterion of instability for two-parameter solitary waves investigated in details for the case of three-wave resonant interaction in a diffractive medium (Buryak et al., 1996b). The threshold of the soliton instability is defined by the condition

$$\frac{\partial P_u}{\partial v}\frac{\partial M_{\rm tot}}{\partial \beta} - \frac{\partial P_u}{\partial \beta}\frac{\partial M_{\rm tot}}{\partial v} = 0\,. \tag{5.15}$$

To simplify the discussion of stability, Buryak et al. (1996a) considered the case $v = 0$ when the first term in Eq. (5.15) vanishes because $\partial P_u/\partial v \to 0$ for $v \to 0$. This factorizes the general stability condition into *two conditions* which can be understood as symmetric (or bright-type) and

antisymmetric (or dark-type) instabilities. For the solitons of the lower branch in Fig. 18a, $\partial P_u/\partial\beta > 0$, and thus these dark–bright solitons are always stable with respect to bright-type instability which results in a symmetric growth of the amplitude of the u-component. In contrast, for the solitons of the upper branch, the derivative $\partial P_u/\partial\beta$ can be negative (see, e.g., Fig. 18a), and thus these solitons can become unstable with respect to symmetric perturbations.

The analysis of the dark-type instability shows that the solitons of the upper branch (see Fig. 18b) are always unstable to antisymmetric perturbations. On the other hand, because of the relation $\partial M_{\rm tot}/\partial v = \partial M_w/\partial v - r(\rho^2/2)P_u$, the stability criterion defined by the second condition becomes $\partial M_w/\partial v < r(\rho^2/2)P_u$, and it predicts instability for the solitons of the lower branch if the parameter ρ is small enough, i.e., for $\rho < \rho_{\rm cr}(\sigma, \eta, \beta)$, and it predicts stability otherwise. Stability diagram was found and also verified numerically by Buryak et al. (1996a), and it is shown in Fig. 19. This diagram proves that stable dark–bright solitons can exist even in the case of the opposite dispersions when there exist no linear guided modes trapped by a dark soliton. These dark–bright solitons can be however stable only if the power of a bright component is not too high and the corresponding dark component does not have a phase-jump. This condition is not restricted by a particular choice of σ, but with increase of σ in Eqs. (5.3) and (5.4), the instability threshold $\rho_{\rm cr}$ also rapidly increases.

5.4. Polarization instability and domain walls

An interesting class of localized solutions with nonvanishing boundary condition was shown to exist in the case of vectorial interaction between polarizations in an isotropic medium [see, e.g., Haelterman and Sheppard (1994a–e); Malomed (1994)].

Following Haelterman and Sheppard (1994c,e), we consider propagation of polarized light in an isotropic Kerr medium which in dimensionless units can be described by a system of symmetrically

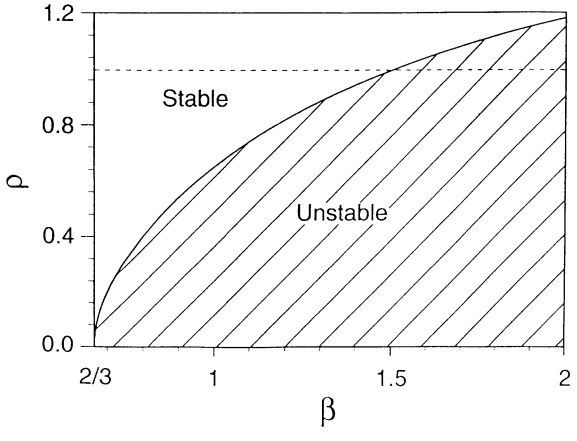

Fig. 19. Stability diagram for the dark–bright solitons of the lower branch of Fig. 18a. Stability threshold is given by the $\rho_{\rm cr}(\beta)$-dependence (Buryak et al., 1996a,b).

coupled NLS equations:

$$\mathrm{i}\frac{\partial E_+}{\partial z} - \frac{1}{2}\frac{\partial^2 E_+}{\partial x^2} + (|E_+|^2 + \sigma|E_-|^2)E_+ = 0\,, \tag{5.16}$$

$$\mathrm{i}\frac{\partial E_-}{\partial z} - \frac{1}{2}\frac{\partial^2 E_-}{\partial x^2} + (|E_-|^2 + \sigma|E_+|^2)E_- = 0\,, \tag{5.17}$$

where E_+ and E_- are the circular polarization components and $\sigma = (1 + B)/(1 - B)$ is the coefficient of the cross-phase modulation. These equations can also describe the case of a highly birefringent optical fibers for which σ is a function of the fiber parameters and $E_\pm$ are the amplitudes of elliptically polarized fiber eigenmodes (Menyuk, 1989).

The simplest solution of Eqs. (5.16) and (5.17) describes the steady state of (linearly polarized) cw mode

$$E_+ = E_- = E_0 \exp\{\mathrm{i}(1 + \sigma)\, E_0^2 z\}\,.$$

The linear stability analysis of this solution was carried out by several authors [e.g., Berkhoer and Zakharov (1970), Agrawal (1987) and Haelterman and Sheppard (1994c)]. We use the standard ansatz $E_\pm = (E_0 + a_\pm)\exp\{\mathrm{i}(1 + \sigma)E_0^2 z\}$, and linearize the NLS equation for small $a_\pm$ looking for the solution in the form $a_\pm = \alpha_\pm \exp(\lambda z)\cos(\Omega x)$. This leads to a characteristic polynomial of the fourth degree in λ, and determines the instability eigenvalue

$$\lambda_1 = \Omega\sqrt{(\sigma - 1)P_0 - \Omega^2/4}\,, \tag{5.18}$$

where P_0 is the power of the cw polarization components, $P_0 = E_0^2$. The maximum gain of the modulational instability is found to be $\lambda_{\max} = (\sigma - 1)P_0$ which corresponds to the optimal frequency $\Omega_\mathrm{m} = [2(\sigma - 1)P_0]^{1/2}$. This kind of modulational instability exist for the normal dispersion regime, when there is no instability of a single NLS equation. That is why it can be called extended, or polarization modulational instability. Importantly, if the cross-phase modulation becomes smaller than self-phase modulation, i.e., $\sigma < 1$, the instability no longer occurs.

It is usually believed that modulational instability should be associated with the existence of localized wave solutions. Indeed, as has been mentioned in Section 2.4, scalar bright solitons are associated with the existence of modulational instability of a scalar focusing NLS equation. Using this analogy, Agrawal (1987) suggested the existence of solitary waves of the coupled system of Eqs. (5.16) and (5.17) associated with the extended modulational instability which can exist even in a defocusing medium (or normal dispersion regime) due to intermode interaction. The link between the extended modulational instability discussed above and solitary waves was demonstrated for the first time by Haelterman and Sheppard (1994e) who demonstrated the existence of the so-called *polarization domain walls* as solitary waves associated with this kind of polarization modulational instability.

Exact stationary localized solutions of the system of Eqs. (5.16) and (5.17) can be found only numerically (Haelterman and Sheppard, 1994c,e). We look for solutions of the form,

$$E_+(x, z) = u(x)\,\mathrm{e}^{\mathrm{i}\beta z}\,, \quad E_-(x, z) = v(x)\,\mathrm{e}^{\mathrm{i}\beta z}\,,$$

where the functions $u(x)$ and $v(x)$ are real and β is the propagation constant. Substituting these expressions into Eqs. (5.16) and (5.17) brings us to the system of two coupled ordinary differential

equations:

$$\frac{1}{2}\frac{d^2u}{dx^2} = -\beta u + u^3 + \sigma v^2 u\,, \tag{5.19}$$

$$\frac{1}{2}\frac{d^2v}{dx^2} = -\beta v + v^3 + \sigma u^2 v\,, \tag{5.20}$$

Eqs. (5.19) and (5.20) describe the motion of a unit mass in the (u, v) plane in the potential

$$U(u, v) = \beta(u^2 + v^2) - \tfrac{1}{2}(u^4 + v^4) - \sigma u^2 v^2\,.$$

The solitary wave solutions correspond to the separatrix trajectories of this potential. The separatrices that connect the pairs of opposite maxima correspond to the circularly polarized NLS dark solitons,

$$u(x) = \sqrt{\beta}\tanh(\sqrt{\beta}x)\,, \qquad v(x) = 0\,,$$

$$u(x) = 0\,, \qquad v(x) = \sqrt{\beta}\tanh(\sqrt{\beta}x)\,.$$

The separatrices connecting opposite saddle points correspond to the linearly polarized NLS dark solitons,

$$u(x) = \pm v(x) = \sqrt{\beta/(1+\sigma)}\tanh(\sqrt{\beta}x).$$

The separatrices connecting adjacent maxima of the potential $U(u, v)$ can be found only numerically for each value of σ because the model described by Eqs. (5.19) and (5.20) is generally nonintegrable. They correspond to the kink shape localized solutions, shown in Fig. 20a–d. The solution of this kind connects two domains of orthogonal stable eignepolarizations of the Kerr medium and that is why it can be called a *polarization domain wall*. It describes a change of the field ellipticity $q = (u - v)/(u + v)$ from $q = +1$ to $q = -1$, while $q = 0$ corresponds to a linear polarization state.

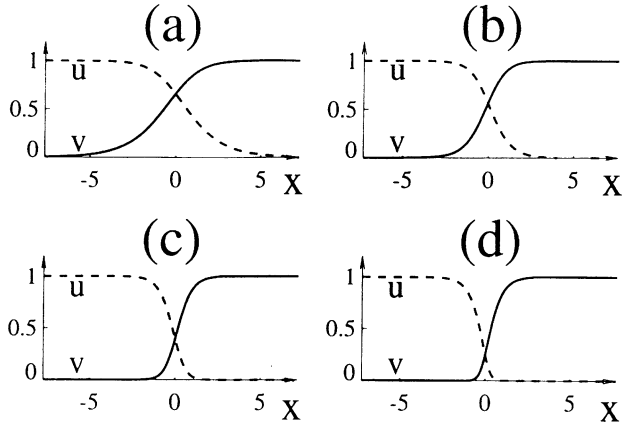

Fig. 20. Envelopes $u(x)$ and $v(x)$ of the polarization domain wall found numerically as localized solutions of Eqs. (5.19) and (5.20) for $\beta = 1$ and (a) $\sigma = 1.2$, (b) $\sigma = 2$, (c) $\sigma = 7$, and (d) $\sigma = 40$.

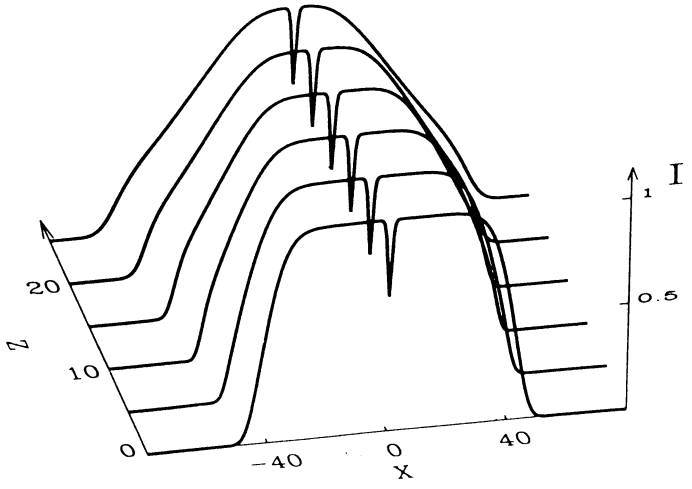

Fig. 21. Numerical simulation of the propagation of the polarization domain wall on a broader square-shaped background. The curves show the total intensity profile of the field $I = E_+^2 + E_-^2$. The polarization state switches from the mode E_+ to the node E_- around $x = 0$ (Haelterman and Sheppard, 1994e).

Haelterman and Sheppard (1994e) demonstrated that the polarization domain wall can be treated as the limiting case of a periodic solution and it can be interpreted as a solitary wave associated with the polarization modulational instability of the coupled NLS Eqs. (5.16) and (5.17). They also checked the stability of this solution by direct numerical simulations of Eqs. (5.16) and (5.17). Fig. 21 shows the example of propagation of the total intensity profile $I = E_+^2(x) + E_-^2(x)$ associated with the polarization domain wall excited on a background beam of a finite extention.

It is important to note that the localized solutions describing domain walls are also known in other fields. Some examples are domain walls between convection patterns of different symmetry being described by the similar system of coupled Ginzburg–Landau equations [see, e.g., Malomed et al. (1990) and Aranson and Tsimring (1995)], and the so-called self-induced gap solitons which separate different standing waves in a discrete lattice (Kivshar, 1993a).

5.5. *Parametric dark solitons in $\chi^{(2)}$ media*

As has been mentioned in Section 2.3, the NLS equation is not valid near resonances where the wave of the fundamental frequency becomes coupled to some other frequency. This means that the solitary waves of the cubic nonlinearity can be drastically modified near such resonant points e.g. due to third-harmonic generation [see, e.g., Sammut et al. (1997)]. Importantly, the similar parametric coupling between waves of different frequencies can lead to solitary waves even in the cases when they are not supported by the leading nonresonant nonlinearity. As has been understood recently, this is the key mechanism leading to solitary waves in optical materials with quadratic (or $\chi^{(2)}$) nonlinearities.

It was shown long time ago [see, e.g., Armstrong et al. (1962) and Ostrovsky (1967)] that a product of second-order nonlinearities can lead to an effective third-order process which resembles a cubic nonlinearity of a Kerr medium. However, only recently experiments have

confirmed (DeSalvo et al., 1992; Nitti et al., 1994) that large nonlinearity-induced phase shift, self-focusing and self-diffraction can be observed in materials with $\chi^{(2)}$ susceptibility due to cascaded $\chi^{(2)}:\chi^{(2)}$ second-order parametric processes. The experimental results have stimulated further efforts in analysing various nonlinearity-induced effects which can be observed due to cascading. In particular, it has been shown that such cascaded nonlinearities can support the intensity-dependent light propagation in the form of spatial (or temporal) bright optical solitons [see Karamzin and Sukhorukov (1974), Schiek (1993), Hayata and Koshiba (1993b), Werner and Drummond (1993, 1994) and Buryak and Kivshar (1994, 1995a–c)]. In particular, it was shown that, for a very special choice of the system parameters, an exact analytical solution exists (Karamzin and Sukhorukov, 1974). Recently, Buryak and Kivshar (1995a) have demonstrated the existence of a family of two-wave bright solitons; this family includes, as a special case, the exact solution found earlier (Karamzin and Sukhorukov, 1974; Hayata and Koshiba, 1993a,b).

Dark solitons in $\chi^{(2)}$ materials have been first discussed by Werner and Drummond (1994) for two particular cases when an effective NLS equation can be derived. These cases are (i) the limit of the large phase mismatch between harmonics and (ii) the zero dispersion of the second harmonics. Hayata and Koshiba (1994) found one particular exact solution for a dark soliton beyond the NLS approximation. The first theory of *two-wave dark solitons* in dispersive optical materials with quadratic nonlinearities was elaborated by Buryak and Kivshar (1995b,c). This theory describes all the cases discussed earlier and also presented families of localized solutions with nonvanishing asymptotics. However, this theory is still not complete because it does not include grey solitons and it does not allow arbitrary value of the walk-off between the harmonics. In this section, we discuss two-wave dark solitons in a $\chi^{(2)}$ medium following the original results obtained by Buryak and Kivshar (1995a–c).

Considering interaction between the first ($\omega_1=\omega$) and second ($\omega_2=2\omega$) harmonics in a dispersive/diffractive dielectric medium with $\chi^{(2)}$ nonlinear susceptibility, we derive the system of two nonlinear equations for slowly varying envelopes E_1 and E_2 coupled through components $\chi^{(2)}_{ijk}$ of the nonlinear second-order susceptibility tensor,

$$
\begin{aligned}
&\mathrm{i}\frac{\partial E_1}{\partial z}+\mathrm{i}\delta_1\frac{\partial E_1}{\partial \xi}+\gamma_1\frac{\partial^2 E_1}{\partial \xi^2}+\chi_1 E_1^{*}E_2\mathrm{e}^{\mathrm{i}\Delta kz}=0\,,\\
&\mathrm{i}\frac{\partial E_2}{\partial z}+\mathrm{i}\delta_2\frac{\partial E_2}{\partial \xi}+\gamma_2\frac{\partial^2 E_2}{\partial \xi^2}+\chi_2 E_1^{2}\mathrm{e}^{-\mathrm{i}\Delta kz}=0\,,
\end{aligned}
\tag{5.21}
$$

where $\chi_1\equiv(4\pi\omega^2/k_1c^2)\chi^{(2)}(\omega;2\omega,\,-\omega)$ and $\chi_2\equiv(8\pi\omega^2/k_2c^2)\chi^{(2)}(2\omega;\omega,\omega)$, z is the propagation distance, and $\Delta k\equiv(2k_1-k_2)$ is the wave vector mismatch between the harmonics. The system of Eq. (5.21) generalizes the standard equations of the second-harmonic generation, and it describes two different physical situations. In the first, *spatial case*, the difference $(\delta_1-\delta_2)$ describes the so-called spatial walk-off effect, ξ stands for the transverse coordinate, and $\gamma_j=1/2k_j$, $(j=1,2)$, so that Eq. (5.21) take into account the effect of diffraction. In the second, *temporal case*, ξ stands for time, $\delta_j=\partial k_j/\partial\omega_j$ and $\gamma_j=-\frac{1}{2}\partial^2 k_j/\partial\omega_j^2$ describe group velocities and group-velocity dispersions, respectively.

For stationary solutions of Eq. (5.21), when the walk-off effect and the wave-vector mismatch are compensated due to the nonlinearity-induced phase-locking effect, the following transformation can be applied, $E_1=w(\kappa/\sqrt{2\sigma\chi_1\chi_2})\exp(\mathrm{i}\beta_1 z+\mathrm{i}\Omega\xi)$, $E_2=u(\kappa/\chi_1)\exp(\mathrm{i}\beta_2 z+2\mathrm{i}\Omega\xi)$, where β_1 and

$\beta_2 \equiv 2\beta_1 - \Delta k$ are the nonlinearity-induced shifts of the propagation constant, $\sigma = |\gamma_1|/|\gamma_2|$, $\kappa = \beta_1 + \delta_1\Omega + \gamma_1\Omega^2$, and $\Omega = (\delta_1 - \delta_2)/2(2\gamma_2 - \gamma_1)$. Then, equations for w and u take the universal dimensionless form:

$$i\frac{\partial w}{\partial \zeta} + r\frac{\partial^2 w}{\partial \tau^2} - w + w^* u = 0\,,$$

$$i\sigma\frac{\partial u}{\partial \zeta} + s\frac{\partial^2 u}{\partial \tau^2} - \alpha u + \frac{1}{2}w^2 = 0\,, \tag{5.22}$$

where $\zeta = \kappa z$, $\tau = (|\kappa|/|\gamma_1|)^{1/2}(\xi - vz)$, $v = (2\gamma_2\delta_1 - \gamma_1\delta_2)/(2\gamma_2 - \gamma_1)$, $r = \text{sign}(\kappa\gamma_1)$, $s = \text{sign}(\kappa\gamma_2)$, and $\alpha = (\beta_2 + 2\delta_2\Omega + 4\gamma_2\Omega^2)\sigma/\kappa$.

For large α, when the derivatives in the equation for u can be neglected, it is possible to show that $u \approx w^2/2\alpha$ and Eq. (5.22) can be formally reduced to a single NLS equation for w (Werner and Drummond, 1993) for which dark solitons exist at $r = -1$. Similar results may be found in the case when the dispersion of the second harmonic vanishes (Werner and Drummond, 1994).

Stationary solutions are described by Eq. (5.22) with ζ-derivatives omitted. The real functions $w(\tau)$ and $u(\tau)$ can be then considered as two coordinates in the corresponding mechanical problem with Hamiltonian $H = rp_w^2/2 + sp_u^2/2 + U(w, u)$, where $p_w = \mathrm{d}w/\mathrm{d}\tau$, $p_u = \mathrm{d}u/\mathrm{d}\tau$, and $U(w, u)$ is the two-dimensional potential, $U(w, u) = \frac{1}{2}(w^2 u - \alpha u^2 - w^2)$. For $r = -1$ and large α, dark-soliton solutions can be found in the form of the asymptotic series in α^{-1} (Buryak and Kivshar, 1994; Buryak, 1996)

$$w = \sqrt{2\alpha}\tanh Z + \frac{(\sqrt{2}Z - \tanh Z)}{\sqrt{\alpha}\cosh^2 Z} + O(\alpha^{-3/2})\,, \tag{5.23}$$

$$u = \tanh^2 Z + \frac{[5 - 4\cosh^2 Z + (Z/2)\tanh Z]}{\alpha\cosh^4 Z} + O(\alpha^{-2})\,, \tag{5.24}$$

where $Z = \tau/\sqrt{2}$. The asymptotic series, Eqs. (5.23) and (5.24), does not display any difference between the cases of normal and anomalous dispersions, i.e. between the cases $s = 1$ and $s = -1$. However, as was pointed out by Buryak and Kivshar (1995a), the type of the stationary solutions of the system, Eq. (5.22), depends crucially on the sign of dispersion s.

The importance of dispersion may be already seen in the analysis of modulational instability of two-wave interaction in a $\chi^{(2)}$ medium first by Buryak and Kivshar (1995b,c) and Trillo and Ferro (1995). Such cw solutions are given by the nonlinear stationary eigenmodes of $\chi^{(2)}$ media (Trillo et al., 1992; Kaplan, 1993), and here they appear as asymptotic tails of dark solitons which connect two cw solutions of the same amplitude but different phases. The analysis of the linear stability of the simplest cw solution $w_0 = \pm\sqrt{2\alpha}$, $u_0 = 1$ against modulations $\sim \exp(iq\zeta + i\rho\tau)$ reveals *two branches* for the dispersion relation (Buryak and Kivshar, 1995b; Buryak, 1996),

$$q_{1,2}^2(\rho^2) = [-B \pm \sqrt{B^2 - D}]\,,$$

where

$$B = [(s\rho^2 + \alpha)^2 + 4\alpha\sigma + r\rho^2\sigma^2(r\rho^2 + 2)]/(2\sigma^2)\,,$$

$$D = \rho^2(2r + s\alpha + \rho^2)(\rho^4 + s\alpha\rho^2 - 2rs\alpha)/\sigma^2\,.$$

These two spectrum branches resemble 'optical' and 'acoustic' modes of a diatomic lattice and they exist due to relative and collective dynamics of w and v components, respectively. It is important that instabilities can appear due to both acoustic (as for a single NLS equation) and optical branches (parametric modulational instability). As was first found by Buryak and Kivshar (1995a) the cw solution can be modulationally stable only for the case $r = 1$ and $s = +1$ for some σ and α. Therefore, stable dark solitons of Eq. (5.22) can be expected only when *dispersion coefficients of the fundamental and second harmonic modes have opposite signs, so that there exist no stable spatial dark solitons* supported by $\chi^{(2)}$ nonlinearity.

Indeed, in the case $r = -1$, $s = +1$ and positive α, a continuous family of dark one-soliton solutions has been found by Buryak and Kivshar (1995b). The dependence $u(0)$ vs. α and two characteristic representatives of this family (with monotonous and nonmonotonous tails) are

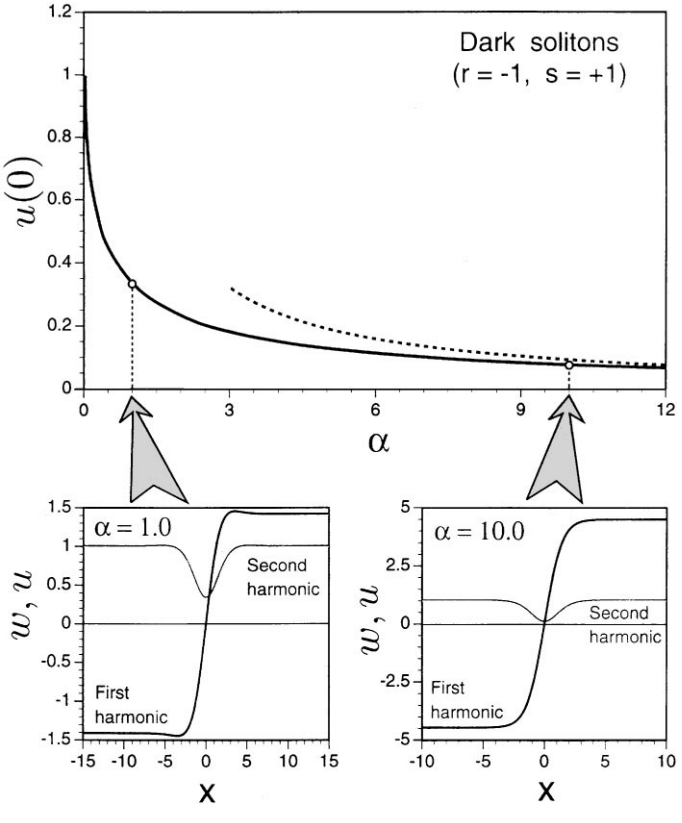

Fig. 22. Characteristic profiles of two-wave dark solitons at $\alpha = 1.0$ and $\alpha = 10.0$. Dependence $u(0)$ vs. α characterizes the whole continuous family of localized solutions found numerically whereas the dashed curve $u(0) = 1/\alpha$ corresponds to the NLS asymptotic solution (Buryak and Kivshar, 1995b).

shown in Fig. 22 where the dashed curve corresponds to the similar dependence $u(0) = 1/\alpha$ found for the asymptotic solution, Eqs. (5.23) and (5.24). Dark solitons of this family exist for every positive value of α. However, the modulational instability analysis predicts that at $r = -1$ and $s = +1$ the cw background, which supports these dark solitons, can be stable only provided $\alpha > 2$ and $\sigma > \sigma_{cr}$ ($\sigma_{cr} \approx 1.689$). Additionally, as was found by Buryak and Kivshar (1995b), the dark solitons may possess nonmonotonous tails if $2 < \alpha < 8$. The existence of the nonmonotony tails leads to important consequences for the soliton interaction in the adiabatic approach when dark solitons are treated as effective particles interacting through exponentially decaying forces, such nonmonotonous tails produce local minima in the effective interaction potential of weakly overlapping solitons, and, therefore, a dark soliton with nonmonotonous tails can trap another dark soliton creating *multi-hole dark soliton bound states* (Buryak and Kivshar, 1995c).

For the case $r = s = -1$ the corresponding results are summarized in Fig. 23 (Buryak and Kivshar, 1995c). In this case, instead of a continuous family, there is only a discrete set of dark-soliton solutions. The simplest one (shown as a black circle) is the exact solution found by Hayata and Koshiba (1994): $w(\tau) = \pm\sqrt{2}u(\tau) = \pm\sqrt{2}[1 - (3/2)\mathrm{sech}^2(\tau/2)]$, which may be

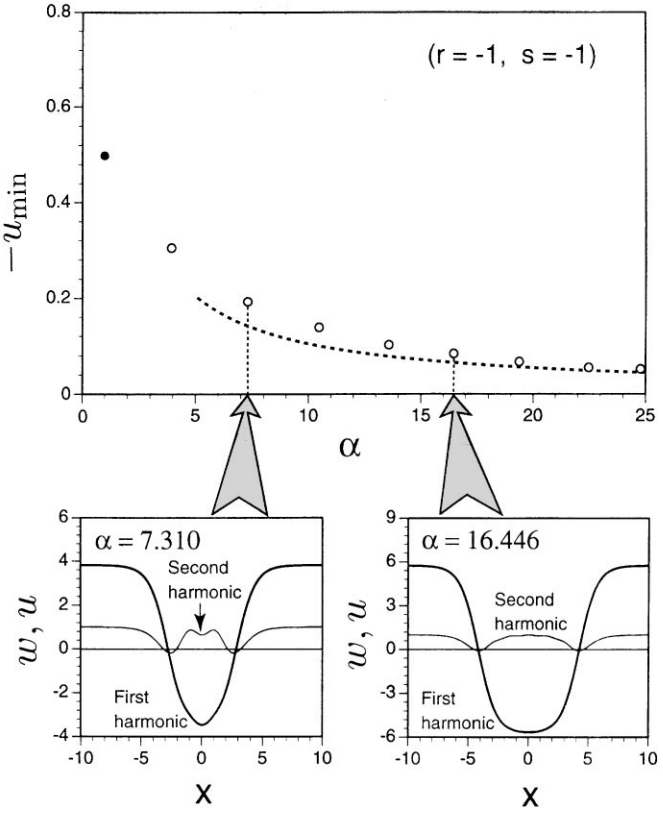

Fig. 23. Discrete set of stationary localized solutions of Eq. (5.22). Dashed curve $u_{min} = -1/\alpha$ is given by the asymptotic soliton of the NLS equation. The filled circle corresponds to the exact solution found by Werner and Drummond (1993) which are unstable (Buryak and Kivshar, 1995b).

considered as a dark soliton of the *lowest order*. Importantly, as follows from the analysis presented above, all dark solitons of this type are modulationally unstable, and this result has been confirmed by direct numerical simulations.

It is important to note that all solutions found in this second case ($r = s = -1$) are very different from each other, and each of them exists only at a particular value of α. This phenomenon was explained as being produced by a trapped radiation when a single dark soliton does not exist as a stationary object but two- (or multi-) soliton bound states are still possible provided some resonant conditions are satisfied [see Buryak and Kivshar (1995a) and Buryak (1995, 1996)].

6. Experimental verifications

6.1. Dark solitons in fibers

6.1.1. General remarks

It is well known that *optical bright solitons* can be used for long-distance optical communications to drastically increase the bit rate of fiber transmission systems (see, e.g., Hasegawa (1989), Hasegawa and Kodama (1995) and Haus and Wong (1996)]. Similar uses have been proposed for *dark solitons.*

The technical difficulties to be considered when dark solitons are used for long-distance optical communications can be split into two main areas, *generation and modulation*, and *propagation*, with concerns which overlap from one area to the other.

Generation is less straightforward than for bright solitons because dark solitons require both a local change in phase as well as amplitude of the background wave (to avoid a large amount of radiation). Various techniques have been proposed and demonstrated for generating single or multiple dark soliton pulses. The first experiments involved either the generation of single dark solitons (Emplit et al., 1987; Weiner et al., 1988) or a pair of dark solitons (Krökel et al., 1988) on a bright pulse background. Several authors studied the generation of quasi-continuous trains of dark solitons by colliding two bright pulses in an optical fibre (Rothenberg and Heinrich, 1992; Williams et al., 1994). Although it was suggested some years ago that continuous dark soliton pulse trains could be generated using electro-optic modulators (Zhao and Bourkoff, 1990), until recently such pulse trains had only been generated using either temporal shaping by high resolution spectral filtering (Haelterman and Emplit, 1993) or by beating together two cw signals in a dispersion tapered fibre (Richardson et al., 1994). For a long time there was no method for encoding the dark soliton train to form a data sequence. Recently, however, Nakazawa and Suzuki (1995a,b) used an electro-optic modulator as an effective technique for simultaneously generating and modulating a stream of dark solitons. Their impressive results will no doubt stimulate further the work in this direction.

Propagation studies are implicit in much of the above work and include, for example, the observation of reshaping of even or odd symmetry dark pulses into grey or black dark solitons in the presence of positive group-velocity dispersion in optical fibres (Krökel et al., 1988; Weiner et al., 1988). Raman scattering has been shown to lead to decay of the dark soliton pulses at high optical powers (Weiner et al., 1989), whilst recently Foursa and Emplit (1996a) used Raman gain to compensate for linear fibre losses encountered during dark soliton transmission. Observation

of dark soliton propagation over distances relevant to telecommunications was reported by Emplit et al. (1993), whilst Nakazawa and Suzuki (1995b) recently demonstrated transmission of a 10Gbit/s pseudorandom dark soliton data train over 1200 km.

Other interesting features of dark soliton propagation, not yet experimentally demonstrated, include their improved stability with respect to Gordon-Haus jitter (Hamaide et al., 1991; Kivshar et al., 1994a) and interactions over a longer length scale than bright solitons (Zhao and Bourkoff, 1989b). However, because the overall phase of the dark soliton rotates at twice the rate of the bright soliton phase, dark solitons are more sensitive to periodic perturbations than the equivalent bright soliton over the same absolute distance.

There remain many open questions to be answered about temporal dark solitons. The main reason to study them is the amount of fibre in the ground optimized for transmission in the normal dispersion regime. Other reasons include the development of 1.3 μm amplifiers using praseodymium, and the fact that dark solitons can tolerate a smaller mark : space ratio than bright. This means that the average power needed to transmit bright and dark solitons can be of a similar order of magnitude.

6.1.2. Generation of dark solitons

Although both bright and dark solitons in optical fibers were predicted in 1973 by Hasegawa and Tappert (1973a,b) almost simultaneously and bright solitons were already experimentally observed by Mollenauer, Stolen, and Gordon in 1980 (Mollenauer et al., 1980), dark solitons remained a mathematical curiosity until quite recently. This is because of the relative difficulty of generating a short 'dark pulse' on a continuous or long background pulse as a seed to the evolution of a dark soliton with well-defined phase. The first attempt to study dark pulse propagation in optical fibers experimentally was made by Emplit et al. (1987). They created odd-symmetry dark pulses using a spectral filtering technique from a beam containing a π-phase step. They observed that the dark pulses had properties similar to those of a fundamental dark soliton although their experimental results did not demonstrate dark soliton propagation because of the rather long dark pulses that were used ($\sim$ 5 ps at 600 nm). As a result, fiber losses could not be neglected because the characteristic length for soliton propagation ($\sim$ 220 m) was greater than the fiber attenuation length of $\sim$ 140 m. Thus, these experiments did not provide clear enough evidence of dark-soliton generation.

Later Krökel et al. (1988) provided the first experimental results on dark soliton propagation when they showed experimentally that an even dark pulse evolved into a symmetric pair of low-constant (small-amplitude) dark pulses that propagate unmistakably as solitons in accordance with earlier numerical results by Blow and Doran (1985) and a general theory of this pair generation developed by Gredeskul and Kivshar (1989a,b). In Krökel et al. experiments 0.3 ps duration dark pulses were generated on a 100 ps duration 532 nm background pulse from a frequency doubled Nd : YAG laser by using a 15 mm long, optical Kerr effect fibre modulator. The pulses were launched into a 10 m single mode polarization preserving fiber and the output signals measured using the autocorrelator at different input power levels. At high powers ($>$ 9 W) the input pulse evolved into a pair of dark soliton pulses with opposite velocities relative to the background and these could be clearly distinguished from the structures produced during linear propagation. Their results were in very good agreement with numerical solutions of the NLS equation.

The creation of a pair of dark solitons with opposite velocities and equal amplitudes as observed by Krökel et al. (1988) is a simple consequence of the fact that the input pulse did not contain the phase jump needed to create a single dark soliton (see Section 2.4). Any input pulse with the same phase on its leading and trailing edge will lead to the creation of a symmetric pair of dark solitons (Gredeskul and Kivshar, 1989a). To create a single dark soliton, one needs to prepare a background pulse containing an appropriate phase jump as was achieved in the attempt by Emplit et al. (1987).

The first successful experiments in which single dark soliton propagation was confirmed were reported by Weiner et al. (1988). Using a pulse tailoring technique that relies on spatial filtering within a standard grating decompressor they propagated 185 fs duration antisymmetric input dark pulses, which closely corresponded to the form of the fundamental dark soliton, through a 1.4 m length of single-mode optical fiber. Their experimental results are presented in Fig. 24a–e by dotted lines. Fig. 24a shows an intensity cross-correlation measurements of the input pulse. The duration of the central hole was 185 fs (intensity FWHM), and the background duration 1.76 ps FWHM. Cross-correlation traces of the output pulses from the 1.4 m fiber are plotted in Fig. 24b–e for various power levels. At the lowest power (1.5 W peak input power), propagation was almost linear. As the power was increased, the background pulse broadened and acquired a square profile because of the combined effects of nonlinearity and dispersion. Same time, the width of the output dark pulse decreased. At 300 W peak input power, the output dark pulse was of essentially the same duration as the input. Thus the dark pulse underwent soliton-like propagation and emerged from the fiber almost unchanged, even in the presence of significant broadening and chirping of the finite-duration background pulse. Computer solutions of the NLS

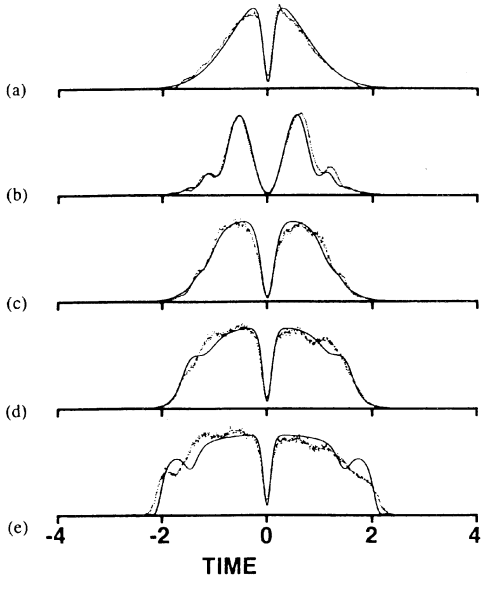

Fig. 24. Measured (dotted lines) and calculated (solid lines) cross-correlation data for the odd-symmetry dark pulse. (a) Input dark pulse. (b)–(e) Pulses emerging from the fiber for peak input power of (b) 1.5, (c) 52.5, (d) 150, and (e) 300 W (Weiner et al., 1988).

equation, shown in Fig. 24a–e by solid curves, were in qualitative agreement with the experimental data.

By changing the spatial mask in the decompressor, even symmetry pulses could be obtained. The results in this case are plotted in Fig. 25a–e. Fig. 25a shows a measurement of the input pulse, and cross-correlation measurements of the output pulses from the fiber are shown in Fig. 25b–e. The trends are similar to those reported by Krökel et al. (1988). At low power the background pulse was reshaped by interference with the chirped, temporally broadened dark pulse. As the power was increased, one may observe the formation of two low-contrast holes, separated by ≈ 2.3 ps at 285 W peak input power. Again, the data agree closely with numerical solutions to the NLS equation shown as solid lines in Fig. 25a–e. Therefore, the experiments confirmed the crucial importance of the phase profile of the input pulse: an odd dark pulse propagates undistorted as a black soliton, while an even dark pulse splits into a pair of gray solitons.

Nonlinear propagation of 5.3 ps odd-symmetry dark pulses through a 1 km long single-mode fiber at 850 nm was reported by Emplit et al. (1993). The choice of this wavelength allowed them to study dark soliton propagation in conditions more compatible with telecommunications. It was demonstrated that the soliton-like propagation is possible in a fiber 2.5 times longer than the soliton characteristic distance z_0 despite a finite background and fiber loss. A quantitative agreement with numerical simulations was found for both temporal and spectral measurements.

Weiner et al. (1989) also reported the effect of temporal and spectral self-shifts of dark solitons in fibers. Such an effect is well-known for bright optical solitons [see, e.g., Hasegawa (1989) and Hasegawa and Kodama (1995)]. In the case of dark solitons these shifts become increasingly pronounced as the intensity and the fiber length are increased. As has been shown, the experimental

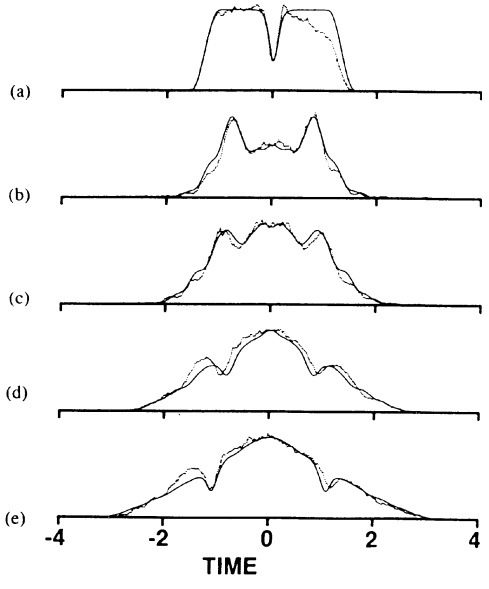

Fig. 25. The same as in Fig. 24, but for the even-symmetry dark pulse. (a) Input pulse. (b)–(e) Pulse emerging from the fiber for peak input power of (b) 2.5, (c) 50, (d) 150, and (e) 285 W (Weiner et al., 1988).

data are in a good agreement with numerical simulations made in the framework of the modified NLS equation that includes the Raman contribution to the nonlinear refractive index. Analytical description of the effect was proposed by Kivshar (1990a,b) (see also Section 3.2.2 above where another version of the analytical approach is presented).

The Raman effect was employed to advantage in the work by Foursa and Emplit (1996a) where Raman amplification was used to compensate for fibre losses. A highly Ge-doped single mode fibre, 395 m long, was used as the gain medium into which was launched a 2.7 ps long dark pulse imposed upon a 39 ps duration 883 nm background. The output pulses were analysed using a streak camera. A counter-propagating pump pulse at 850 nm with an average power of 190 mW was used to produce a Raman gain of up to 3 dB compensating fully the 6 dB/km absorption losses in the fibre.

Although these single pulse propagation studies confirmed the basic properties of dark solitons, the generation of pulse trains is essential for application in optical communications. In initial experiments dark soliton trains were created by colliding two right pulses launched with a time delay between them into an optical fibre in conditions of normal dispersion (Rothenberg and Heinrich, 1992; Williams et al., 1994). This process for creating dark soliton trains involves three stages. In the first stage the two pulses broaden nonlinearity forming rectangular frequency-chirped pulses. The chirped pulses eventually broaden sufficiently that they start to overlap and linearly interfere forming a pulse with sinusoidal density modulation and alternating phase. Finally the nonlinearity acts on this modulation producing a train of dark solitons in a similar way to that which occurs during amplification (Dianov et al., 1989).

The first experimental observation of this effect was reported by Rothenberg and Heinrich (1992) following the earlier numerical predictions of Rothenberg (1991). A 2 ps duration pulse from a dye laser was split into an input pulse pair using an interferometer and focussed into an optical fibre 100 m long. The output pulses were analysed using a streak camera. By varying the pulse separation and power the transition from nearly sinusoidal modulation to a characteristic dark soliton-like structure was observed. The later work of Williams et al. (1994) extended the process to create high repetition dark pulse trains (up to 60 GHz) and propagated these trains for distances up to 2 km.

The generation of dark solitons on a background containing a noise component was reported by Grudinin et al. (1988). Such an experimental observation is related to the work by Gredeskul et al. (1990) [see also Gredeskul and Kivshar (1989a)] who demonstrated analytically that any dip (deterministic or random) on a cw background will evolve into at least one pair of dark solitons.

The first high repetition rate continuous train of dark soliton pulses was generated by Richardson et al. (1994). In their work the CW beams from a pair of single frequency DFB lasers temperature tuned to have their frequencies separated by 100 GHz were focussed into a 1.5 km length of fibre with slowly decreasing normal dispersion. Dark soliton pulses 1.6 ps in duration were measured at the output of the fibre using an autocorrelator. The technique is similar to that already predicted (Dianov et al., 1989) and demonstrated (Chernikov et al., 1992) for the generation of bright soliton trains.

So far the problem of encoding information onto dark soliton trains had remained unsolved. However, quite recently Nakazawa and Suzuki (1995b) demonstrated both encoding and detection of a pseudorandom data train of dark solitons. Fundamental to their work was the availability of a fast Lithium Niobate push–pull electro-optic modulator. An non-return-to-zero (NRZ) data

pattern and clock pattern were combined in an 'and' gate. The 'and' data stream as then converted to a Q and $\bar{Q}$ outputs to drive the Mach–Zehnder interferometer using a T-flip-flop circuit, see Fig. 26a and Fig. 26b. Dark solitons about 50 ps long were generated.

Detection (Fig. 27a and Fig. 27b) involved the separation of the incoming dark soliton train into two arms of Mach–Zehnder interferometer with a one-bit shift in time introduced between them at

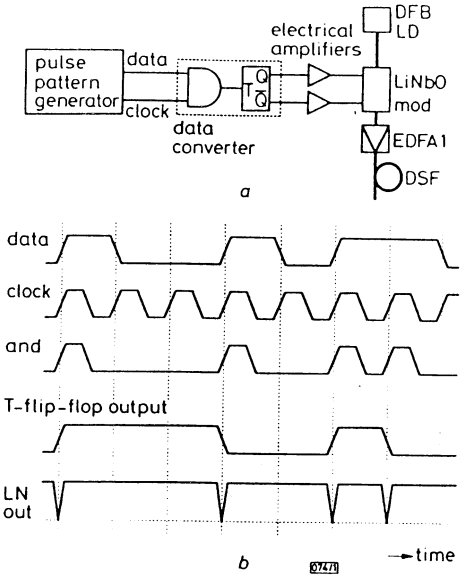

Fig. 26. Generation scheme for pseudorandom binary sequence dark soliton train: (a) block diagram, (b) operating principle (Nakazawa and Suzuki, 1995b).

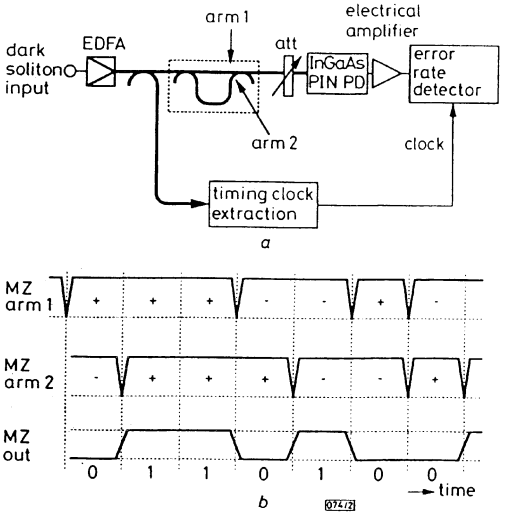

Fig. 27. Detection scheme for pseudorandom binary sequence dark soliton train using one-bit-shifting with Mach-Zehnder interferometer: (a) block diagram, (b) operating principle (Nakazawa and Suzuki, 1995b).

the output. Interference between these two signals created an inverted version of the original NRZ data train.

In subsidiary experiments (Nakazawa and Suzuki, 1995a) propagated the dark soliton trains through dispersion shifted optical fibre demonstrating a 2.5 dB power penalty was required to maintain a BER or 10^{-10} after 1200 km.

These last results clearly indicate that most of the basic issues involved with the generation, encoding and detection of dark soliton pulse trains can be overcome although higher bit rates will require more sophisticated equipment. Hence, the basic possibility of using dark soliton pulse transmission in normally dispersive fibre has now been established.

6.1.3. Interaction between dark solitons

The first experimental investigation of the interaction between black and grey solitons in an optical fiber has been recently reported by Foursa and Emplit (1996b). Experiments were carried out using a 1 km single-mode fiber with an effective core area of 28 μm^2 and dispersion of 90 ps/nm/km. The fiber length equaled to approximately 7 soliton distances. A pair of dark solitons with adjustable 'blackness' were generated using a pair of phase plates inserted in the frequency dispersed part of the beam within a grating decompressor. The coupled signal power slightly exceeded the level of the fundamental dark soliton in order to partially compensate for the fiber losses. The output pulses were analysed with a streak camera with the interaction between the pair of solitons investigated by measuring the change in arrival time relative to the interaction-free case.

The streak camera images shown in Fig. 28a–c show temporal profiles of various inputs (left) and the fiber outputs (right). In Fig. 28a a single grey pulse with the grayness parameter $B^2 = 0.78$ (see Section 2.3) was observed to walk from the leading edge (-10 ps) to the trailing

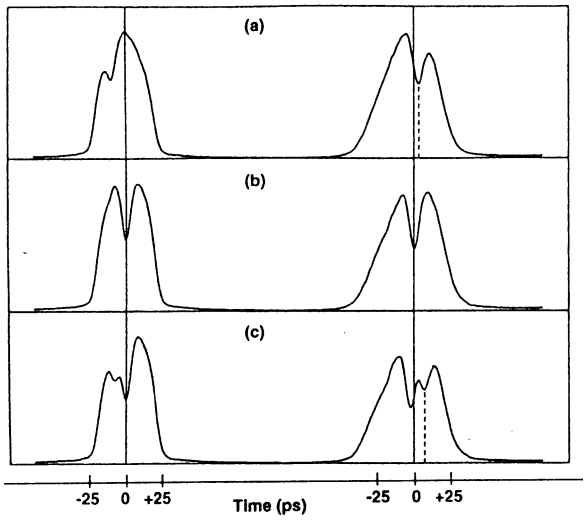

Fig. 28. Streak camera images of the pulses at the shaping output (left) and the fiber output (right) for the grayness parameter $B^2 = 0.78$. (a) Single gray pulse, (b) single black pulse, and (c) gray and black pulse pair. Black solitons are marked by solid cursors and gray pulses at the fiber output by dotted lines (Foursa and Emplit, 1996b).

edge (+ 4 ps) of the background pulse. At the same time the carrier pulse lengthened in time because of the effects of dispersion and self-phase modulation. The soliton also became broader after propagation because the fiber losses decrease the amplitude of the background pulse. Fig. 28 shows the case of a black soliton positioned originally at the centre of the background pulse where no relative motion was expected or observed. The temporal measurements when both dark and gray solitons were present at the same time, showed the following behaviour. The gray soliton walked through the black pulse during propagation through the fibre but as a result of the interaction its walk off increased by 3 ps (compare Fig. 28a and Fig. 28c). At the same time dark pulse also changes its position towards the leading edge of the carrier pulse by 2 ps (see Fig. 28b and Fig. 28c).

These results provided evidence of the basic repulsive nature of the interaction between the coherent dark solitons and were well reproduced by numerical simulations based on the scalar cubic NLS equation carried out by Foursa and Emplit (1996b) [see also Thurston and Weiner (1991) and Diankov and Uzunov (1995)].

6.2. Spatial dark solitons

6.2.1. General remarks

Experimental studies of bright spatial solitons in self-focussing glasses and semiconductors had already demonstrated the main features predicted by the cubic NLS equation (Aitchinson et al., 1990; Reynaud and Barthelemy, 1990) before any experimental work on dark spatial solitons had been attempted. The first experimental investigations of dark spatial solitons in self-defocusing media were performed almost simultaneously for a bulk medium, by Andersen et al. (1990) and Swartzlander et al. (1991), and for planar waveguides, by Allan et al. (1991) and Skinner et al. (1991).

Andersen et al. (1990) and Swartzlander et al. (1991) reported the generation of dark soliton stripes, grids and crosses on the transverse cross-section of an optical beam propagating through a bulk self-defocusing medium.

Although it is well known that such quasi-one-dimensional structures should suffer from a transverse modulational instability and hence do not exist as stable analytical solutions for dark solitons in the (2 + 1)-dimensional NLS equation, the experimental and numerical data presented in these papers using various two-dimensional amplitude and phase masks provided strong evidence that the observed phenomenon were indeed due to the creation of dark spatial solitons. A number of experimental factors contributed to the absence of the long wavelength transverse modulational instability in these experiments. Firstly, the moderate beam intensities led to stabilization due to the finite size of the laser beam (that is the fastest growing unstable mode had a period much larger than the beam size). Secondly, in experiments using thermal media (Swartzlander et al., 1991), the diffusive nature of the nonlinearity led to stabilization, the effect known also to suppress collapse of light beam [see, e.g., Turitsyn (1985) and Suter and Blasberg (1993)].

The transverse modulational instability will not, however, always be suppressed. Quite recently (Mamaev et al., 1996a; Tikhonenko et al., 1996a) it was observed in experiments where higher nonlinearity with an essentially local response was available. The instability led to a snake like distortion of the soliton stripe and eventually breakup to form pairs of optical vortex solitons (Tikhonenko et al., 1996a).

By analogy with the case of grey temporal solitons, grey spatial solitons have a finite transverse velocity relative to the background beam that supports them. A convenient way of understanding this motion is to recognize that a nonzero on-axis intensity can only occur if a travelling crosses the soliton. Since the background is a plane wave (i.e., it is characterized by a single k-vector) then the soliton must propagate at some angle to this background wave to generate the travelling wave component. The direction of the soliton is determined by its grayness which in turn is determined by the change of phase across the soliton. It follows that adjusting the phase change across the soliton allows it to be scanned relative to the background wave. This was first demonstrated by Luther-Davies and Yang (1992b) for single dark solitons and later by Bosshard et al. (1994) and Mamyshev et al. (1994) for an array of dark solitons [see also West and Kennedy (1993) where dark soliton trains were investigated analytically with the help of the inverse scattering transform].

The ability to change the propagation direction of a dark spatial soliton is useful when they are considered for use in optical switching. Although large number of concepts for optical switching have been suggested, reconfigurable light induced waveguides is of particular interest. Spatial solitons can be thought of as self-guided waves, that is they 'write' a waveguide into the nonlinear material in which they are created and propagate as modes of that waveguide. Bright solitons are bound modes of the waveguides they induce whilst dark solitons are reflectionless radiation modes (Snyder et al. (1993), see also Section 2.6).

As a result of this concept, quite a lot of attention has been paid to 'writing' ideal structured waveguides into nonlinear materials using dark spatial solitons. The creation of a pair of grey solitons from an amplitude hole in a pulse is well-known from the results on temporal solitons. In the spatial domain a pair of solitons which emerge from a square intensity dip in an input beam provides an optical structure similar to a waveguide Y-junction. This was first demonstrated by Luther-Davies and Yang (1992a) and recently by Z. Chen et al. (1996a) and Taya et al. (1996) in photorefractive materials.

Another interesting property of dark spatial solitons is their behaviour during collisions. Numerical simulations have demonstrated that the soliton induced X-junctions created by such collisions form lossless transmission junctions (Luther-Davies and Yang, 1996a). Experimentally the X-junction is difficult to realize in materials with diffusive nonlinearities but recently they have been observed in photorefractive materials (Segev et al., 1996).

Dark and bright solitons in photorefractive media have attracted considerable attention in recent years (Valley et al., 1994; Taya et al., 1995; Iturbe-Castillo et al., 1995; Taya et al., 1996; Z. Chen et al., 1996a,b; Segev et al., 1996). The work on photorefractive solitons will be dealt with in one of the following sections.

6.2.2. Dark soliton stripes and grids

A report of the first experiments on dark spatial solitons were published by Swartzlander et al. (1991). A cw frequency-stabilized dye laser with a beam of power $P_{\text{in}} \sim 100\,\text{mW}$ was passed through a wire mesh and then imaged with a lens into a $L = 18\,\text{mm}$-long cell containing $\sim 10^{12}$ atoms/cm^3 of sodium vapor. By tuning the laser below the atomic D_2 resonance, a strong defocussing response with an effective nonlinearity n_2 up to $\simeq -3 \times 10^{-7}\,\text{cm}^2/\text{W}$ was obtained. Far-field intensity profiles were recorded at the distance of > 1 m from the output of the cell. When the laser was detuned far from the resonance the normal Fraunhofer pattern due to linear

diffraction from the grid was observed. However as the D_2 resonance was approached this pattern underwent a remarkable transformation to form a well-organised array of square dots. Numerical simulations of the NLS equation showed that the formation of regular patterns of dark stripes within the background field was a universal phenomenon, most likely associated with the production of multiple dark spatial solitons. From these far-field patterns the authors observed that these (2 + 1)-dimensional dark stripes behaved very similarly to the analytical (1 + 1)-D dark solitons.

To confirm that dark solitons were indeed being created, a further series of experiments was undertaken this time using a weakly absorbing liquid as a thermally defocussing nonlinear material. Near field images at the output of the medium were recorded at high power (nonlinear propagation) and low power (linear propagation). The use of either an amplitude mask (a wire cross) or a π phase mask (again in the form of a cross) led respectively to the creation of pairs of or single crossed dark soliton-like stripes on a uniform background in the nonlinear regime. The transverse velocity of the pair of stripes generated from the amplitude mask varied with the width of the wire in the manner predicted for (1 + 1)-D dark spatial solitons. A similar result had been published by Andersen et al. (1990) from experiments where a single wire was used to mask an input beam to a thermally defocussing nonlinear medium and multiple (higher order) dark soliton stripes with transverse velocities predictable from the theory of Zakharov and Shabat (1973), were created.

Numerical study of controllable branching of optical beams by dark soliton stripes depending on a proper choice of the initial phase profile and the width of the crossed dark stripes and the background beam intensity was analyzed by Neshev et al. (1997b).

Although such dark-soliton stripes should be unstable to transverse modulations (see Section 7.2 below), the experimental data described above and numerical simulations carried out for a Kerr medium did not show any manifestation of this instability. The natural explanation is that the finite-width beam used by Andersen et al. (1990) and Swartzlander et al. (1991) prevented the development of long-wavelength instabilities. Nevertheless, for stronger light intensities stripe breakup should be observed with the subsequent generation of vortex paris, as we describe below in Section 7.4.1.

Almost simultaneously with the work of Swartzlander et al. (1991), there appeared two reports of dark soliton generation in ZnSe bulk semiconductors (Allan et al., 1991; Skinner et al., 1991). In these experiments 30 ps duration pulses from a frequency doubled Nd : YAG laser were passed through phase or amplitude masks into a $5 \times 5 \times 2$ mm single crystal of ZnSe. ZnSe has an instantaneous defocussing component of the nonlinear refractive index at $\lambda = 532$ nm, due to the dispersive change associated with two-photon absorption. The output from the crystal was imaged onto the slit of a streak camera aligned orthogonal to the axis of the expected dark soliton stripe to provide time resolution. Interferograms of the beam emerging from the crystal were also recorded.

When a π phase mask was used the streak records showed intensity dependent narrowing of the central dark zone accompanied by defocussing of the background indicating the creation of a dark soliton. Allan et al. (1991) were able to confirm that the soliton constant (the product of the square of the width and the peak dark irradiance) was conserved in their experiments. Interferograms of the output beam for π phase or amplitude masks showed the phase structures expected for black and grey solitons respectively. The results thus gave quantitative evidence of the fact that the irradiance minimum propagates as a dark spatial soliton.

6.2.3. Dark soliton induced waveguides

All spatial solitons are self-guided waves and hence it is useful to think of them as optical modes of the waveguides they induce in the nonlinear medium [see, e.g., Snyder et al. (1993)]. Using this concept it is immediately clear that soliton induced waveguides could be used as light guides for co-propagating beams (De la Fuente et al., 1991). In the case of dark spatial solitons the guided beam is localized as a bound mode within the dark zone of the background wave. When the power in the guided mode is infinitesimally small, it does not perturb the dark soliton, whereas at high powers it is possible for the two waves to form a bound dark–bright soliton pair (see Sections 5.1 and 6.3).

The first results on dark soliton induced waveguides with co-propagating guided modes were reported by Luther-Davies and Yang (1992a,b). In those experiments the beam from a multiline argon-ion laser was passed through a dispersing prism to separate the different wavelengths. The 514 nm radiation passed unfocused through a polarizing beam splitter into a 10 cm long cell containing a thermally nonlinear liquid. The output beam from the cell was imaged onto a screen by using a 50 mm focal-length lens and a CCD camera and a frame grabber used to capture the images. The on-axis beam intensity at the input to the cell was ≈ 30 W/cm^2 for 514 nm powers of 1 W. The 476 nm argon line was routed by an attenuator and injected into the nonlinear medium through the polarizing beam splitter coaxial with the 514 nm beam. The probe beam was focused to a spot size suitable for launching into the various soliton structures.

Two types of perturbation were used to create structured dark soliton induced waveguides using the 514 nm beam. The first was a simple π phase jump formed by evaporating a 530 nm thick SiO_2 layer across one half of a glass slide. The phase jump was positioned across the middle of the 514 nm beam at different distances from the input to the cell. The separation of mask and cell determined the width of the zone over which the π phase change occurred in the input field by varying the amount of linear diffraction. When the width of this zone was much greater than the width of the dark soliton in the medium, a transition region was created as the dark soliton formed, and this region had the shape of a tapered waveguide. The experimental data, supported by numerical simulations, showed that this tapered waveguide was able to adiabatically couple an input beam launched coaxial with the dark zone at the input into a bound mode of the dark soliton induced waveguide, thus forming an ideal adiabatic taper. In fact it is generally the case that structured waveguides formed by the creation or interaction between spatial solitons have almost ideal optical properties. This is qualitatively due to the absence of abrupt interfaces in these light induced structures.

A second type of input perturbation was also used: an amplitude jump formed by placing a fine ($= 40$ μm) diameter wire across the beam 1 cm from the input to the nonlinear medium. In this case, the lowest-order soliton solution corresponds to the formation of a diverging pair of dark solitons. However the solitons only form some distance from the input and the overall structure linking the pair of diverging dark solitons to the single dark input stripe is equivalent to a waveguide Y-junction. Numerical simulations showed that the Y-junction should be essentially lossless, and this was supported by the experimental results. The experimental measurements of the input and output fields from the Y-junction are shown in Fig. 29. Note that the use of dark soliton stripes in this experiment meant that divergence in the vertical direction was not controlled. The overall transmission of the Y-junction structure was $> 85\%$ and it is possible this figure to be further improved by more careful attention to the launch conditions.

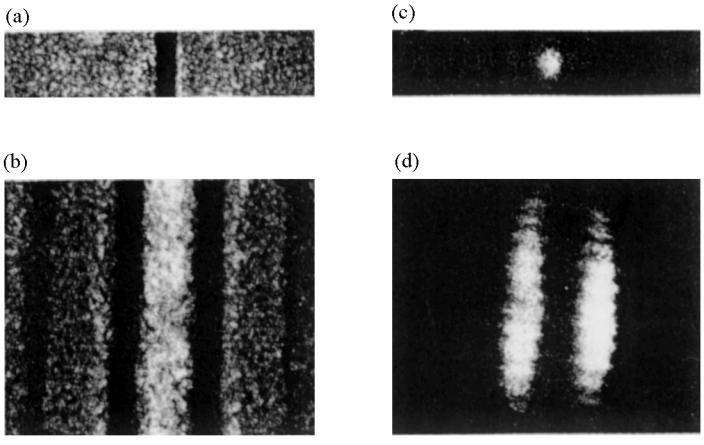

Fig. 29. Experimental beam profiles: (a) the input soliton-forming-beam pattern, (b) the output dark-soliton pattern, (c) the input probe-beam pattern, (d) the output probe-beam pattern (Luther-Davies and Yang, 1992b).

A useful feature of soliton induced structures is that they can be reconfigured by changing the launch conditions. An important example which creates steerable waveguides is based on the use of grey solitons whose phase can be controlled. It is well known that dark solitons propagate at an angle, determined by their phase, to the plane wave background in which they are embedded. Luther-Davies and Yang (1992b) demonstrated that an adjustable phase mask within the input beam could, therefore, be used to scan the position of a dark soliton at the output of a nonlinear medium over several soliton widths (limited only by the available nonlinear change in the refractive index and the propagation distance). It was also pointed out that different dark soliton channels could cross (forming X-junctions) and that the signals propagating in those channels would pass without loss across those junctions. This would in principle allow a large number of cross-connects between an array of input and output channels without cross talk.

The theory of the dark solitons arrays was developed by West and Kennedy (1993) who used the technique of the inverse scalleting transform [see also, Swartzlander (1992) and Lundquist et al. (1995), where the multiple dark soliton generation was also discussed]. Experimentally, the generation and steering of arrays of dark solitons and the beams guided within them was reported by Mamyshev et al. (1994) and Bosshard et al. (1994). To create the dark soliton array the principal proposed for generating dark soliton pulse trains in optical fibres by beating two laser frequencies in the presence of adiabatic amplification was extended to the spatial case. A beam from an Argon ion laser was spatially filtered and expanded before being split into two beams that were directed at different angles into a nonlinear medium to form an interference pattern with a period of 100 μm. A cylindrical lens was used to focus the beam along the axis parallel to the fringes, thereby increasing the beam intensity as a function of propagation distance through the nonlinear medium and providing effective amplification. The experimental data confirmed that this procedure generated the new spatial structures in the far field pattern of the emerging beam which were essential for dark soliton creation and good agreement was observed between the experiments and numerical solution of the $(1 + 1)$-dimensional NLS equation. It was demonstrated that these soliton arrays could guide a co-propagating beam as a bound mode of the array. Steering of the

array as reported by Bosshard et al. (1994) required only a relative change in the intensity of the two beams.

Although induced X-junctions based on collision of dark solitons are also of potential importance, only results from simplified models (Sheppard, 1993; Miller, 1996) or numerical simulations (Sheppard, 1993; Yang et al., 1993) have so far been reported. A major reason for this has been the reliance for the creation of dark spatial solitons on nonlinear media with a diffusive nature where X-junctions do not appear to form.

6.2.4. Dark solitons in photorefractive materials

In the past two years, interest in spatial solitons has increased markedly through the use of photorefractive nonlinear materials. For the first time, dark solitons were mentioned in connection with the photorefractive effect by Belanger and Mathieu (1987) who used the concept of dark solitons for a qualitative explanation of the optical branching effect observed by Jerominek et al. (1985, 1986) in Ti : $LiNbO_3$ slab waveguide. However, that time the experimental results were not sufficient to make that explanation more convincing.

Now, it is well established that in these materials, *three different types* of photorefractive response can lead to the beam self-trapping and localized structures. The first type of self-localization occurs when diffraction is suppressed by two-wave mixing involving refractive index grating within the photorefractive material in the presence of an applied field. The shift in the grating phase due to the external field provides phase coupling between incident and scattering waves necessary to compensate for diffraction (note that in the absence of the field two-wave mixing leads to energy coupling which cannot compensate for diffraction). The effect is *transient* (lasting a fraction of a second to several seconds depending on the materials properties) since the external field will eventually be screened by the background conductivity. The effective nonlinearity in this situation is nonlocal, and can be changed from self-focussing to defocussing by changing the direction of the externally applied field. An important property of the corresponding self-localized beams is their independence of the absolute light intensity (Segev et al., 1992; Crosignani et al., 1993; Duree et al., 1993).

The second and third types of photorefractive response give a birth to spatial solitons known as *screening* solitons (Segev et al., 1994a,b) and *photovoltaic* solitons (Valley et al., 1994), respectively, result from nonuniform screening (the former) or from photovoltaic fields (the latter) which appear in the crystal in steady-state conditions. Unlike the first type of photorefractive soliton, the effective nonlinearity is local and hence the shape and width of screening or photovoltaic solitons depend on intensity. It is a characteristic of photorefractive solitons that they can generally be modelled using a conventional NLS model with a saturating nonlinearity [see, e.g., Christodoulides and Carvalho (1995) and Segev et al. (1996)].

The first experimental observation of photorefractive dark solitons of the nonlocal type was reported by Duree et al. (1995). To observe planar dark solitons, they launched a dark notch associated with a π phase jump in the center of an Argon ion laser beam into a rhodium-doped strontium barium niobate [SBN] crystal. An external electric field of -400 V/cm was applied parallel to the c-axis which also corresponded to the trapping direction. In the absence of the field the 21 μm wide notch at the input diffracted to form a 35 μm wide dark region at the exit face of the crystal. With the field turned on, diffraction was fully compensated and defocussing of the background also occurred. An important signature of the nonlocal photorefractive solitons is their insensitivity to the absolute light intensity. To verify this the authors varied the input power over

2 orders of magnitude, from 3 to 300 μW (intensities of 0.3–30 W/cm^2), and observe no change in the shape or the size of the dark soliton (Duree et al., 1995). In the same paper, the observation of vortex dark solitons was also reported (see Section 7.4).

Screening solitons were first reported by Iturbe-Castillo et al. (1995). The physical process involved is best understood by considering a narrow notch in an otherwise uniform infinite plane wave propagating in a biassed photorefractive medium. In the illuminated regions the conductivity increases and the resistivity decreases. As a result, the voltage drop occurs primarily across the dark region leading to a local increase in the field and a corresponding local change in the refractive index via the pockels effect. Iturbe-Castillo et al. (1995) reported the creation of dark soliton stripes about 20 μm wide when a barium titanate [BTO] crystal was illuminated with He–Ne laser beam in the presence of an applied field up to 7.5 kV/cm and an incoherent background beam. They also demonstrated probe beam guidance by the photorefractive-soliton-induced waveguide.

In fact it has been a common theme in experiments on photorefractive solitons to demonstrate their use as light induced waveguides. This is in part due to the fact that the photorefractive response is rather slow and leads to quasipermanent structures. This is particularly true in the case of photovoltaic spatial solitons where illumination of the nonlinear medium leads to photovoltaic currents which transport charge away from the illuminated region preferentially along the *c*-axis of a ferroelectric crystal. Photovoltaic solitons only exist when there is a component of the intensity gradient along the *c*-axis. Since the physical mechanism for soliton generation involves the separation and trapping of charge, the index perturbation persists in the dark and may be useful in creating semipermanent waveguides for wavelengths where the material is insensitive to light.

Recently, planar dark solitons due to the bulk photovoltaic effect in lithium niobate were observed (Taya et al., 1995). A 488 nm beam from an argon ion laser containing a π phase step illuminated a nominally undoped sample of lithium niobate at low power level (20 mW) normal to the crystal *c*-axis. At intensities of the order of 10 W/cm^2 dark solitons with widths of approximately 20 μm formed after 15 min of exposure. It was demonstrated that solitons only formed when the intensity gradient was parallel to the *c*-axis as predicted and the induced waveguides could trap 514 nm radiation as a bound mode. These photovoltaic waveguides lasted up to 39 h after the soliton forming beam was removed. In recent work (Taya et al., 1996) also demonstrated the formation of a waveguide *Y*-junction using photovoltaic solitons.

Much of the most recent experiments with photorefractive materials has concentrated on screening solitons (Z. Chen et al., 1996a,d; Mamaev et al., 1996a–c). Uniform illumination to the edges of the crystal is important in creating the localized screening region and this can be achieved either by the use of an incoherent background illumination (Iturbe-Castillo et al., 1995) or by extending the soliton background field to cover the full crystal aperture (Z. Chen et al., 1996a). Most recently screening solitons have been used to demonstrate the creation of waveguide *Y*-junctions and higher order solitons (Z. Chen et al., 1996b), dark-bright solitons pairs (Z. Chen et al., 1996d), the transverse breakup of dark soliton stripes (Mamaev et al., 1996a,b) and instability and splitting of vortex solitons (Mamaev et al., 1996c).

Many exciting results have now been reported using photorefractive materials. The main impediment to applications in photonics is the current switching speed which in many cases is limited by the response time of the material to several seconds or longer. Some prospects exist to meet that challenge and in some materials response speeds can be improved dramatically by changing carrier and trap densities, whilst retaining the high photorefractive sensitivity.

6.3. Coupled dark–bright solitons

Experimental observation of the simultaneous propagation of dark and bright solitons of *different wavelength* (1064 and 532 nm) interacting due to the cross-phase modulation effect in a Kerr medium of the focusing type has been reported by Shalaby and Barthelemy (1992). Dark pulse was created by reshaping of a longer pulse, and both pulses with parallel polarizations were launched in a cell of 15 mm length filled with CS_2. The propagation distance corresponded approximately to four Rayleigh lengths associated with the bright wave. The intensity ratio between the two soliton beams was varied by rotating a help wave plate followed by a polarizer in the infrared path. When the dark infrared beam and the bright visible beam are simultaneously launched, the interaction manifests itself by both the narrowing of the central hole in the exiting infrared profile and the reshaping of the green output into a fundamental soliton like wave. The experimental results were compared to the numerical simulations of the linear and nonlinear propagation, with a qualitatively good agreement. The dark beam launched alone was completely destroyed during its propagation in a focusing medium.

The first observation of incoherently coupled dark–bright spatial soliton pairs in a biased bulk strontium barium niobate photorefractive crystal has been reported by Z. Chen et al. (1996d). This kind of solitary waves have been predicted in the context of photorefractive materials by Christodoulides et al. (1996) where it was shown that a coupled bright–dark soliton pair can propagate in a biased photorefractive crystal provided that the two pairing beams share the same polarization and wavelength and are mutually *incoherent*. As a matter of fact, such a soliton pair involves two steady-state photorefractive screening solitons which propagate collinearly in the crystal and experience a refractive-index modulation induced by both beams. The coupled soliton pair can be in dark–bright as well as bright–bright and dark–dark realizations. A stable dark–bright photorefractive soliton pair can only be realized using a self-defocussing nonlinearity and when the peak intensity of dark component is higher than that of the bright component. In earlier experiments (Z. Chen et al., 1996c) the coupling and decoupling between two bright screening solitons was demonstrated.

First, Z. Chen et al. (1996d) generated a coupled dark–bright soliton pair, see Fig. 30a and Fig. 30b. The width of dark notch was 14 mm and that of the bright beam was 11 mm, see Fig. 30a.

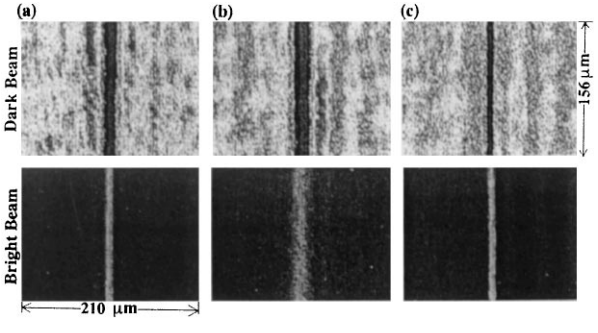

Fig. 30. Photographs showing a coupled fundamental dark–bright soliton pair: (a) input, (b) output (normal diffraction), and (c) output coupled soliton pair (Z. Chen et al., 1996d).

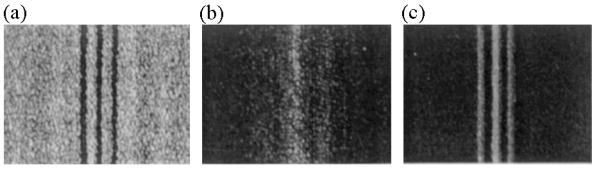

Fig. 31. Photographs showing (a) the output dark and (b) the bright beams when the pair is decoupled. (c) Bright beam guided in the triple-soliton induced waveguide (Z. Chen et al., 1996d).

Without the external field, each beam diffracts after 5 mm of propagation in the crystal, as shown in Fig. 30b. By applying a voltage of -400 V (negative relative to the *c*-axis) between the two electrodes (spaced by 4.5 mm), Z. Chen et al. (1996c) observed that the output beams coupled to a steady-state dark–bright soliton pair. They monitored the bright and dark components of the soliton pair by blocking one and sampling the other within a time interval of 0.1 s, so the refractive index modulation induced by the coupled soliton pair cannot respond in such a short time to the change due to blocking of one beam. Fig. 30c shows the photographs of the output dark and bright components taken by Z. Chen et al. (1996d) immediately (less than 0.1 s) after the pairing beam is blocked. In this way, it is possible to distinguish between the components despite that they have the same frequency and polarization. The two beams are coupled to form a fundamental soliton pair.

Z. Chen et al. (1996d) presented also an elegant proof that each of the two beams cannot maintain the form of a fundamental soliton when they are decoupled, i.e., when one of the beams is blocked and a new steady-state is reached. Fig. 31a and Fig. 31b show photographs of the dark and bright beam, respectively, taken after the pairing beam is blocked for a time (1 min) much longer than the crystal response time. Since the polarity of the applied voltage is not appropriate for the bright soliton, the bright beam alone diffracts and experiences self-defocussing, see Fig. 31b. In the case of dark beam alone, the applied voltage is too high to maintain the fundamental dark soliton without the presence of the bright beam. The dark beam, instead, evolves into a triple-soliton structure shown in Fig. 31a when the bright beam is absent and all other experimental conditions remain unchanged. Interestingly, as Z. Chen et al. (1996d) unblocked the bright beam, guidance of the bright beam into the triple channels (waveguide) induced by the high-order dark soliton was observed (Fig. 31c). This waveguide persisted for a few seconds before the bright beam gets defocussed by the bias field. Eventually, a fundamental dark soliton was retrieved without the bright beam by readjusting the voltage to -250 V.

7. Dark solitons in higher dimensions

7.1. Introductory remarks

In the waveguide geometry light beams are confined by a slab waveguide and, with a good accuracy, guided waves can be regarded as $(1+1)$-dimensional objects. However, in a bulk medium there exists one more, transverse, direction and therefore the concept of solitary waves should be extended to higher dimensions. The simplest way to do this is just to consider *quasi-one-dimensional dark solitons* in a bulk medium. This idea leads to different kinds of

superpositions of such plane solitary waves, including grids and crosses of dark solitons (Swartzlander et al., 1991), a superposition of bright and dark plane solitons (Hayata and Koshiba, 1993a), etc. In spite of the fact that such *plane solitary waves* are expected to be similar to (1 + 1)-dimensional solitons, the freedom to extend to the other direction brings a completely new physics: It is generally believed that all kinds of plane solitary waves are unstable to transverse modulation with a finite-width instability band [see, e.g., Kuznetsov et al. (1986) and references therein]. In the case of dark solitons, the linear stability analysis was first developed for a defocussing Kerr medium (i.e., for the cubic NLS equation) by Kuznetsov and Turitsyn (1988) who demonstrated that plane dark solitons (i.e., *dark soliton stripes*), are unstable to transverse long-wavelength modulations.

This instability can be suppressed provided a stripe is bent to form a loop (or ring dark soliton) with the radius less than the smallest possible wavelength of the instability domain (Kivshar and Yang, 1994c). However, such a ring dark soliton cannot exist as a stationary object, and it expands or collapses depending on initial conditions.

An important physical question then is: *What kind of stable stationary structures can exist in the* (2 + 1)*-dimensional geometry*? In the focussing case, it is known that transverse instability of a plane, (1 + 1)-dimensional bright soliton leads to the creation of (2 + 1)-dimensional bright solitons of circular symmetry that can be stable in a non-Kerr bulk medium [see, e.g., Kuznetsov et al. (1986)]. A similar scenario is expected for dark solitons. Indeed, numerical simulations (Law and Swartzlander, 1993; McDonald et al., 1993; Josserand and Pomeau, 1995; Tikhonenko et al., 1996a; Mamaev et al., 1996a,b), asymptotic analytical theory (Pelinovsky et al., 1995), and recent experimental results (Tikhonenko et al., 1996a; Mamaev et al., 1996a,b) have demonstrated that the transverse instability of plane dark solitons leads to a generation of pairs of optical *vortex solitons* with alternate polarities.

Optical vortex solitons are the only stable (2 + 1)-dimensional stationary structures which have been reported up to now to exist in a bulk optical medium with the nonlinear defocussing refractive index. In the context of optics, the vortex solitons have been predicted theoretically by Snyder et al. (1992) as '*stable black self-guided beams of circular symmetry*'. As a matter of fact, these objects have been known much earlier, since the pioneering paper by Pitaevsky (1961) [see also Ginzburg and Pitaevsky (1958)], as topological excitations of an imperfect Bose gas in the theory of superfluids. Experimental observation of optical vortex solitons has been already reported by several groups and in the following sections we discuss generation, properties, and experimental observation of optical vortex solitons.

Furthermore, vortex solitons themselves can be generalized to include polarization properties of light. There exist two types of such generalization. First, we can allow the field of different polarizations to have a vortex-like structure. This kind of *double vortex solitons* is known in other fields [see, e.g., Perivolaropoulos (1993) and Pismen (1994a,b) and references therein] and it was recently introduced in nonlinear optics (Law and Swartzlander, 1994; Velchev et al., 1996). Second, a vortex of one polarization can guide the field of the other polarization giving rise to the (2 + 1)-dimensional generalization of the bright–dark solitons discussed in Section 5.1 [see, e.g., Pismen (1994b) and Sheppard and Haelterman (1994)].

To conclude this introductory section, we would like to mention that the (2 + 1)-dimensional beam propagation can be generalized to include one more dimension. This is the case when we allow *nonstationary beam propagation* and introduce time as an extra variable. In fact, this

extension leads to the concept of *light bullets* introduced by Silberberg (1990b) for the (3 + 1)-dimensional generalization of bright solitons. In the case of dark solitons, a vortex soliton in the (3 + 1)-dimensional space (i.e. two transverse and one propagation coordinates plus time) forms the so-called vortex line which itself is unstable to transverse modulations (Kuznetsov and Rasmussen, 1995). It is expected that this instability should lead to the formation of 'dark light bullets' which are known to exist in the anomalous group-velocity dispersion regime (Y. Chen and Atai, 1995) [while for the normal dispersion the situation is far from clear, even for a focussing medium, e.g., Chernev and Petrov (1992)]. These interesting objects still require the further analysis of their structure, stability, and interaction. A scenario of the decay of a vortex line as well as the existence of localized multidimensional waves in the case of the normal dispersion still remain unknown.

7.2. Transverse instability of plane solitons

In the case of two transverse dimensions, i.e., for a stationary propagation in a bulk medium, dark solitons can be observed experimentally as dark stripes or grids with the properties similar to those of one-dimensional dark solitons (see Section 6.2.2 above). However, the linear stability analysis shows that a plane dark soliton is unstable to transverse long-wavelength modulations [Kuznetsov and Turitsyn (1988); see also Kuznetsov and Rasmussen (1995)]. Numerical calculations show that, as a result of the development of this instability, a dark stripe may decay into a sequence of optical vortex solitons of alternative polarities [e.g., Law and Swartzlander (1993), McDonald et al. (1993), Tikhonenko et al. (1996a) and Mamaev et al. (1996a,b)].

From the mathematical point of view, the problems mentioned above can be described in the framework of the cubic NLS equation with a transverse coordinate y included,

$$i\frac{\partial u}{\partial z} + \frac{1}{2}\nabla^2 u + (1 - |u|^2)u = 0\,, \tag{7.1}$$

where the dimensionless, slowly varying field amplitude u has nonzero asymptotics, $|u| \to 1$ for $x, y \to \pm\infty$, and the vector operator ∇ is defined as $\nabla = (\partial/\partial x, \partial/\partial y)$, so that $\nabla^2 \equiv \nabla \cdot \nabla$.

As has been shown in Section 2.3, the NLS Eq. (7.1) has an exact one-dimensional solution describing a dark soliton stripe parallel to the y-axis, which we write here in the following form:

$$u_s(x, z) = k \tanh[k(x - vz)] + iv\,, \tag{7.2}$$

where the amplitude parameter k $(0 < k < 1)$ and the transverse velocity v $(v^2 \leq 1)$ are coupled through the relation $k^2 + v^2 = 1$. According to Kuznetsov and Turitsyn (1988), the plane dark soliton, Eq. (7.2), is unstable against transverse perturbations $\sim \cos(py)$ with the wave numbers $p < p_{cr}(k)$ where

$$p_{cr}^2(k) = k^2 - 2 + 2\sqrt{k^4 - k^2 + 1}\,. \tag{7.3}$$

In the parameter plane (p, k), the instability domain is bounded by the curve $p = p_{cr}(k)$, so that if we apply a periodic perturbation with any wave number $p < p_{cr}(k)$, the amplitude of a plane dark

soliton, i.e., a dark-soliton stripe, will grow exponentially in the transverse direction according to the linear stability analysis. Nonlinear regimes of such an instability have been investigated numerically [e.g., Law and Swartzlander (1993) and McDonald et al. (1993)] and also analytically, by means of the asymptotic technique valid near the threshold of the soliton instability (Pelinovsky et al., 1995). In particular, it was demonstrated that a plane dark soliton may decay into a chain of optical vortices of the opposite polarities. This kind of the instability-induced evolution, as was shown by Pelinovsky et al. (1995), is one of the main scenarios of the instability of a plane black soliton, whereas an unstable plane grey soliton may not decay into vortices, instead it displays long-lived oscillations accompanying by emission of linear waves propagating along the background.

Recently, the transverse instability of a plane dark soliton in a strongly saturable optical medium has been studied analytically and numerically by Kivshar et al. (1997b) in the framework of the generalized NLS equation. By employing an asymptotic expansion technique for perturbations with small wavenumbers, Kivshar et al. (1997b) derived an analytical expression for the growth rate $\lambda_\perp$ of the transverse modulations ($p^2 \ll 1$),

$$\lambda_\perp^2 = a^2 p^2 , \qquad a = \left[\left(\frac{\partial P_s}{\partial v} \right) H_s \right]^{1/2} , \tag{7.4}$$

where $P_s(v)$ and $H_s(v)$ are the renormalized invariants, momentum and Hamiltonian, introduced in Section 2.5. The index 's' stands for those values calculated for the exact (1 + 1)-dimensional solution for a plane dark soliton. The analytical result (7.4) and numerical simulations carried out by Kivshar et al. (1997b) display the main effect of the nonlinearity saturation: it leads to an effective suppression of the dark-soliton transverse instability. Fig. 32 presents the numerically calculated maximum growth rate $(\lambda_\perp)_{max}$ of the transverse instability of a black (i.e., the dark soliton at $v = 0$) plane soliton in a standard model of saturable nonlinearity which clearly displays the suppression of instability.

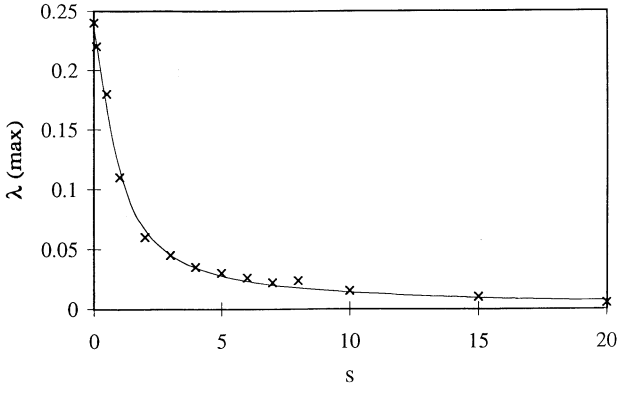

Fig. 32. Maximum growth rate of the transverse instability of a plane black soliton in a saturable defocussing medium vs. the dimensionless saturation parameter s. Crosses are numerical simulation results whereas the solid curve is a numerical approximation (Kivshar et al., 1997b).

7.3. Vortex solitons: theory

7.3.1. Stationary solutions

It is well known that in linear optics and acoustics vortex can appear as a particular mode described by the wave equation and associated with a wavefront screw dislocation (or phase singularity) of the linearly diffracting field (Nye and Berry, 1974; Bazhenov et al., 1992; Heckenberg et al., 1992; Basistiy et al., 1995). These dislocations can be generated, for example, by the wave scattering from a rough surface [e.g., Baranova et al. (1981) and Freund (1994)]. In a self-defocussing nonlinear medium this screw dislocation can create a stationary beam structure with a phase singularity known as a *vortex soliton.*

Existence of vortex solutions of the (2 + 1)-dimensional defocussing NLS equation can be established from an analogy between optics and fluid mechanics. Indeed, using the so-called Madelung transformation [see, e.g., Spiegel (1980), Donelly (1991) and Nore et al. (1993)]

$$u(\boldsymbol{r}, z) = \rho(\boldsymbol{r}, z)\mathrm{e}^{\varphi(r,\ z)}\,,$$

we transform the NLS Eq. (7.1) to the following form:

$$\frac{\partial\rho^2}{\partial z} + \nabla\cdot(\rho^2\nabla\varphi) = 0\,, \tag{7.5}$$

$$\frac{\partial\varphi}{\partial z} + \frac{1}{2}(\nabla\varphi)^2 = 1 - \rho^2 + \frac{\nabla^2\rho}{2\rho}\,. \tag{7.6}$$

Eqs. (7.5) and (7.6) can be treated as the equations of conservation for mass and momentum of a compressible inviscid fluid of density $\sigma = \rho^2$ and velocity $\boldsymbol{V} = \nabla\varphi$ with the pressure defined as $p = \sigma^2/2$. Importantly, this kind of analogy between optics and fluid mechanics still remains valid for the generalized NLS equation with the nonlinearity function $g(|u|^2)$, in this case the effective pressure is defined as

$$p(\sigma) = \int \mathrm{d}x\ \sigma\frac{\mathrm{d}}{\mathrm{d}x}\,g(\sigma)\,.$$

This analogy is however is not exact because, additionally to the standard pressure Eq. (7.6) includes the second term, so-called 'quantum mechanical pressure', which has no analog in fluid mechanics.

The Madelung transformation is singular at the points where $\rho = 0$ and around such points on the plane (x, y) the circulation of $\boldsymbol{V}$ is equal to 2π. These points are *topological defects* of the scalar field called vortices.

To find the structure of the stationary solution for the vortex soliton (or dark soliton with the circular symmetry), we look for the solutions of the normalized NLS Eq. (2.3) for the cubic nonlinearity in the polar coordinates r and θ,

$$u(r, \theta; z) = u_0 U(r)\mathrm{e}^{\mathrm{i}m\theta}\mathrm{e}^{\mathrm{i}u_0^2 z}\,, \tag{7.7}$$

where u_0 is the background intensity, the integer m is the so-called winding number (or the vortex charge), and the modulus function $U(r)$ satisfies the (normalized) boundary value problem,

$$\frac{d^2U}{dr^2} + \frac{1}{r}\frac{dU}{dr} - \frac{m^2}{r^2}U + (1 - U^2) = 0\,, \tag{7.8}$$

for positive r and the boundary conditions,

$$U(0) = 0\,, \quad U(\infty) = 1\,.$$

The continuity of u at $r = 0$ forces the first condition, while $U(\infty) = 1$ is consistent with a locally uniform state as $r \to \infty$. Asymptotic behavior of $U(r)$ may be established directly from Eq. (7.8):

$$U(r) \sim ar^{|m|} + \mathcal{O}(r^{|m|+2})\,, \quad \text{as } r \to 0\,,$$

$$U(r) \sim 1 - \frac{m^2}{2r^2} + \mathcal{O}(1/r^4)\,, \quad \text{as } r \to \infty\,.$$

Fig. 33 depicts profiles of the normalized function $U(r)$ found numerically for four different values m [e.g., Neu (1990); see also Velchev et al. (1997)]. The neighborhood of $r = 0$ where the function U is significantly less than one is called *the vortex core*.

Generally speaking, the structure of the vortex soliton can be also defined in a similar way for any nonlinear medium by solving numerically the equation for the amplitude function $U(r)$ similar to Eq. (7.8). This analysis was carried out for the NLS model with nonlinearity saturation (Y. Chen, 1992a,b; Tikhonenko et al., 1997). No qualitatively new features were discovered. As was mentioned by Tikhonenko et al. (1997), in a saturable medium the effective diameter of the vortex core

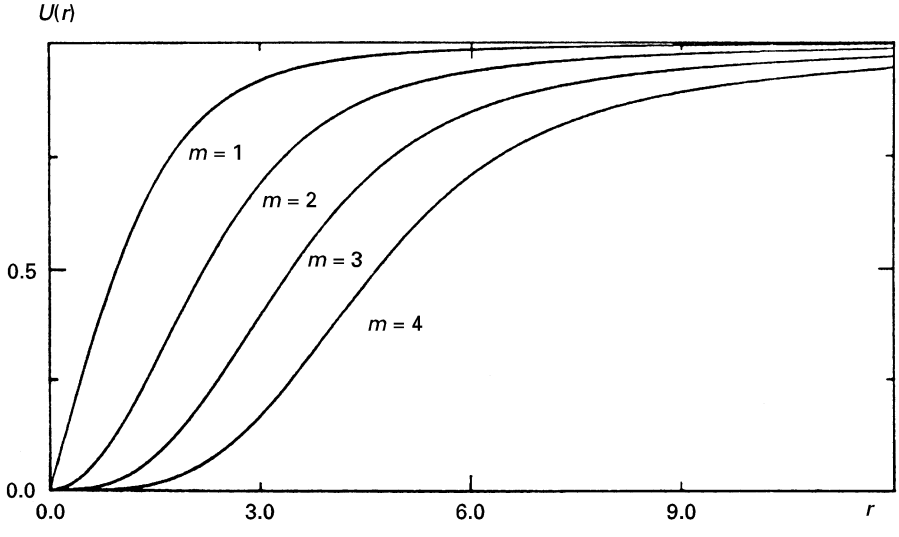

Fig. 33. Numerical solution for the vortex profile in a Kerr medium for different values of the vortex charge, $m = 1, 2, 3,$ and 4 (Neu, 1990).

increases almost linearly with the dimensionless saturation parameter defined as $s = I_0/I_s$, where I_s and I_0 are the saturation and maximum background intensities.

Stability of vortex solitons in a generalized NLS equation has been not addressed so far. However, it is usually believed that the vortices with the winding numbers $m = \pm 1$ are *topologically stable*, whereas those with larger values of $|m|$ are unstable against decay into $|m|$ single-charge vortices. This later statement requires the further analysis because, as was recently demonstrated by Aranson and Steinberg (1996) in the context of a model of superflow, the multicharged vortex solitons are surprisingly very long-lived objects, contrary to the accepted opinion.

7.3.2. Vortex rotation and drift

Being excited experimentally on a diffracting background beam of finite extend, a vortex soliton displays a nontrivial dynamics. The effects such as the vortex rotation and radial drift relatively to the Gaussian carrier-wave beam are indeed observed experimentally, and they cannot be predicted from the analysis of stationary solutions. Describing these effects theoretically requires the development of special analytical techniques for analyzing the vortex motion. This was done in the papers by Christou et al. (1996) and Kivshar et al. (1997a).

Following Kivshar et al. (1997a), we consider the propagation of a monochromatic scalar electric field $\mathscr{E}$ in a bulk optical medium with an intensity-dependent refractive index, $n = n_0 + n_{nl}(I)$, where n_0 is the linear refractive index of the unperturbed medium, and $n_{nl}(I)$ describes the change in the index due to the field intensity $I = |E|^2$. In the so-called paraxial approximation, Maxwell's equations can be reduced to the generalized NLS equation for the slowly varying envelope $\mathscr{E}(z, \boldsymbol{r}) = E(z, r)\exp(-ik_0 n_0 z)$ of the electric field [cf. Eq. (2.3)],

$$2ik_0 n_0 \frac{\partial \mathscr{E}}{\partial z} + \nabla^2 \mathscr{E} + g(I)\mathscr{E} = 0\,, \tag{7.9}$$

where k_0 is the free-space wave number, and the gradient operator ∇ was defined above. The function $g(I) = 2n_0 k_0^2 n_{nl}(I)$ describes the nature of nonlinearity, and it is determined by the intensity-dependent correction $n_{nl}(I)$ to the refractive index. Analysing the interaction of a vortex soliton with a *background field*, we look for solutions of Eq. (7.9) in the form (Kivshar and Yang, 1994b)

$$E(z, \boldsymbol{r}) = \sqrt{I_b}\, e^{i\theta_b}\, u(z, \boldsymbol{r})$$

and assume that both the background intensity $I_b(z, \boldsymbol{r})$ and phase $\theta_b(z, \boldsymbol{r})$ satisfy Eq. (7.9). This yields the equation for the auxiliary field $u(z, \boldsymbol{r})$,

$$2ik_0 n_0 \frac{\partial u}{\partial z} + \nabla^2 u + [g(I_b|u|^2) - g(I_b)]u = -\nabla u \cdot \boldsymbol{f}, \tag{7.10}$$

where the complex vector $\boldsymbol{f}$ is defined by gradients of the background field,

$$\boldsymbol{f} = \boldsymbol{f}^r + i\boldsymbol{f}^i \equiv \nabla \ln I_b + 2i\nabla\theta_b\,, \tag{7.11}$$

and the boundary condition $|u| \to 1$ applies for large $\boldsymbol{r}$.

In the particular case of a defocussing Kerr medium, i.e., when $n_{nl}(I) = -|n_2|I$, Eq. (7.10) takes the form of a perturbed NLS equation [cf. Eq. (7.1)]

$$2ik_0 n_0 \frac{\partial u}{\partial z} + \nabla^2 u + 2k_0^2 n_0 |n_2| I_b (1 - |u|^2) u = -\nabla u \cdot \boldsymbol{f}. \tag{7.12}$$

Kivshar et al. (1997a) applied the method of matched asymptotic expansions to analyze a slow vortex motion in a shallow-gradient background field. The expansions near and far form the vortex core followed from the asymptotic matching at an intermediate distance. We mention here the most important steps of this derivation which follows a similar analysis (Rubinstein and Pismen, 1994) that, in its turn, draws on the application of the same technique in other settings (Neu, 1990; Pismen and Rodriguez, 1990; Pismen and Rubinstein, 1991; Rubinstein and Pismen, 1994).

We assume that the function u describes a vortex with the centre coordinate $\boldsymbol{r}_0(z)$, and the fields I_b and θ_b vary slowly in comparison with the vortex scales. Then, the problem is to describe a change of the position of the vortex (i.e., the so-called vortex drift) for the field u under the action of these slowly varying background fields. To clarify the idea of a 'background field', one may picture it as the field which would exist if the vortices were somehow removed. We rescale to dimensionless coordinates by using the value of the background field at the vortex centre, $I_0 = I_b(\boldsymbol{r}_0)$, so that $z \to z/(k_0 n_0 |n_2| I_0)$ and $\boldsymbol{r} \to \boldsymbol{r}/(k_0 n_0 \sqrt{2|n_2| I_0/n_0})$, then set $\boldsymbol{f} = \varepsilon \boldsymbol{F}$ where $|\boldsymbol{F}| = O(1)$. In this case Eq. (7.12) becomes

$$i\frac{\partial u}{\partial z} + \nabla^2 u + \frac{I_b}{I_0}(1 - |u|^2) u = -\varepsilon \nabla u \cdot \boldsymbol{F}, \tag{7.13}$$

where $\boldsymbol{F}$ has also been rescaled. The vortex velocity, in this new coordinate scale, is assumed to be small, producing the same small parameter ε as the background gradients, so that

$$\frac{d\boldsymbol{r}_0}{dz} = \boldsymbol{w} = \varepsilon \boldsymbol{V}, \tag{7.14}$$

where $|\boldsymbol{V}| = O(1)$.

Next, we need to solve Eq. (7.13) in the vicinity of the vortex core in the reference frame moving with the vortex drift velocity $\boldsymbol{w}$. Since the background field does not change significantly on the scale of the core, the term I_b/I_0 can be expanded as

$$I_b/I_0 \approx 1 + \boldsymbol{r} \cdot \nabla \ln I_b|_{\boldsymbol{r}=\boldsymbol{r}_0} \equiv 1 + \varepsilon \boldsymbol{r} \cdot \boldsymbol{F}_0^r, \tag{7.15}$$

where the rescaled complex vector $\boldsymbol{F}_0$ is calculated at the position of the vortex, $\boldsymbol{F}_0 \equiv \boldsymbol{F}|_{\boldsymbol{r}=\boldsymbol{r}_0}$. Thus, Eq. (7.13) becomes

$$\nabla^2 u + (1 - |u|^2) u = \varepsilon[(iV - F) \cdot \nabla u - \boldsymbol{r} \cdot \boldsymbol{F}_0^r (1 - |u|^2) u]. \tag{7.16}$$

We expand also the field u as $u = u_0 + \varepsilon u_1 + \cdots$ and substitute it into Eq. (7.16). In the zero-order approximation in ε we find the standard stationary NLS equation for the vortex

$$\nabla^2 u_0 + (1 - |u_0|^2) u_0 = 0, \tag{7.17}$$

so that, in the polar coordinates of the moving frame, its solution is given by the expression

$$u_0 = \rho(r) e^{im\phi} \tag{7.18}$$

where $m = \pm 1$ is the vortex charge (polarity), and the function $\rho(r)$ that verifies

$$\frac{\mathrm{d}^2\rho}{\mathrm{d}r^2} + \frac{1}{r}\frac{\mathrm{d}\rho}{\mathrm{d}r} + \left(1 - \frac{1}{r^2} - \rho^2\right)\rho = 0 \tag{7.19}$$

is the well known vortex amplitude profile, first studied in the superfluid context, and known numerically [Pitaevsky (1961); see also Donelly (1991) and references therein].

The first-order approximation yields the inhomogeneous equation,

$$\mathscr{L}(u_1, u_1^*) = \Psi(\boldsymbol{r}) \tag{7.20}$$

with the homogeneous part

$$\mathscr{L}(u_1, u_1^*) = \nabla^2 u_1 + u_1 - 2|u_0|^2 u_1 - u_0^2 u_1^*, \tag{7.21}$$

and the right-hand-side

$$\Psi(\boldsymbol{r}) = (\mathrm{i}\boldsymbol{V} - \boldsymbol{F}_0)\cdot\nabla u_0 - \boldsymbol{r}\cdot\boldsymbol{F}_0^{\mathrm{r}}(1 - |u_0|^2)u_0 . \tag{7.22}$$

Solvability condition of the linear Eq. (7.20) can be used to derive the equation of motion for the vortex core. These conditions follow from the orthogonality of the inhomogeneous part, $\Psi(\boldsymbol{r}\}$, to the two components of the translational eigenfunction, ∇u_0^*, of the adjoint homogeneous equation. Using the method of matched asymptotics allows to present the solvability conditions in the following vector form (Kivshar et al., 1997a)

$$\boldsymbol{w} = \boldsymbol{f}_0^{\mathrm{i}} + m\boldsymbol{J}\boldsymbol{f}_0^{\mathrm{r}} \ln\left(\tfrac{1}{4}c|\boldsymbol{f}_0^{\mathrm{r}}|\mathrm{e}^{\gamma}\right) \tag{7.23}$$

where c is found numerically (for the cubic nonlinearity $c \approx 1.126$), γ is the Euler constant ($\gamma \approx 0.577$), $\boldsymbol{J}$ is the operator of rotation by $\pi/2$ defined by the matrix

$$\boldsymbol{J} = \begin{pmatrix} 0 & -1 \\ 1 & 0 \end{pmatrix},$$

and the force components, $\boldsymbol{f}$, are defined by Eq. (7.11), but evaluated at the vortex core.

In the dimensional units which are required to compare with the experimental results (see Section 7.4.2 below), the motion equation for the vortex core can be presented, by rescaling Eq. (7.23), as the following:

$$k_0 n_0 \frac{\mathrm{d}\boldsymbol{r}_0}{\mathrm{d}z} = \left(-\nabla\theta_{\mathrm{b}} + \frac{m}{2} C\boldsymbol{J}\nabla \ln I_{\mathrm{b}}\right)\Bigg|_{\boldsymbol{r}=\boldsymbol{r}_0}, \tag{7.24}$$

where $\boldsymbol{J}$ is the operator introduced above, and C is slowly varying function of I_{b}. In the particular case of the Kerr medium, the coefficient C has been derived above:

$$C = -\ln\left(\frac{c\mathrm{e}^{\gamma}|\nabla I_{\mathrm{b}}|}{4k_0 n_0\sqrt{2n_2 I_0/n_0}}\right)$$

but in general case of non-Kerr medium we can expect a similar form of the motion equation. Indeed, for a general function $g(I)$ in Eq. (7.10), the coordinates are rescaled by $g(I_0)$ rather than

I_0 as before, and Eq. (7.13) becomes

$$i\frac{\partial u}{\partial z} + \nabla^2 u + \frac{g(I_b)}{g(I_0)}\left[1 - \frac{g(|u|^2 I_b)}{g(I_b)}\right]u = -\varepsilon \nabla u \cdot \boldsymbol{F}\,. \tag{7.25}$$

Expanding as in Eq. (7.15) and proceeding exactly as in the Kerr case gives in the zero-order a modified equation for the stationary vortex profile

$$\nabla^2 u_0 + (1 - G(|u_0|)^2)u_0 = 0\,, \tag{7.26}$$

where $G(x) = g(I_0 x)/g(I_0)$. In the first-order approximation Eq. (7.20) is again obtained, but with a modified coefficient on the $\boldsymbol{r}\cdot\boldsymbol{F}_0^r$ term. Thus, all results are obtained as before with a modified numerical coefficient c and with a rescaled coefficient

$$C = -\ln\left(\frac{c e^{\gamma} |\nabla I_b|}{4k_0 n_0 \sqrt{2n_{nl}(I_0)/n_0}}\right)$$

In particular, for the important case of a saturable nonlinearity we take

$$g(I) = \frac{I}{1 + sI}\,,$$

where the dimensionless parameter s characterizes, as above, the inverse saturation intensity I_s relative to the background intensity I_0; larger values of s correspond to a stronger saturation of the nonlinearity. Calculation of the coefficient c for this model yields $c = 1.126$ at $s = 0$ (non-saturable case), $c = 1.412$ at $s = 1$, and $c = 1.639$ at $s = 2$ (Kivshar et al., 1997a).

As follows from the analysis presented above, to describe the vortex drift induced by the diffracting background field, one should know the evolution of this field a priori, so that the radial and angular velocity components for the vortex motion can be calculated according to Eq. (7.24). It is assumed that the background field in the absence of the vortex evolves in approximately the same manner as it would when hosting a vortex. Thus, even qualitative knowledge of the propagation behaviour of a field may be used, along with the vortex equation of motion, to predict the action of a vortex subsequently nested in that field. The following example of a vortex nested in a Gaussian beam serves to illustrate how vortex motion may be simply predicted (Christou et al., 1996).

The transverse 'velocity' of a vortex, according the model, Eq. (7.24), has two components arising separately from the transverse phase and intensity gradients of its background field, evaluated at the position of the vortex. The first component, $-\nabla\theta_b$, is directed normal to the wavefront of the background, that is in the direction of energy flow in the background field, giving rise to *radial motion* of a vortex in a Gaussian beam [see also Christou et al. (1996)]. The second component, $\frac{1}{2}mC\boldsymbol{J}\nabla \ln I_b$, is directed along the intensity contour (isophote) of the background upon which the vortex is positioned, with the sense of direction given by the vortex charge, $m = \pm 1$. For a Gaussian background, the isophote in any transverse plane is a circle, and so the second component of velocity describes the *angular motion* of the vortex, first observed experimentally by Luther-Davies et al. (1994). The flattening of the intensity profile under nonlinear action reduces the intensity gradient and thus subtracts from the rotation experienced by a vortex in linear propagation. For flatter intensity profiles (plane waves), the motion of the vortex becomes more

dependent on the background wavefront solely, and results of other work which have examined this behaviour (Staliunas, 1994a,b; Roux, 1995) may be recovered.

A simple analysis can be made for 'beam-like' field, employing a Gaussian ansatz to approximate the evolution of the background field in a self-defocussing medium (Christou et al., 1996). Using the Gaussian ansatz, we can make explicit calculations in Eq. (7.24), and the resulting equations for the vortex core can be integrated to yield

$$r_0(z) = \frac{w(z)}{w(0)} r_0(0)\,, \tag{7.27}$$

$$\phi(z) = \phi(0) + \frac{mC}{k_0 n_0} \int_0^z \frac{\mathrm{d}\zeta}{w^2(\zeta)}\,, \tag{7.28}$$

where the polar coordinates r_0 and ϕ characterize the vortex position at a propagation distance z. Here $w(z)$ is the beam radius which can be calculated by various methods [e.g., Butylkin et al. (1989)]. These equations have been found to effectively characterize aspects of vortex behaviour important to the problem of vortex steering (Christou et al., 1996; Kivshar et al., 1997a). Although linear propagation is outside the parameters set in the derivation of the equation of motion, exact agreement is obtained, in this case, with vortex dynamics calculated by other methods (Indebetouw, 1993), provided that $C \to 1$.

Vortex *interaction* is also adequately accounted for by considering the host beam for one vortex as being comprised of the underlying background field along with the remaining vortices. A single vortex has circular isophotes centred on the vortex core and also circular energy flow. Thus one vortex interacting with the background field generated by another, will move in the direction normal to the line connecting its core with the background vortex. The situation is exactly the same reversing the roles of the vortices in the pair. The resultant motion of the vortex pair can therefore be only circular or parallel, depending on the vortex chirality. It is also possible to include the effect of a non-planar background in this picture, in order to estimate any influence on the observed interactions between vortices, as observed experimentally by Luther-Davies et al. (1994).

A simple physical argument underlies this form for the vortex equation of motion used in the above examples, which may clarify the mechanisms underlying vortex behaviour. Consider the 'momentum', $\int I \nabla\theta$, of a small element of the transverse field surrounding the vortex core. In the first case, assume that the intensity is uniform, then the momentum of the element is proportional to the sum of the vortex phase gradient around the core, which is zero, and the sum of the background phase gradient around the core. Thus the element around the core has a momentum approximately proportional to the background phase gradient at the vortex position, giving rise to the first velocity component in the equation of motion. In the second case, assume that the background phase is uniform, then the background phase gradient around the core is zero. The momentum of the element is thus proportional to the sum of the vortex phase gradient weighted by the background intensity, around the core. Using the ideas of vector summation, it is apparent that an imbalance in background intensity, over the small region around the vortex core, gives rises to a net momentum component in the direction normal to the intensity gradient, i.e., along the isophote, sourcing the second velocity component in the equation of motion. That the origin of vortex dynamical effects may be justified in this way imparts a generality to the equation of motion,

suggesting that it may retain some validity even outside the specific parameters set in its formal derivation.

7.4. Vortex solitons: experiments

7.4.1. Transverse instability of dark soliton stripes

Most of the experiments on dark spatial solitons reported in Section 6 involved the creation of dark soliton stripes in a (2 + 1)-dimensional geometry. As noted, such stripes should be unstable due to transverse modulational instability which leads to stripe breakup (Kuznetsov and Turitsyn, 1988) and the eventual creation of optical vortex solitons (Law and Swartzlander, 1993; McDonald et al., 1993). The instability was avoided in the early experiments by the use of finite-sized background beams and weak nonlinearity.

By increasing the nonlinearity, however, the transverse instability should be observed even with finite sized beams. Experiments to verify the existence of this transverse instability, and through it the creation of optical vortex solitons, have been performed by Tikhonenko et al. (1996a) using a continuous wave, Ti : sapphire laser and a nonlinear medium comprised of atomic rubidium vapour. Very similar observations, with less evidence of the stripe decay into vortex solitons, were performed simultaneously by Mamaev et al. (1996a,b) for photorefractive dark solitons.

In the experiments using rubidium vapor (Tikhonenko et al., 1996a), the laser output was a linearly polarized slightly elliptical Gaussian beam with a wavelength tuned close to the rubidium atom resonance line at 780 nm. A π phase jump was imposed across the beam centre using a mask and the resulting beam imaged into the nonlinear medium. The rubidium vapour concentration could be increased up to 10^{13} cm^{-3} by changing the cell temperature. Images of the beam at the output of the cell were recorded by a CCD camera and frame capture system. A schematic of this experimental arrangement, used also to observed optical vortex solitons, is shown in Fig. 34.

The important step in observing the instability was to resonantly enhance the value of nonlinearity of the medium by tuning the laser frequency close (-0.4 GHz to -1.0 GHz) to the rubidium atom D_2 line and the use of the maximum vapour pressure consistent with tolerable absorption. The power in the beam at the input face of the cell was 240 mW with a $1/e^2$ waist of 0.3 mm. A maximum nonlinear refractive index change of order of 10^{-4} was achieved.

Fig. 35 shows a series of output intensity profiles, calculated numerically (left column) and observed experimentally (right column), with increasing cell temperature and with the detuning fixed at approximately 0.85 GHz. For vanishingly small vapour concentration, the beam underwent linear propagation through the medium, leading to the output intensity profile shown in Fig. 35a. With increasing temperature (i.e., increasing nonlinearity), the output beam developed a vertically uniform dark soliton stripe, as shown in Fig. 35b. Further increase in the temperature

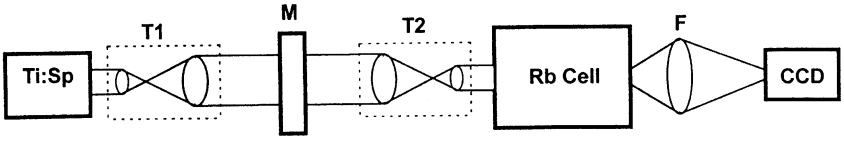

Fig. 34. Schematic presentation of the experimental setup for the observation of the dark soliton decay into vortex solitons and the measurement of the vortex parameters.

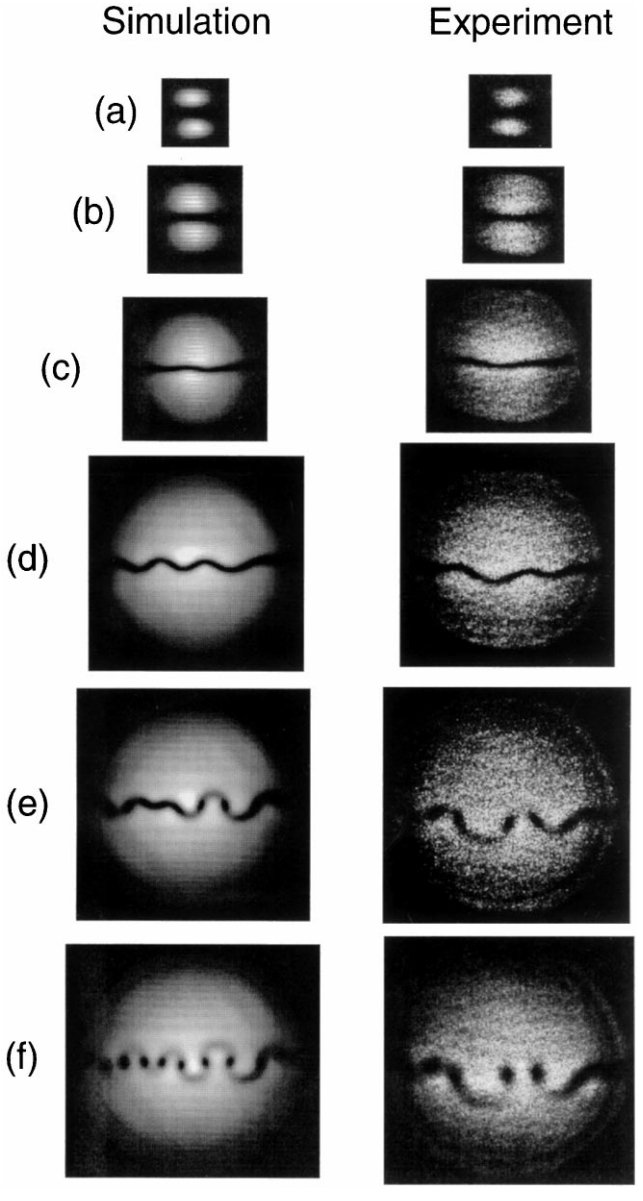

Fig. 35. Output beam intensity profiles demonstrating the instability of a dark soliton stripe as the nonlinearity is increased. The vapor concentration increases from vanishingly small in (a) to the order of 10^{13} cm^{-2} in (f). The cell temperatures were (a) 40, (b) 72, (c) 82, (d) 90, (e) 112, and (f) 125. *Left*: Results of numerical simulations. *Right*: Experimental results. Laser detuning was held constant at 0.85 GHz, and the power of the beam at the cell was 240 mW, corresponding to a maximum intensity of approximately 170 W/cm^2 (Tikhonenko et al., 1996a).

led to the growth of a periodic modulation of the uniformity of the stripe (see Fig. 35c). As the temperature was further increased, the breakup of the stripe began, initially appearing as a growing, 'snake-type' bending (Fig. 35d), then as breaking, with field coalescing into dark spots at the

inflection points in the bends (Fig. 35e). At the highest nonlinearity the dark spot assumed close to circular symmetry consistent with the predicted formation of a pair of optical vortex solitons (Fig. 35f and insert).

The process of breakup was found to be sensitive to the size of the phase step on the input beam. Misalignment of the phase mask from the optimum (which provided a phase jump closest to π) caused the final stages in evolution of the instability involving the creation of optical vortex pairs, to disappear. Under such conditions, only the snake-type bending of the soliton stripe was observed. This supported the theoretical prediction (see Section 7.2) that the growth rate of the instability should be lower for grey soliton stripes.

Tikhonenko et al. (1996a) also carried out numerical simulations based on the generalized NLS equation including saturation and dissipative effects for comparison with the experimental results (see Fig. 35, left column). The calculated output intensity distributions showed the same dynamics observed experimentally with increasing nonlinearity. The beam defocussing, power depletion and instability growth rates seen in experiments appeared to be well approximated by the simulations. However, the period of the transverse perturbation corresponding to the maximum growth rate appeared to be *smaller* than that seen in experiment, by a factor of 1.5–2. This discrepancy is most likely due to (i) the physically complicated nonlinear response of rubidium vapour, which was only approximated by the model used in the simulations; (ii) the difficulty in accurately characterizing the initial field which was found to sensitively affect the simulations. It should be noted that this sensitivity was not observed in the experiments, suggesting that the breakup process may have been partially stabilized by some physical mechanisms not included in the model (e.g., nonlocality in the form of diffusion).

Similar experimental results were reported by Mamaev et al. (1996a) [see also Mamaev et al. (1996b), where the instability of a bright-soliton stripe was also reported]. In their experiments a biassed photorefractive SBN crystal, irradiated with a 10 mW He–Ne laser beam containing a phase step, was used as the nonlinear medium. Numerical simulations using the generalized NLS equation with a saturable nonlinearity demonstrated a similar breakup of the initial stripe into a set of optical vortex solitons as reported by Tikhonenko et al. (1996a,b). The effectively nonlinearity could be varied by increasing the bias voltage on the crystal. When zero voltage was applied, the dark stripe spread due to diffraction as did the background beam. As the applied voltage increased the background beam underwent self-defocussing and a dark-stripe soliton was clearly formed. A further increase in the voltage up to 990 V [the maximum voltage reported was 1410 V (Mamaev et al., 1996a) and 2000 V (Mamaev et al., 1996b)] led to the appearance of the snake-like bending of the dark soliton stripe. However, the final state was markedly different from that shown in Fig. 34f because it did not present clear evidence of the creation of optical vortex soliton pairs. However, the authors reported the observation of zeroes in the electromagnetic field from interferometric measurements of the output beam with the distances between the zeroes being about 40 μm. This measurement indicates that wave-front dislocations similar to single vortices were being formed.

7.4.2. Optical vortex solitons

The seminal work of Nye and Berry (1974) on wavefront dislocations in optical beams has led to a substantial growth of interest in screw dislocations (optical vortices) in linearly diffracting beams [see, e.g., Heckenberg et al. (1992) and Basistiy et al. (1993)]. In a self-defocussing nonlinear

medium screw dislocations can form dark optical vortex solitons as predicted by Snyder et al. (1992) and first demonstrated experimentally by Swartzlander and Law (1992, 1993).

In Swartzlander and Law's experiment (1992) a thermally nonlinear medium was irradiated with an Argon laser beam which had passed through a mask used to impose an approximation to the helical phase structure of an optical vortex. This mask contained regions of '0', 'π' and '2π' phase thickness surrounding a single point in the plane of the mask. At the exit from the medium a dark spot localized at this point was observed and interferometric measurements demonstrated the presence of a phase dislocation at that point, supporting the idea that an optical vortex soliton had formed. The authors also demonstrated that the $(2 + 1)$-dimensional induced waveguide existed in the vicinity of the vortex by co-propagating a He–Ne beam as a guided mode through the induced structure.

A more practical method of creating the helical vortex field in the input beam was suggested by Heckenberg et al. (1992). By numerically calculating the interference pattern between either an on-axis spherical wave or off-axis plane wave and the optical vortex they computer-generated diffracting masks which could be used to create single optical vortices in the first order diffracted beams from a Gaussian input. This method was used in the work by Swartzlander and Law (1993), Luther-Davies et al. (1994), Tikhonenko et al. (1995), Tikhonenko et al. (1996a,b), and Christou et al. (1996). The advantage with this method is that beams with arbitrarily placed numbers of vortices with selectable chirality (clockwise or anti-clockwise) can be generated. The final method of vortex creation recognizes that far field of a single vortex is identical to the $p = 1$, Gauss-Laguerre mode of an optical resonator (Duree et al., 1995).

A diffracting mask was used to create pairs of like-charged vortices in a single beam by Luther-Davies et al. (1994) to demonstrate rotation of the solitons around beam axis at the output of a nonlinear medium with increasing nonlinearity. An off-axis vortex rotates around the axis of a Gaussian beam by 90° as it propagates from the beam waist to infinity (Indebetouw, 1993). This rotation exactly matches the so-called Guoy shift which characterizes the change of on-axis phase of the Gaussian beam with propagation relative to that of a plane wave. The defocussing action of the nonlinear medium acts to flatten the phase fronts of the background beam which reduces the effective Guoy shift at a given distance. Hence the action of the nonlinearity is to subtract from the natural rotation the vortex experiences during linear propagation in a nonuniform Gaussian beam (the effect is absent in a uniform plane wave).

Using Rb vapour pumped resonantly using a Ti : sapphire laser near 780 nm as the nonlinear medium and a focussed Gaussian beam with its confocal parameter much shorter than the cell length, it was demonstrated that a change in vortex rotation of $\sim 90^\circ$ could be obtained with increasing nonlinearity with little change in radial position of the vortex. It was suggested that this motion could be used to create an optical rotary switch using the light guiding properties of the dark vortex soliton.

A number of other papers have dealt with the creation, dynamics and waveguiding properties of optical vortex solitons in saturating nonlinear media (Law and Swartzlander, 1993; Segev et al., 1994a,b; Duree et al., 1995; Tikhonenko and Akhmediev, 1996; Tikhonenko et al., 1996a, 1997; Christou et al., 1996; Luther-Davies et al., 1997).

Segev et al. (1994a,b) and Duree et al. (1995) provided the first experimental demonstration of the creation of optical vortex solitons in photorefractive media using the nonlocal response in a biassed SBN crystal. They used an input beam which was either the coherent 'donut' mode of a laser, or

constructed the 'donut' mode by summing two beams: one with a vertical notch and the other with a horizontal notch, with an appropriate $\pi/2$ relative phase between them. Both methods produced a Gauss–Laguerre beam that possessed the desired azimuthal phase dependence to create an optical vortex soliton at the output of the medium. In spite of the anisotropy of the nonlinear response in the photorefractive material nearly circular vortex solitons were obtained although it was noted that this would depend on the input conditions.

Spatial dynamics of single-charged vortices in an anisotropic photorefractive medium has been also studied by Mamaev et al. (1996c) which results a bit different from those reported earlier by Duree et al. (1995). In particular, the experimental and numerical results presented by Mamaev et al. (1996c) indicated a stretching of the vortex in a media with an anisotropic nonlocal nonlinearity, and its subsequent decay. At the same time, Mamaev et al. (1996c) demonstrated the existence of a bound state of a counterrotating vortex pair *created* from a single vortex soliton. All these results clearly indicate a high sensitivity to the initial conditions for generating vortex solitons in photorefractive media, and also the importance of a finite-width background that can lead to a chance of the vortex charge. Definitely, further experimental studies will be necessary to clarify these issues.

Tikhonenko and Akhmediev (1996) studied the creation of single optical vortices in Rubidium vapor [for experimental details, see Luther-Davies et al. (1994, 1997)]. They compared numerical predictions of the output field distributions and demonstrated that saturation and absorption must be taken into account to obtain a reasonable agreement. They also described a new method of steering solitons, and hence the waveguides they induce, based on an interaction with a weak coherent background wave. This idea is closely related to a steering phenomenon earlier described for vortices nested in linearly propagating beams (Basistiy et al., 1993).

Christou et al. (1996) demonstrated this steering method experimentally, using a coherent background wave whose intensity was $\sim 20\%$ of that of a beam containing an off-axis vortex. By adjusting the relative phase of the background wave, the position of the vortex could be moved to any selectable angular position in the output beam. Christou et al.'s work (1996) [see also Kivshar et al. (1997a)] also introduced a simple analytic model to describe the vortex motion as has been discussed above in Section 7.3.2. It showed that the position of the vortex could be described as a result of a radial drift proportional to the gradient of the phase of the background beam and an azimuthal drift proportional to the gradient of the intensity [this effect was observed earlier in numerical simulations by McDonald et al. (1992)]. Using a Gaussian approximation for the defocussing background wave, this resulted in a magnification of the absolute radial displacement of the vortex in proportion to the ratio of the beam radii with and without defocussing. Experimental results confirmed this prediction, see Fig. 36a and Fig. 36b, even under the conditions where the background deviated from the assumed Gaussian form. To assess the affect of a non-Gaussian background, simulations of the beam propagation were carried out which yielded an excellent fit with the experimental and numerical data. Interestingly a small but definite saturation of the transfer function can be observed when the vortex is launched very near the edges of the beam.

A detailed comparison between the theoretical and experimentally measured vortex diameters in a saturable defocusing medium was reported by Tikhonenko et al. (1997). First, the authors developed an analytical theory to find the stationary, radially symmetric localized solitons of the generalized NLS equation with a saturating nonlinearity. Saturation was characterized by

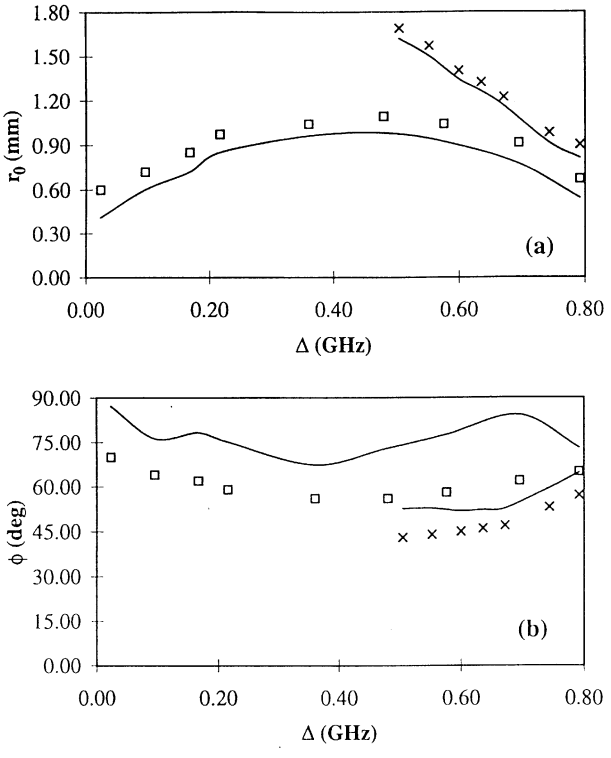

Fig. 36. Radial (a) and angular (b) position of the vortex at the output of the cell as a function of the detuning below the resonance. Two sets of the data show results for a cell temperature 88C (boxes) and 108C (crosses). Solid curves show the interpolated analytical results (Kivshar et al., 1997a,b).

a dimensionless saturation parameter $s = I_0/I_{sat}$, I_0 being the background intensity and I_{sat}, the saturation intensity. It was noticed that the vortex profile and diameter depended strongly on the degree of saturation and that the FWHM diameter of the vortex increased almost linearly with s. To link the theory, which deals with stationary solutions on an infinite uniform background, and the experiments, where an input beam with a somewhat arbitrary intensity profile and helical phase is used, Tikhonenko et al. (1997) analyzed the transition from several typical input profiles to a vortex soliton. For comparison the dynamics of the vortex propagation was investigated experimentally using Rb vapour as a medium with a variable saturating nonlinearity. Some novel phenomena were reported such as rotation of initially elliptic vortex core as the soliton formed. Measurements of the vortex diameter as a function of the effective saturation showed (see Fig. 37) that the almost linear growth with s, predicted by the theory, could only be observed in the region of high saturation where the effective propagation distance, shown in Fig. 37 by a dotted curve, was long enough to approximate to the stationary case. For lower saturations, the measured vortex diameters were observed to be less than the corresponding stationary values (see Fig. 37) indicating the experimentally observed vortex was still far from a steady-state regime.

At last, as one of the future possible practical application of vortex solitons, we would like to mention the recently demonstrated three-dimensional trapping of low-index particles (20 μm

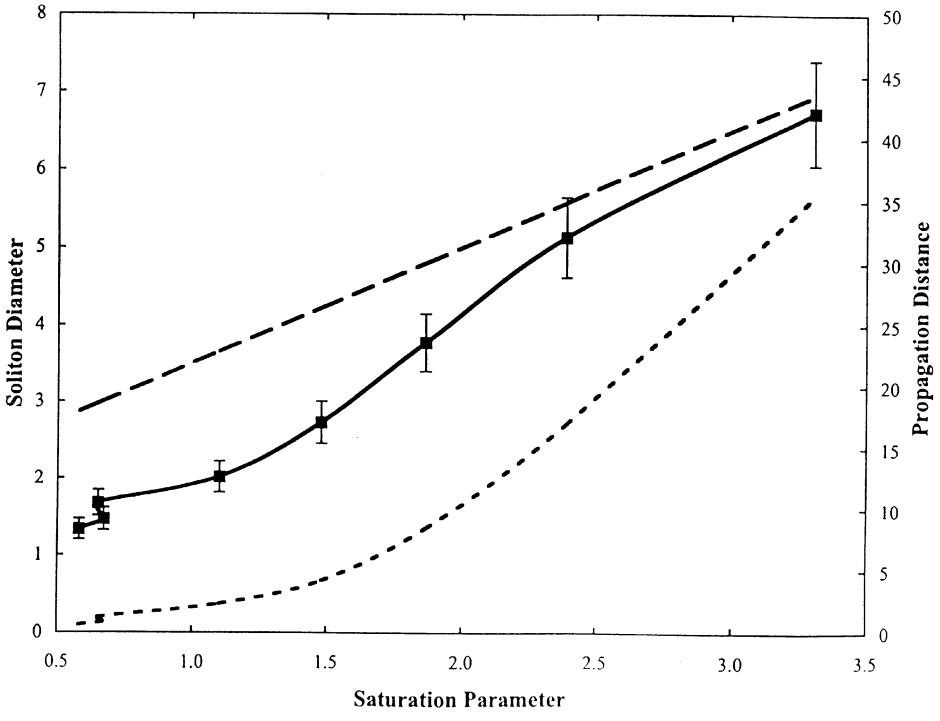

Fig. 37. Comparison between the theory and experiment for the vortex diameters in a saturable medium. Shown are the experimentally measured mean value of the vortex diameter (solid curve with marks) as a function of the dimensionless saturation s. The similar value obtained from the stationary vortex profile is shown as a dashed line. Dotted line displays the variation of the dimensionless propagation distance at the output of the cell (Tikhonenko et al., 1997).

diameter hollow glass spheres in water) by using a single, strongly focused, Gaussian beam containing an optical vortex (Gahagan and Swartzlander, 1996). Transverse trapping was attributed to gradient directed toward the vortex core, that allowed to trap and form ring patterns of high-index particles. In their studies, Gahagan and Swartzlander (1996) used the computer-generated holographic technique to generate an optical vortex.

7.5. Ring dark solitons

As has been shown in Sections 7.2 and 7.4.1, dark-soliton stripes are unstable to transverse long-wavelength modulations. The instability band is characterized by the maximum modulation wave number p_{cr}, so that a soliton stripe is stable to the transverse periodic perturbations of the short wavelength $\lambda_\perp$ provided $\lambda_\perp < \lambda_{cr}$, where $\lambda_{cr} \equiv 2\pi/p_{cr}$. Let us consider *a dark-soliton loop* which is formed by a quasi-two-dimensional dark soliton of the length L. From the physical point of view it becomes clear that such transverse instabilities should be suppressed provided the condition $L < \lambda_{cr}$ holds. The loop of the lowest energy is expected to have a circular symmetry, therefore, one may expect the instability to be stabilized for *ring dark solitary waves* in self-defocussing materials. This simple reasoning allowed Kivshar and Yang (1994c) to introduce the so-called *ring dark solitons.*

Following Kivshar and Yang (1994c) [see also Kivshar and Yang (1994d)], we treat radially symmetric solutions of the (2 + 1)-dimensional NLS equation on the unit-intensity background in the form of a dark soliton ring with slowly varying parameters,

$$u(z, r) = \mathrm{e}^{-\mathrm{i}z}[\cos\phi(z)\tanh\Theta + \mathrm{i}\sin\phi(z)]\,, \tag{7.29}$$

$$\Theta = \cos\phi(z)\{r - R(z)\}\,, \tag{7.30}$$

where $\phi(z)$ ($|\phi| < \pi/2$) and $R(z)$ are the slowly varying soliton angle and its centre coordinate, respectively. The physical meaning of these parameters is the following: the soliton angle ϕ describes the contrast of a ring dark soliton, $B = \cos^2\phi$, and it is connected with the phase jump across the ring, 2ϕ, if we calculate the phase difference between the outer and inner regions separated by the ring. The effective variable $R(z)$ is the radius of the ring at the propagation distance z.

For large values of the soliton radius, the ring soliton can be regarded as quasi-one dimensional object with the curvature treated as a perturbation. This allows the evolution of the soliton parameters to be analysed using the adiabatic approximation of the perturbation theory for dark solitons (see Section 3.1 above), where the term $\sim r^{-1}$ is an effective perturbation. The resulting evolution equations derived from the perturbation-induced dynamics of the system Hamiltonian, take the form (Kivshar and Yang, 1994c,d)

$$\frac{\mathrm{d}\phi}{\mathrm{d}z} = \frac{(D-1)}{3R}\cos\phi\,, \quad \frac{\mathrm{d}R}{\mathrm{d}z} = \sin\phi\,. \tag{7.31}$$

Combining these equations, we find the radial velocity of the ring dark soliton as a function of its radius R,

$$W \equiv \frac{\mathrm{d}R}{\mathrm{d}z} = \kappa\left[1 - \cos^2\phi(0)\left(\frac{R(0)}{R}\right)^{(2/3)(D-1)}\right]^{1/2}, \tag{7.32}$$

where $\kappa = \mathrm{sgn}[\sin\phi(0)] = \pm 1$, $\phi(0)$ and $R(0)$ being the initial values of the parameters. Eq. (7.32) shows that the minimum radius of the collapsing ring dark soliton is defined by the initial conditions,

$$R_{\min} = R(0)[\cos\phi(0)]^{3/(D-1)}, \tag{7.33}$$

and at $R = R_{\min}$ the dark soliton has the maximum contrast. Depending on the initial value $\phi(0)$ of the soliton phase ϕ, the dark soliton can collapse to reach $R_{\min}$, or it diverges decreasing its contrast.

The linear stability analysis (Kuznetsov and Turitsyn, 1988) predicts that the dark soliton stripe is stable when the condition (in our notations)

$$p_\perp > p_{\mathrm{cr}}(\phi) = [2\sqrt{\sin^4\phi + \cos^2\phi} - (1 + \sin^2\phi)]^{1/2} \tag{7.34}$$

is satisfied, $p_\perp$ being the wave number of the transverse perturbations. The result of Eq. (7.34) shows that the instability band vanishes for small amplitude dark solitons when $\cos\phi \to 0$. Thus, when the limit length of the ring $2\pi R_{\min}$ is smaller than the minimum wavelength $2\pi/p_{\mathrm{cr}}(0)$ for the instability region, we expect the ring dark soliton to be stable because, being expanded, it gets 'grey'

and even more stabilized. This gives the condition

$$R_{\min} p_{\mathrm{cr}}(0) < 1 \,. \tag{7.35}$$

Numerical simulations of the NLS equation for both cases mentioned above were carried out by Kivshar and Yang (1994c) and excellent agreement with the analytical results was demonstrated. One of the cases of the evolution of a ring dark soliton at $D = 2$ is shown in Fig. 38a–d. When the dark ring soliton collapses, it reaches its minimum radius, see Fig. 38c, and then it expands again (Fig. 38d). At the turning point, the validity of the adiabatic approximation breaks down, and the dark ring expands along the trajectory slightly different from that predicted by the theory. Nevertheless, this solitary wave is robust and it perfectly conserves its radial symmetry as is shown in Fig. 38a–d.

Importantly, in the small-amplitude approximation discussed in Section 2.5.2 for (1 + 1)-dimensional dark solitons, the ring dark solitons can be described by the so-called cylindrical Korteweg de Vries equation (Kivshar and Yang, 1994c) which is known to be exactly integrable.

A very interesting idea has been suggested by Dreischuh et al. (1996b) who studied theoretically the guiding of multiple bright signal beams by a single ring dark soliton. The authors proposed to use a (1 + 1)-dimensional bright dark soliton as an induced all-optical cable to transmit (2 + 1)-dimensional bright pulses, see Fig. 39a. It is clear that, even not mentioned explicitly in that work, this idea equally applies to the transmission of light bullets through waveguides 'written' by dark solitons. However, since a dark soliton stipe suffers from a transverse modulational instability,

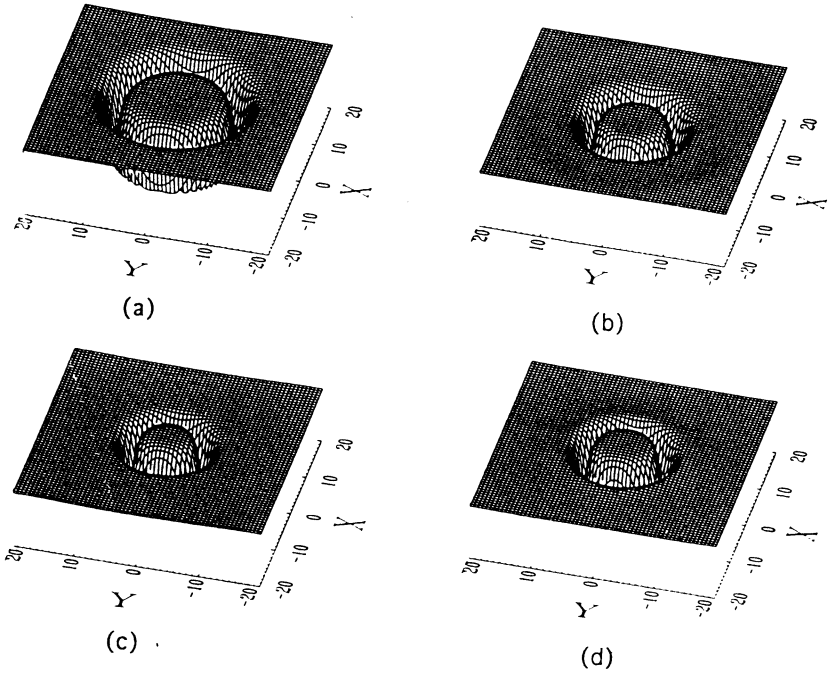

Fig. 38. Evolution of a ring dark soliton in a Kerr medium for collapsing regime, (a) $z = 0$ and (b) $z = 3.0$, and divergence regime: (c) $z = 6.0$ and (d) $z = 9.0$ (Kivshar and Yang, 1994c).

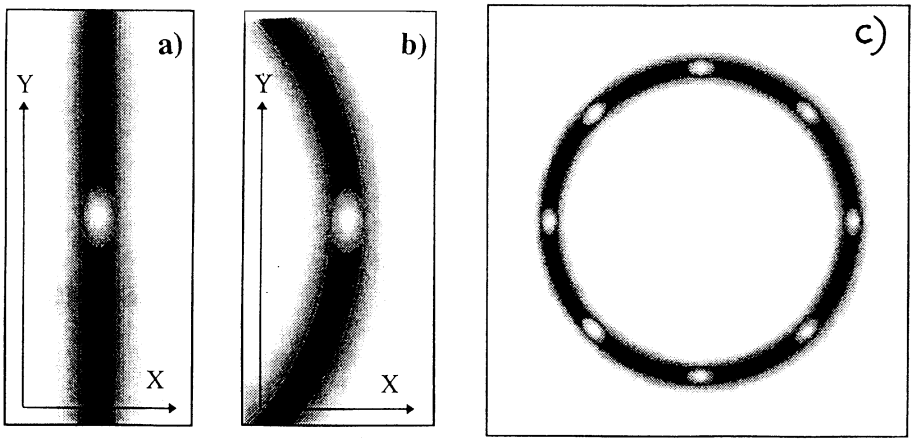

Fig. 39. Scheme of the (2 + 1)-dimensional dark soliton guiding: (a) a planar soliton waveguide, (b) a curved waveguide formed by a ring dark soliton, and (c) multi-soliton guiding by a ring dark soliton. The positions of elliptical signal beams are shown as bright spots (Dreischuh et al., 1996b).

Dreischuh et al. (1996b) suggested to use a ring dark soliton as a curved waveguide shown in Fig. 39b. This idea is a nontrivial generalization of the concept of the soliton-induced waveguide discussed above for (1 + 1)-dimensional dark solitons, and it allows to use more than one single beam. For example, Fig. 39c shows the grayscale image of a ring dark soliton that guides 8 elliptic bright signal beams. Dreischuh et al. (1996b) demonstrated also a misalignment stability of the guiding scheme, similar to the inherent stability of a bright–dark soliton pair.

Experimental results demonstrating the existence of these ring dark solitons were reported by Baluschev et al. (1995a,b). To provide the initial conditions, the authors placed an amplitude mask consisting of opaque dots ranging from 50 to 250 μm in diameter in front of a thermally nonlinear medium (ethanol containing a red absorbing dye). A copper vapour laser ($P = 4$ W) was used to produce the background beam. Single and double (at higher power) dark ring structures separating regions of roughly uniform intensity confirmed that ring dark solitons were created. Baluschev et al. (1995b) also measured the dependence of the transverse velocity of a ring on the intensity for a fixed value of the dark-beam diameter. The results were qualitatively in good agreement with the theory and numerical simulations reported earlier by Kivshar and Yang (1994c) [see also Kanemov et al. (1997)]. Quite recently the phase profile of ring dark solitons has also been measured (Dreischuh et al., 1996a; Neshev et al., 1997a) and it was shown that the rings correspond to regions where a phase step $< \pi$ occurs in the background beam, as expected for a ring dark soliton.

8. Conclusion and open problems

We have presented different aspects of the physics of *optical dark solitons*, including analytical, numerical, and experimental results. They demonstrate a number of very interesting properties of these nonlinear waves which can exist on a (modulationally stable) background being characterized

by a nontrivial phase distribution of the field. In many cases discussed in this review, these dark solitary waves can be not only described analytically and numerically for a variety of nonlinear models, but, and this is the most amazing fact, they can be also verified, with a relatively good accuracy, by direct measurements of the pulse propagation in optical fibers and beam propagation through a defocussing nonlinear medium.

As has been already mentioned, the application of dark solitons to optical communications still remains unclear, it is likely that the answer on this question depends on a general success of the application of bright optical solitons to long-distance fiber communications. As for spatial solitons, many problems involving the light-guiding-light concept are still not solved experimentally, and this definitely will require more efforts to be done making this concept a practical reality. Searching and employing new materials with strong nonlinear properties may sufficiently speed up this process.

As the list of important *theoretical problems* which still remain unsolved, we would like to mention the following.

(a) *Stability theory for dark solitons and vortex solitons* is not completed yet, in the sense of a solution of the corresponding linear eigenvalue problem. In fact, the completeness of eigenfunctions is still questionable.

(b) *Classification and stability of vector dark solitons* calls for numerical solutions of the coupled NLS equations with nonequal (nonzero) boundary conditions. The analytical solution found by Kivshar and Turitsyn (1993) is just one member of the whole family of localized solutions not yet known. It is expected that the general solution of this kind will involve two independent parameters, the soliton velocity and the difference between the propagation constants, and it will describe a dark soliton on a rotating background. Stability of this vector solitons is also an open problem.

(c) *Dark solitons in* $\chi^{(2)}$ *media* have been shown to be *unstable* for the case of the mode dispersions of the same sign. This is also the important case of spatial dark solitons. *Can parametric interactions in a* $\chi^{(2)}$ *medium support spatial dark solitons*? We expect that the effect of the next order, cubic nonlinearity or nondegenerated three-wave mixing on dark solitons may suppress this instability and finally lead to suggestions for experimental verifications.

(d) *Dark solitons created by resonantly interacting waves* in a diffractive (or dispersive) medium have been not investigated theoretically yet. When the effect of the wave walk-off, in the spatial domain, or the group-velocity mismatch, in the temporal domain, are important, only coupled states of bright–dark solitons have been found. More general types of solitary waves on a background field are expected when diffraction becomes important. This also includes dark solitons in the systems of three and four resonantly interacting waves and the effect of harmonic generation near the parametric coupling between the waves provided the matching condition is satisfied.

(e) The use of *dark spatial solitons for light guiding light* is an important theoretical concept useful for physical applications. However, the analysis of the soliton-based devices such as X- and Y-junctions is usually restricted by integrable models. The work to extend this concept to more realistic physical situations has been just started. Also, increasing the amplitude of a guided beam we break the validity of the linearized equations describing the probe beam guidance, the problem becomes naturally *nonlinear*, and it describes *dark–bright soliton pairs*. Properties of this kind of soliton become more and more clear after recent theoretical and experimental works on this topic,

but a general approach to this problem is still absent. This includes the classification and stability analysis of bright–dark vector solitons. In particular, we expect that the polarization domain walls should appear as a special limit case of the general solution for the bright–dark solitons.

Among numerous *experimental problems* related to dark solitons, it is worth to mention just a few.

(a) *Polarization properties of dark solitons and vortex solitons* require an experimental study. Observation of vectorial properties of dark solitons was, to the best of our knowledge, never reported. This also includes incoherent interaction between dark solitons. In particular, some theoretical papers described polarization-induced instability (Law and Swartzlander, 1994) and interaction between vortex solitons of different backgrounds (Velchev et al., 1996).

(b) *Possibility of steerable light guiding by dark solitons* in a bulk medium, e.g. by plane, ring, or vortex solitons, has been discussed theoretically but never realized in practice. This will require, in fact, an additional theoretical analysis of guiding properties of dark solitons in higher dimensions and $(3 + 1)$-dimensional generalizations of dark solitons ('dark bullets' and 'donut modes').

(c) Recent demonstrations, presented by Nakazawa and Suzuki (1995a,b), of the potential use of dark solitons for *data coding and signal transmission* should open room for experimental activity in this direction. Increased interest in the effect of nonlinearity on a standard non-return-to-zero (NRZ) communication schemes [see, e.g., Kodama and Wabnitz (1995)] will also require some efforts to understand if dark solitons might 'coexist' with the NRZ transmission [see, e.g., interesting ideas in the paper by Ngo et al. (1996)].

Will spatial and temporal dark solitons be useful in the future? For spatial dark solitons, with their relatively popular appeal, the answer may be *yes*. But for temporal dark solitons, which are less popular than their bright relatives, the answer – though closer to *no* – is harder to predict.

Acknowledgements

It is a great pleasure for us to thank all colleagues and students with whom we had discussed and worked on this subject for the last several years. We should like to name especially Vsevolod Afanasjev, Philippe Emplit, Sergei Gredeskul, Marc Haelterman, Wieslaw Królikowski, Len Pismen, Moti Segev, Allan Snyder, Vladimir Tikhonenko, and also our great team of students: Alexander Buryak, Jason Christou, Dmitry Pelinovsky, Adrian Sheppard, Vika Steblina, and Yang Xiaoping.

This work was supported by the Australian Photonics Cooperative Research Centre through the theoretical and experimental projects on nonlinear waveguides and light guiding light.

References

Acioli, L.H., Gomes, A.S.L., Hickmann, J.M., de Araujo, C.B., 1990. Appl. Phys. Lett. 56, 2279.
Afanasjev, V.V., Kivshar, Yu.S., Konotop, V.V., Serkin, V.N., 1989a. Opt. Lett. 14, 805.
Afanasjev, V.V., Dianov, E.M., Serkin, V.N., 1989b. IEEE J. Quantum Electron. 25, 2656.

Afanasjev, V.V., Kivshar, Yu.S., Menyuk, C.R., 1996. Opt. Lett. 21, 1975 *.
Agrawal, G.P., 1987. Phys. Rev. Lett. 59, 880.
Agrawal, G., 1989. Nonlinear Fiber Optics. Academic Press, Boston, MA.
Aitchinson, J.S., Weiner, A.M., Silberberg, Y., Oliver, M.K., Jackel, J.L., Leaird, D.E., Vogel, E.M., Smith, P.W.E., 1990. Opt. Lett. 15, 471 *.
Akhmanov, S.A., Sukhorukov, A.P., Khokhlov, R.V., 1967. Usp. Fiz. Nauk 93, 19 [Sov. Phys. Uspekhi 10 (1968) 609].
Allan, G.R., Skinner, S.R., Andersen, D.R., Smirl, A.L., 1991. Opt. Lett. 16, 156.
Allen, K.M., Doran, N.J., Williams, J.A.R., 1994. Opt. Lett. 19, 2086.
Allen, K.M., Doran, N.J., Smith, N.J., Williams, J.A.R., 1995. In: Nonlinear Guided Waves and Their Applications, February 23–25, 1995. Dana Point, CA, OSA Technical Digest Series, Vol. 6, pp. 236–238.
Andersen, D.R., Hooton, D.E., Swartzlander, G.A. Jr., Kaplan, A.E., 1990. Opt. Lett. 15, 783 ***.
Andersen, D.R., Skinner, S.R., 1991a. J. Opt. Soc. Am. B 8, 759.
Andersen, D.R., Skinner, S.R., 1991b. J. Opt. Soc. Am. B 8, 2265.
Ankiewicz, A., Karlsson, M., Akhmediev, N., 1994. Opt. Commun. 111, 116.
Aranson, I., Steinberg, V., 1996. Phys. Rev. B 53, 75.
Aranson, I., Tsimring, L., 1995. Phys. Rev. Lett. 75, 3273.
Armstrong, J.A., Bloembergen, N., Ducuing, J., Pershan, P.S., 1962. Phys. Rev. 127, 1918.
Askar'yan, G.A., 1962. Sov. Phys. JETP 15, 1088.
Baluschev, S., Dreischuh, A., Velchev, I., Dinev, S., Marazov, O., 1995a. Phys. Rev. E 52, 5517 *.
Baluschev, S., Dreischuh, A., Velchev, I., Dinev, S., Marazov, O., 1995b. Appl. Phys. B 61, 121.
Baranova, N.B., Zel'dovich, B.Ya., Mamaev, A.V., Pilipetsky, N.F., Shkukov, V.V., 1981. Pis'ma Zh., Eksp. Teor. Fiz. 33, 206 [JETP Lett. 33 (1981) 195].
Barashenkov, I.V., 1996. Phys. Rev. Lett. 77, 1193 **.
Barashenkov, I.V., Gosheva, A.D., Makhankov, V.G., Puzynin, I.V., 1989. Physica D 34, 240.
Barashenkov, I.V., Kholmurodov, Kh.T., 1986. JINR Preprint P17-86-698, Dubna (in Russian).
Barashenkov, I.V., Makhankov, V.G., 1988. Phys. Lett. A 128, 52.
Barashenkov, I.V., Panova, E.Yu., 1993. Physica D 69, 114 **.
Basistiy, I.V., Bazhenov, V.Yu., Soskin, M.S., Vasnetsov, M.V., 1993. Opt. Commun. 103, 422 *.
Basistiy, I.V., Soskin, M.S., Vasnetsov, M.V., 1995. Opt. Commun. 119, 604 *.
Bass, F.G., Konotop, V.V., Puzenko, S.A., 1992. Phys. Rev. A. 46, 4185.
Bazhenov, V.Yu., Soskin, M.S., Vasnetsov, M.V., 1992. J. Mod. Opt. 39, 985 *.
Belanger, P.A., Mathieu, P., 1987. Appl. Opt. 26, 111.
Berkhoer, A.L., Zakharov, V.E., 1970. Zh. Eksp. Teo. Fiz. 58, 903 [Sov. Phys. JETP, 31 (1970) 486].
Blow, K.J., Doran, N., 1985. Phys. Lett. A 107, 55 *.
Boardman, A.D., Xie, K., 1993. Radio Sci. 28, 891.
Bogdan, M.M., Kovalev, A.S., Kosevich, A.M., 1989. Fiz. Nizk. Temp. 15, 511 (in Russian).
Bosshard, C., Mamyshev, P.V., Stegeman, G.I., 1994. Opt. Lett. 19, 90.
Burtsev, S., Camassa, R., 1997. J. Opt. Soc. Am. B, in press.
Buryak, A.V., 1995. Phys. Rev. E 52, 1156.
Buryak, A.V., 1996. Solitons due to quadratic nonlinearities. Ph.D. Thesis, ANU, Canberra, Australia.
Buryak, A.V., Kivshar, Yu.S., 1994. Opt. Lett. 19, 1612.
Buryak, A.V., Kivshar, Yu.S., 1995a. Phys. Lett. A 197, 407.
Buryak, A.V., Kivshar, Yu.S., 1995b. Opt. Lett. 20, 834.
Buryak, A.V., Kivshar, Yu.S., 1995c. Phys. Rev. A 51, R41.
Buryak, A.V., Kivshar, Yu.S., Parker, D.F., 1996a. Phys. Lett. A 215, 57.
Buryak, A.V., Kivshar, Yu.S., Trillo, S., 1996b. Phys. Rev. Lett. 77, 5210 **.
Butylkin, V.S., Kaplan, A.E., Khronopulo, Yu.G., Yakubovich, E.I., 1989. Resonant Nonlinear Interactions of Light with Matter. Springer, Berlin.
Cai, D., Bishop, A.R., Grønbech-Jensen, N., Malomed, B.A., 1997. Phys. Rev. Lett. 78, 223.
Cao, W., Zhang, Y., 1996. Opt. Commun. 128, 23.

Chen, M., Tsankov, M.A., Nash, J.M., Patton, C.E., 1993. Phys. Rev. Lett. 70, 1707.
Chen, Y., 1991a. J. Appl. Phys. 70, 5694.
Chen, Y., 1991b. Phys. Rev. A. 44, 7524.
Chen, Y., 1992a. Opt. Commun. 90, 317.
Chen, Y., 1992b. Phys. Rev. A 45, 6922.
Chen, Y., Atai, J., 1992. J. Opt. Soc. Am. B 9, 2252.
Chen, Y., Atai, J., 1995. Opt. Lett. 20, 133.
Chen, Z., Mitchell, M., Shih, M., Segev, M., Garrett, M.H., Valley, G.C., 1996a. Opt. Lett. 21, 629 *.
Chen, Z., Mitchell, M., Segev, M., 1996b. Opt. Lett. 21, 716.
Chen, Z., Segev, M., Coskun, T.H., Christodoulides, D.N., 1996c. Opt. Lett. 21, 1436.
Chen, Z., Segev, M., Coskun, T.H., Christodoulides, N., Kivshar, Yu.S., Afanasjev, V.V., 1996d. Opt. Lett. 21, 1821 ***.
Chernev, P., Petrov, V., 1992. Opt. Lett. 17, 172.
Chernikov, S.V., Mamyshev, P.V., Dianov, E.M., Richardson, D.J., Laming, R.I., Payne, D.N., 1992. Sov. J. Lightwave Technol. 2, 161.
Chiao, R.Y., Garmire, E., Townes, C.H., 1964. Phys. Rev. Lett. 13, 479.
Chiao, R.Y., Deutsch, I.H., Garrison, J.C., Wright, E.M., 1993. In: Walter, H. et al. (Ed.), Frontiers in Nonlinear Optics (The Sergei Akhmanov Memorial Volume). Institute of Physics Publishing, Bristol, p. 151.
Christodoulides, D.N., 1988. Phys. Lett. A 132, 451.
Christodoulides, D.N., 1991. Opt. Comm. 86, 431.
Christodoulides, D.N., Carvalho, M.I., 1995. J. Opt. Soc. Am. B 12, 1628 *.
Christodoulides, D.N., Joseph, R.I., 1988. Opt. Lett. 13, 53.
Christodoulides, D.N., Singh, S.R., Carvalho, M.I., Segev, M., 1996. Appl. Phys. Lett. 68, 1763 *.
Christou, J., Tikhonenko, V., Kivshar, Yu.S., Luther-Davies, B., 1996. Opt. Lett. 21, 1649 ***.
Coutaz, J.L., Kull, M., 1991. J. Opt. Soc. Am. B 8, 95.
Crosignani, B., DiPorto, P., 1981. Opt. Lett. 6, 329.
Crosignani, B., DiPorto, P., 1982. J. Opt. Soc. Am. 72, 1136.
Crosignani, B., Segev, M., Engin, D., DiPorto, P., Yariv, A., Salamo, G., 1993. J. Opt. Soc. Am. B 10, 449.
De Bouard, A., 1995. SIAM J. Math. Anal. 26, 566.
De la Fuente, R., Barthelemy, A., Froehly, G., 1991. Opt. Lett. 16, 21.
Denardo, B., Galvin, B., Greenfield, A., Larraza, A., Putterman, S., Wright, W., 1992. Phys. Rev. Lett. 68, 1730.
Denardo, B., Wright, W., Putterman, S., Larraza, A., 1990. Phys. Rev. Lett. 64, 1518.
DeSalvo, R., Hagen, D.J., Sheik-Bahae, M., Stegeman, G., Van Stryland, E.W., 1992. Opt. Lett. 17, 28.
Diankov, G.L., Uzunov, I.M., 1995. Opt. Commun. 117, 424.
Dianov, E.M., Mamyshev, P.V., Prokhorov, A.M., Chernikov, S.V., 1989. Opt. Lett. 14, 1008.
Donelly, R.J., 1991. Quantized Vortices in Helium II. Cambridge University Press, Cambridge.
Dreischuh, A., Fliesser, W., Velchev, I., Dinev, S., Windholz, L., 1996a. Appl. Phys. B 62, 139 *.
Dreischuh, A., Kamenov, V., Dinev, S., 1996b. Appl. Phys. B 63, 145.
Duree, G., Morin, M., Salamo, G., Segev, M., Crosignani, B., DiPorto, P., Sharp, E., Yariv, A., 1995. Phys. Rev. Lett. 74, 1978.
Duree, G., Shultz, J.L., Salamo, G., Segev, M., Yariv, A., Crosignani, B., DiPorto, P., Sharp, E., Neurgaonkar, R., 1993. Phys. Rev. Lett. 71, 533.
Emplit, Ph., Haelterman, M., Hamaide, J.-P., 1993. Opt. Lett. 18, 1047.
Emplit, Ph., Hamaide, J.P., Reynaud, F., Froehly, G., Barthelemy, A., 1987. Opt. Commun. 62, 374 ***.
Enns, R.H., Mulder, L.J., 1989. Opt. Lett. 14, 509 *.
Feit, M., Fleck, J., 1988. J. Opt. Soc. Am. B 5, 633.
Feng, J., Kneubühl, F.K., 1993. IEEE J. Quantum Electron. 29, 590 *.
Fibich, G., 1996. Phys. Rev. Lett. 76, 4356.
Foursa, D., Emplit, Ph., 1996a. Electron. Lett. 32, 919.
Foursa, D., Emplit, Ph., 1996b. Phys. Rev. Lett. 77, 4011 ***.
Frantzeskakis, D.J., 1996. J. Phys. A 29, 3631.
Freund, I., 1994. J. Opt. Soc. Am. A 11, 1644.

Gagnon, L., 1989. J. Opt. Soc. Am. B 6, 1477.
Gagnon, L., 1993. J. Opt. Soc. Am. B 10, 469.
Gahagan, K.T., Swartzlander, G.A. Jr., 1996. Opt. Lett. 21, 827.
Gatz, S., Herrmann, J., 1991. J. Opt. Soc. Am. B 8, 2296.
Gatz, S., Herrmann, J., 1992. Opt. Lett. 17, 484.
Giannini, J.A., Joseph, R.I., 1990. IEEE J. Quantum Electron. 26, 2109.
Gibbon, J.D., 1990. In: Fordy, A.P. (Ed.), Soliton Theory: A Survey of Results. Manchester University Press, Manchester, pp. 133–151.
Ginzburg, V.L., Pitaevsky, L.P., 1958. Zh. Eksp. Teor. Fiz. 34, 1240 [Sov. Phys. JETP 7 (1959) 858] **.
Gordon, J.P., 1986. Opt. Lett. 11, 662.
Gordon, J.P., Haus, H.A., 1986. Opt. Lett. 11, 665 *.
Gredeskul, S.A., Kivshar, Yu.S., 1989a. Phys. Rev. Lett. 62, 977 *.
Gredeskul, S.A., Kivshar, Yu.S., 1989b. Opt. Lett. 14, 1281.
Gredeskul, S.A., Kivshar, Yu.S., Yanovskaya, M.V., 1990. Phys. Rev. A 41, 3994.
Grimshaw, R., Afanasjev, V.V., Kivshar, Yu.S., 1997. Phys. Lett. A, submitted.
Grudinin, A.B., Dianov, E.M., Prokhorov, A.M., Khaidarov, D.V., 1988. Pisma Zh. Tekhn. Fiz. 14, 1010.
Gustafson, T.K., Kelley, P.L., Chiao, R.Y., Brewer, R.G., 1968. Appl. Phys. Lett. 12, 165.
Haelterman, M., Emplit, Ph., 1993. Electron. Lett. 29, 356.
Haelterman, M., Sheppard, A.P., 1994a. Opt. Lett. 19, 96.
Haelterman, M., Sheppard, A.P., 1994b. Chaos, Solitons and Fractals 4, 1731.
Haelterman, M., Sheppard, A.P., 1994c. Phys. Rev. E 49, 3389 **.
Haelterman, M., Sheppard, A.P., 1994d. Phys. Rev. E 49, 4512 *.
Haelterman, M., Sheppard, A.P., 1994e. Phys. Lett. A 185, 265.
Hamaide, J.P., Emplit, Ph., Haelterman, M., 1991. Opt. Lett. 16, 1578.
Hasegawa, A., 1989. Solitons in Optical Fibers. Springer, Berlin *.
Hasegawa, A., Kodama, Y., 1995. Solitons in Optical Communications. Oxford University Press, Oxford *.
Hasegawa, A., Tappert, F., 1973a. Appl. Phys. Lett. 23, 142.
Hasegawa, A., Tappert, F., 1973b. Appl. Phys. Lett. 23, 171 **.
Haus, H.A., Wong, W.S., 1996. Rev. Mod. Phys. 68, 423.
Hayata, K., Koshiba, M., 1993a. Phys. Rev. E 48, 2312.
Hayata, K., Koshiba, M., 1993b. Phys. Rev. Lett. 71, 3275; Erratum: Phys. Rev. Lett. 72 (1994) 178.
Hayata, K., Koshiba, M., 1994. Phys. Rev. A 50, 675.
Heckenberg, N.R., McDuff, R., Smith, C.P., White, A.G., 1992. Opt. Lett. 17, 221.
Herrmann, J., 1992. Opt. Commun. 91, 337.
Hong, B.J., Yang, C.C., Wang, L., 1991. J. Opt. Soc. Am. B 8, 464.
Huang, G., Velarde, M.G., 1996. Phys. Rev. E 54, 3048.
Iizuka, T., Wadati, M., Yajima, T., 1991. J. Phys. Soc. Jpn. 60, 2862.
Indebetouw, G., 1993. J. Mod. Opt. 40, 73 *.
Ikeda, T., Matsumoto, M., Hasegawa, A., 1995. Opt. Lett. 20, 1113.
Ikeda, T., Matsumoto, M., Hasegawa, A., 1997. J. Opt. Soc. Am. B 14, 136 *.
Iturbe-Castillo, M.D., Sánchez-Mondragon, J.J., Stepanov, S.I., Klein, M.B., Wechsler, B.A., 1995. Opt. Commun. 118, 515.
Jeffrey, A., Kawahara, T., 1982. Asymptotic Methods in Nonlinear Wave Theory. Pitman, London.
Jerominek, H., Delisle, C., Tremblay, R., 1986. Appl. Opt. 25, 732.
Jerominek, H., Tremblay, R., Delisle, C., 1985. J. Lightwave Technol. 3, 1105.
Jin, R., Liang, M., Khitrova, G., Gibbs, M.M., Peyghambarian, N., 1993. Opt. Lett. 18, 494.
Jones, C.A., Roberts, P.M., 1982. J. Phys. A 15, 2599.
Jones, C.K.R.T., Moloney, J.V., 1986. Phys. Lett. A 117, 175.
Josserand, C., Pomeau, Y., 1995. Europhys. Lett. 30, 43.
Josserand, C., Rica, S., 1997. Phys. Rev. Lett. 78, 1215.
Kanemov, V., Dreischuh, A., Dinev, S., 1997. Phys. Scr. 55, 68.

Kaplan, A.E., 1985a. Phys. Rev. Lett. 55, 1291.
Kaplan, A.E., 1985b. IEEE J. Quantum Electron. 21, 1538.
Kaplan, A.E., 1993. Opt. Lett. 18, 1223.
Karamzin, Yu.N., Sukhorukov, A.P., 1974. JETP Lett. 20, 339.
Karpman, V.I., 1993. Phys. Lett. A 181, 211.
Kim, A.D., Kath, W.L., Goedde, C.G., 1996. Opt. Lett. 21, 465.
Kivshar, Yu.S., 1989. J. Phys. A 22, 337.
Kivshar, Yu.S., 1990a. Phys. Rev. A 42, 1757.
Kivshar, Yu.S., 1990b. Opt. Lett. 15, 1273.
Kivshar, Yu.S., 1991a. Phys. Rev. A 43, 1677.
Kivshar, Yu.S., 1991b. Opt. Lett. 17, 1322.
Kivshar, Yu.S., 1992. Opt. Lett. 17, 1322.
Kivshar, Yu.S., 1993a. Phys. Rev. Lett. 70, 3055.
Kivshar, Yu.S., 1993b. IEEE J. Quantum Electron. 28, 250 ***.
Kivshar, Yu.S., 1995. Phys. Rev. E 51, 1613.
Kivshar, Yu.S., Afanasjev, V.V., 1991a. Phys. Rev. A 44, R1446.
Kivshar, Yu.S., Afanasjev, V.V., 1991b. Opt. Lett. 16, 285.
Kivshar, Yu.S., Afanasjev, V.V., 1996. Opt. Lett. 21, 1135.
Kivshar, Yu.S., Afanasjev, V.V., Snyder, A.W., 1996. Opt. Commun. 126, 348.
Kivshar, Yu.S., Anderson, D., Lisak, M., 1993. Phys. Scr. 47, 679.
Kivshar, Yu.S., Christou, J., Tikhonenko, V., Luther-Davies, B., Pismen, L., 1997a. Phys. Rev. E, submitted.
Kivshar, Yu.S., Chubykalo, O.A., Usatenko, O.V., Grinyoff, D.V., 1995. Int. J. Mod. Phys. B 9, 875.
Kivshar, Yu.S., Gredeskul, S.A., 1990. Opt. Commun. 79, 285.
Kivshar, Yu.S., Haelterman, M., Emplit, Ph., Hamaide, J.-P., 1994a. Opt. Lett. 19, 19 *.
Kivshar, Yu.S., Haelterman, M., Sheppard, A.P., 1994c. Phys. Rev. E 50, 3161.
Kivshar, Yu.S., Królikowski, W., 1995a. Opt. Comm. 114, 353.
Kivshar, Yu.S., Królikowski, W., 1995b. Opt. Lett. 20, 1527 **.
Kivshar, Yu.S., Malomed, B.A., 1989. Rev. Mod. Phys. 61, 763 *.
Kivshar, Yu.S., Malomed, B.A., 1991. Phys. Rev. Lett. 60, 129.
Kivshar, Yu.S., Malomed, B.A., 1993. Opt. Lett. 18, 485.
Kivshar, Yu.S., Pelinovsky, D.E., Christou, J., Tikhonenko, V., Luther-Davies, B., 1997b. unpublished.
Kivshar, Yu.S., Turitsyn, S.K., 1993. Phys. Rev. A 47, R3502.
Kivshar, Yu.S., Yang, X., 1994a. Phys. Rev. E 49, 1657 **.
Kivshar, Yu.S., Yang, X., 1994b. Opt. Comm. 107, 93.
Kivshar, Yu.S., Yang, X., 1994c. Phys. Rev. E 50, R40 **.
Kivshar, Yu.S., Yang, X., 1994d. Chaos, Solitons and Fractals 4, 1745.
Kodama, Y., Wabnitz, S., 1995. Opt. Lett. 20, 2291.
Konotop, V.V., Vekslerchik, V.E., 1994. Phys. Rev. E 49, 2397.
Kosevich, A.M., Kovalev, A.S., 1989. Introduction into Nonlinear Physical Mechanics. Naukova Dumka, Kiev, p. 298 (in Russian).
Krökel, D., Halas, N.J., Giuliani, G., Grischkowsky, D., 1988. Phys. Rev. Lett. 60, 29.
Królikowski, W., Akhmediev, N.N., Luther-Davies, B., 1993. Phys. Rev. E 48, 3980.
Królikowski, W., Akhmediev, N.N., Luther-Davies, B., 1996. Opt. Lett. 21, 782.
Królikowski, W., Luther-Davies, B., 1992. Opt. Lett. 17, 1414.
Królikowski, W., Luther-Davies, B., 1993. Opt. Lett. 18, 188.
Kuznetsov, E.A., Rasmussen, J.J., 1995. Phys. Rev. E 51, 4479.
Kuznetsov, E.A., Rubenchik, A.M., Zakharov, V.E., 1986. Phys. Rep. 142, 113.
Kusmartsev, F.V., 1989. Phys. Rep. 183, 1.
Kuznetsov, E.A., Turitsyn, S.K., 1988. Zh. Eksp. Teor. Fiz. 94 (1988) 119 [Sov. Phys. JETP 67, 1583].
Law, C.T., Swartzlander, G.A., 1993. Opt. Lett. 18, 586 *.
Law, C.T., Swartzlander, G.A. Jr., 1994. Chaos, Solitons and Fractals 4, 1759.

Lawrence, B., Cha, M., Torruellas, W.E., Stegeman, G.I., Eteman, S., Baker, G., Kajzer, F., 1994a. Appl. Phys. Lett. 64, 2773.
Lawrence, B., Torruellas, W.E., Cha, M., Sundheimer, M.L., Stegeman, G.I., Meth, J., Eteman, S., Baker, G., 1994b. Phys. Rev. Lett. 73, 597.
Lederer, F., Biehlig, W., 1994. Electron. Lett. 30, 1871.
Lisak, M., Andersen, D., Malomed, B.A., 1991. Opt. Lett. 16, 1936.
Lundquist, P.B., Andersen, D.R., Swartzlander, G.A. Jr., 1995. J. Opt. Soc. Am. B 12, 698.
Luther-Davies, B., Christou, J., Tikhonenko, V.V., Kivshar, Yu.S., 1997. J. Opt. Soc. Am. B, in press.
Luther-Davies, B., Powles, R., Tikhonenko, V., 1994. Opt. Lett. 19, 1816 **.
Luther-Davies, B., Yang, X., 1992a. Opt. Lett. 17, 496 ***.
Luther-Davies, B., Yang, X., 1992b. Opt. Lett. 17, 1775 **.
Maker, P.D., Terhune, R.W., Savage, C.M., 1964. Phys. Rev. Lett. 12, 507.
Makhankov, V.G., 1990. Soliton Phenomenology. Kluwer, Dordrecht, p. 218.
Malomed, B.A., 1994. Phys. Rev. E 50, 1565.
Malomed, B.A., Nepomnyashchy, A.A., Tribelsky, M.I., 1990. Phys. Rev. A. 42, 7244.
Mamaev, A.V., Saffman, M., Zozulya, A.A., 1996a. Phys. Rev. Lett. 76, 2262 *.
Mamaev, A.V., Saffman, M., Anderson, D.Z., Zozulya, A.A., 1996b. Phys. Rev. A 54, 870.
Mamaev, A.V., Saffman, M., Zozulya, A.A., 1996c. Phys. Rev. Lett. 77, 4544.
Mamyshev, P.V., Bosshard, Ch., Stegeman, G.I., 1994. J. Opt. Soc. Am. B 11, 1254 **.
Manakov, S.V., 1974. Sov. Phys. JETP 38, 248.
Manassah, J.T., 1991. Opt. Lett. 16, 587.
Maruta, A., Kodama, Y., 1995. Opt. Lett. 20, 1752.
Marburger, J.H., Dawes, E., 1968. Phys. Rev. Lett. 21, 556.
McDonald, G.S., Syed, K.S., Firth, W.J., 1992. Opt. Commun. 94, 469 *.
McDonald, G.S., Syed, K.S., Firth, W.J., 1993. Opt. Commun. 95, 281 *.
Menyuk, C.R., 1989. IEEE J. Quantum Electron. 25, 2674.
Menyuk, C.R., 1993. J. Opt. Soc. Am. B 10, 1585.
Menyuk, C.R., Wai, P.K.A., 1992. In: Taylor, J.R. (Ed.), Optical Solitons – Theory and Experiment. Cambridge Univ. Press, pp. 332–346, 359–369.
Micallef, R.W., Afanasjev, V.V., Kivshar, Yu.S., Love, J.D., 1996. Phys. Rev. E 54, 2936.
Miller, P.D., 1996. Phys. Rev. E 53, 4137.
Miranda, J., Andersen, D.R., Skinner, S.R., 1992. Phys. Rev. A 46, 5999.
Mitchell, D.J., Snyder, A.W., 1993. J. Opt. Soc. Am. B 10, 1574.
Mitschke, F.M., Mollenauer, L.F., 1986. Opt. Lett. 11, 659.
Mollenauer, L.F., Neubelt, M.J., Evangelides, S.G., Gordon, J.P., Simpson, J.R., Cohen, L.G., 1990. Opt. Lett. 15, 1203.
Mollenauer, L.F., Stolen, R.H., Gordon, J.P., 1980. Phys. Rev. Lett. 45, 1095.
Mulder, L.J., Enns, R.H., 1989. IEEE J. Quantum Electron. 25, 2205.
Nakazawa, M., Suzuki, K., 1995a. Electron. Lett. 31, 1076 ***.
Nakazawa, M., Suzuki, K., 1995b. Electron. Lett. 31, 1084 ***.
Neshev, D., Dreischuh, A., Kamenov, V., Stefanov, I., Dinev, S., Fliesser, W., Windholz, L., 1997a. Appl. Phys. B 64, 429.
Neshev, D., Dreischuh, A., Dinev, S., Windholz, L., 1997b. Controllable branching of optical beams by quasi-2D dark spatial solitons. J. Opt. Soc. Am. B, submitted.
Neu, J.C., 1990. Physica D 43, 385 *.
Ngo, N.Q., Binh, L.N., Dai, X., 1996. Opt. Commun. 132, 389.
Nitti, S., Tan, H.M., Banfi, G.P., Degiorgio, V., 1994. Opt. Commun. 106, 263.
Nore, C., Brachet, M.E., Fauve, S., 1993. Physica D 65, 154.
Nye, J.F., Berry, M.V., 1974. Proc. R. Soc. Lond. A 336, 165 **.
Ostrovsky, L.A., 1967. Pis'ma Zh. Eksp. Teor. Fiz. 5, 331 [JETP Lett. 5 (1967) 272].
Oughstun, K.E., Xiao, H., 1997. Phys. Rev. Lett. 78, 642.
Panoiu, N.-C., Mihalache, D., Baboiu, D.-M., 1995. Phys. Rev. A 52, 4182.

Pelinovsky, D.E., Afanasjev, V.V., Kivshar, Yu.S., 1996a. Phys. Rev. E 53, 1940.
Pelinovsky, D.E., Kivshar, Yu.S., Afanasjev, V.V., 1996b. Phys. Rev. E 54, 2015 **.
Pelinovsky, D.E., Stepanyants, Yu.A., Kivshar, Yu.S., 1995. Phys. Rev. E 51, 5016 **.
Perivolaropoulos, L., 1993. Phys. Lett. B 316, 528.
Pismen, L.M., 1994a. Physica D 73, 244.
Pismen, L.M., 1994b. Phys. Rev. Lett. 72, 2557.
Pismen, L.M., Rodriguez, J.D., 1990. Phys. Rev. A 42, 2471.
Pismen, L.M., Rubinstein, J., 1991. Physica D 47, 353.
Pitaevsky, L.P., 1961. Zh. Eksp. Teor. Fiz. 40, 646 [Sov. Phys. JETP 13 (1961) 451] **.
Radhakrishnan, R., Lakshmanan, M., 1995. J. Phys. A: math. Gen. 28, 2683.
Reichert, J.D., Wagner, W.G., 1968. IEEE J. Quantum Electron. QE-4, 221.
Richardson, D.J., Chamberlin, R.P., Dong, L., Payne, D.N., 1994. Electron. Lett. 30, 1326.
Reynaud, F., Barthelemy, A., 1990. Europh. Lett. 12, 401.
Rothenberg, J.E., 1991. Opt. Commun. 82, 107.
Rothenberg, J.E., Heinrich, H.K., 1992. Opt. Lett. 17, 261.
Roussignol, P., Ricard, D., Lukasik, J., Flytzanis, C., 1987. J. Opt. Soc. Am. B 4, 5.
Roux, F.S., 1995. J. Opt. Soc. Am. B 12, 1215.
Rubinstein, J., Pismen, L.M., 1994. Physica D 78, 1.
Ryskin, N.M., 1994. JETP 79, 833.
Sakaguchi, H., 1991. Prog. Theor. Phys. 85, 417.
Sammut, R., Buryak, A.V., Kivshar, Yu.S., 1997. Opt. Lett., submitted.
Schiek, R., 1993. J. Opt. Soc. Am. B 10, 1848.
Segev, M., Crosignani, B., Yariv, A., Fischer, B., 1992. Phys. Rev. Lett. 68, 923.
Segev, M., Salamo, G., Morin, M., Crosignani, B., Di Porto, P., Yariv, A., 1994a. Optics and Photonics News 5 (December), the cover page and the summary on p. 9.
Segev, M., Valley, G.C., Crosignani, B., Di Porto, P., Yariv, A., 1994b. Phys. Rev. Lett. 73, 3211.
Segev, M., Shih, M., Valley, G.C., 1996. J. Opt. Soc. Am. B 13, 706.
Shalaby, M., Barthelemy, A.J., 1992. IEEE J. Quantum Electron. 28, 2736.
Sheppard, A.P., 1993. Opt. Commun. 102, 317.
Sheppard, A.P., Haelterman, M., 1994. Opt. Lett. 19, 859.
Sheppard, A.P., Kivshar, Yu.S., 1997. Phys. Rev. E 55, 4773 **.
Silberberg, Y., 1990a. Opt. Lett. 15, 1005.
Silberberg, Y., 1990b. Opt. Lett. 15, 1282.
Skinner, S.R., Allan, G.R., Andersen, D.R., Smirl, A.L., 1991. IEEE J. Quantum Electron. 27, 2211.
Snyder, A.W., Love, D.J., 1973. Optical Waveguide Theory. Chapman & Hall, London.
Snyder, A.W., Mitchell, D.J., Poladian, L., Ladouceur, F., 1991. Opt. Lett. 16, 21.
Snyder, A.W., Mitchell, D.J., Luther-Davies, B., 1993. J. Opt. Soc. Am. B 10, 2341 *.
Snyder, A.W., Mitchell, D.J., Kivshar, Yu.S., 1995. Mod. Phys. Lett. B 9, 875.
Snyder, A.W., Poladian, L., Mitchell, D.J., 1992. Opt. Lett. 17, 789 **.
Snyder, A.W., Sheppard, A.P., 1993. Opt. Lett. 18, 499.
Spiegel, E.A., 1980. Physica D 1, 236.
Staliunas, K., 1994a. Opt. Commun. 90, 123.
Staliunas, K., 1994b. Chaos, Solitons, and Fractals 4, 1783.
Stolen, R.H., Gordon, J.P., Tomlinson, W.J., Haus, H.A., 1989. J. Opt. Soc. Am. B 63, 1159.
Suter, D., Blasberg, T., 1993. Phys. Rev. A 48, 4583.
Svelto, O., 1974. Self-focusing, self-trapping, and self-phase modulation of laser beams. In: Wolf, E. (Ed.), Progress in Optics, vol. XII, North-Holland, Amsterdam.
Swartzlander, G.A. Jr., Andersen, D.R., Regan, J.J., Yin, H., Kaplan, A.E., 1991. Phys. Rev. Lett. 66, 1583 ***.
Swartzlander, G.A. Jr., 1992. Opt. Lett. 17, 493.
Swartzlander, G.A. Jr., Law, C., 1992. Phys. Rev. Lett. 69, 2503.
Swartzlander, G.A., Jr., C. Law, 1993. Optics and Photonics News 10 (December).

Taniuti, T., Nishihara, K., 1983. Nonlinear Waves. Pitman, Boston.
Taya, M., Bashaw, M.C., Fejer, M.M., Segev, M., Valley, G.C., 1995. Phys. Rev. A 52, 3095 **.
Taya, M., Bashaw, M.C., Feier, M.M., Segev, M., Valley, G.C., 1996. Opt. Lett. 21, 943.
Thurston, R.N., Weiner, A.M., 1991. J. Opt. Soc. Am. B 8, 471.
Tikhonenko, V., Akhmediev, N.N., 1996. Opt. Commun. 126, 108.
Tikhonenko, V., Christou, J., Luther-Davies, B., 1995. J. Opt. Soc. Am. B 12, 2046.
Tikhonenko, V., Christou, J., Luther-Davies, B., Kivshar, Yu.S., 1996a. Opt. Lett. 21, 1129 ***.
Tikhonenko, V., Christou, J., Luther-Davies, B., 1996b. Phys. Rev. Lett. 76, 2698.
Tikhonenko, V., Kivshar, Yu.S., Steblina, V.V., Zozulya, A.A., 1997. J. Opt. Soc. Am. B, in press.
Tomlinson, W.J., Hawkins, R.J., Weiner, A.M., Heritage, J.P., Thurston, R.N., 1989. J. Opt. Soc. Am. B 6, 329.
Tratnik, M.V., Sipe, J.E., 1988. Phys. Rev. A 38, 2011.
Trillo, S., Wabnitz, S., Chisari, R., Cappellini, G., 1992. Opt. Lett. 17, 637.
Trillo, S., Wabnitz, S., Wright, E.M., Stegeman, G., 1988. Opt. Lett. 13, 871.
Turitsyn, S.K., 1985. Teor. Mat. Fiz. 64, 226 [Theor. Math. Phys. 64 (1986) 797].
Uzunov, I.M., Gerdjikov, V.S., 1993. Phys. Rev. A 47, 1582 *.
Vakhitov, M.G., Kolokolov, A.A., 1973. Radiophys. Quantum Electron. 16, 783.
Valley, G.C., Segev, M., Crosignani, B., Yariv, A., Fejer, M.M., Bashaw, M.C., 1994. Phys. Rev. A 50, R4457 *.
Velchev, I., Dreischuh, A., Neshev, D., Dinev, S., 1996. Opt. Commun. 130, 385.
Velchev, I., Dreischuh, A., Dinev, S., 1997. Multiple-charged optical vortex solitons in bulk Kerr media, Opt. Commun., in press.
Wai, P.K.A., Menyuk, C.R., Lee, Y.C., Chen, H.H., 1986. Opt. Lett. 11, 464.
Wai, P.K.A., Chen, H.H., Lee, Y.C., 1990. Phys. Rev. A 41, 426.
Wang, L., Yang, C.C., 1990. Opt. Lett. 15, 474.
Weiner, A.M., 1992. In: Taylor, J. (Ed.), Optical Solitons: Theory and Experiment. Cambridge University Press, Cambridge ***.
Weiner, A.M., Heritage, J.P., Hawkins, R.J., Thurston, R.N., Kirschner, E.M., Learid, D.E., Tomlinson, W.J., 1988. Phys. Rev. Lett. 61, 2445 ***.
Weiner, M.J., Thurston, R.N., Tomlinson, W.J., Heritage, J.P., Leaird, D.E., Kirschner, E.M., Hawkins, R.J., 1989. Opt. Lett. 14, 868.
Weinstein, M.I., 1985. SIAM J. Math. Anal. 16, 472.
Werner, M.J., Drummond, P.D., 1993. J. Opt. Soc. Am. B 10, 2390.
Werner, M.J., Drummond, P.D., 1994. Opt. Lett. 19, 613.
West, C.S., Kennedy, T.A.B., 1993. Phys. Rev. A 47, 1252.
Williams, J.A.R., Allen, K.M., Doran, N.J., Emplit, Ph., 1994. Opt. Commun. 112, 333.
Yang, X., Kivshar, Yu.S., Luther-Davies, B., Andersen, D., 1994. Opt. Lett. 19, 344 *.
Yang, X., Luther-Davies, B., Królikowski, W., 1993. Int. J. Nonlinear Opt. Phys. 2, 339.
Zakharov, V.E., 1972. Sov. Phys. JETP 72, 908.
Zakharov, V.E., Manakov, S.V., Novikov, S.P., Pitaevskii, L.P., 1980. Theory of Solitons: The Inverse Scattering Transform. Nauka, Moscow (English Translation by Consultant Bureau, New York, 1984).
Zakharov, V.E., Shabat, A.B., 1971. Zh. Eksp. Teor. Fiz. 61, 118 [Sov. Phys. JETP 34 (1972) 62].
Zakharov, V.E., Shabat, A.B., 1973. Zh. Eksp. Teor. Fiz. 64, 1627 [Sov. Phys. JETP 37 (1973) 823] ***.
Zakharov, V.E., Sobolev, V.V., Synakh, V.S., 1971. Zh. Eksp. Teor. Fiz. 60, 136 [Sov. Phys. JETP 33 (1971) 77].
Zakharov, V.E., Synakh, V.S., 1975. Zh. Eksp. Teor. Fiz. 68, 940 [Sov. Phys. JETP 41 (1975) 465].
Zhao, W., Bourkoff, E., 1989a. Opt. Lett. 14, 703 *.
Zhao, W., Bourkoff, E., 1989b. Opt. Lett. 14, 1371.
Zhao, W., Bourkoff, E., 1990. Opt. Lett. 15, 405.
Zhao, W., Bourkoff, E., 1992. J. Opt. Soc. Am. B 9, 1134 *.